DRAFT 1 - DRAFT 1

Very Long Baseline Neutrino Oscillation Experiments for Precise Measurements of Oscillation Parameters and Search for $\nu_\mu \to \nu_e$ Appearance and CP Violation.

Report of the Neutrino Working Group to Brookhaven National Laboratory.

D. Beavis, M. Diwan, R. Fernow, J. Gallardo, S. Kahn, H. Kirk, D. Lowenstein, W. Marciano, W. Morse, Z. Parsa, R. Palmer, T. Roser, N. Samios, Y. Semertzidis, N. Simos, B. Viren, W. Weng
Brookhaven National Laboratory Box 5000, Upton, NY 11973-5000

W. Frati, J. R. Klein, K. Lande, A. K. Mann, R. Van Berg and P. Wildenhain
University of Pennsylvania Philadelphia, PA 19104-6396

R. Corey
South Dakota School of Mines and Technology Rapid City, S.D. 57701

D. B. Cline, K. Lee, B. Lisowski, P. F. Smith
Department of Physics and Astronomy, University of California, Los Angeles, CA 90095 USA

I. Mocioiu, R. Shrock
C.N. Yang Institute for Theoretical Physics, State University of New York, Stony Brook, NY 11974 USA

C. Lu, K.T. McDonald
Joseph Henry Laboratories, Princeton University, Princeton, NJ 08544 USA

October 4, 2002

BLANK PAGE

Contents

Abstract

The possibility of making a low cost, very intense high energy proton source at the Brookhaven Alternating Gradient Synchrotron (AGS) along with the forthcoming new large underground detectors at either the National Underground Science Laboratory (NUSL) in Homestake, South Dakota or at the Waste Isolation Pilot Plant (WIPP) in Carlsbad, New Mexico, allows us to propose a program of experiments that will address fundamental aspects of neutrino oscillations and CP-invariance violation. This program of experiments is unique because of the extra-long baseline of more than 2500 km from Brookhaven National Laboratory to the underground laboratories in the West, the high intensity of the proposed conventional neutrino beam, and the possibility of constructing a very large array of water Cerenkov detectors with total mass approaching 1 Megaton. A companion report examines the design and construction of the necessary AGS upgrades and the new neutrino beam which will have a proton beam of power $\sim$1.0 MW. In this report we will examine the potential physics reach of such an experiment. We use the running scenario of a 1 MW AGS, 500 kT of fiducial detector mass, and 5×10^7 secs of running time. With these conditions, we conclude that such an experiment is capable of precisely measuring Δm^2_{32} and $\sin^2 2\theta_{23}$; it has excellent senstivity to $\sin^2 2\theta_{13}$ with a signal spectrum that is very distinctive. Moreover if $\sin^2 2\theta_{13}$ is sufficiently large (> 0.01) the experiment is sensitive to the CP violation parameter δ_{CP} with only neutrino running. Lastly, the very long baseline will allow the measurement of Δm^2_{21} with approximately 15% resolution in the $\nu_\mu \rightarrow \nu_e$ appearance channel if the LMA solution is correct for the Solar neutrino deficit.

1 Introduction

The physics of neutrino masses and mixings is currently very fluid and open to new ideas. Brookhaven National Laboratory started a neutrino working group to identify new opportunities in this field and explore how our laboratory facilities can be used to explore this field of research. The memo to the working group and the charge is included in Appendix I.

This report is the result of the deliberations of the working group. Previously our working group wrote a letter of intent to build a new high intensity neutrino beam at BNL [1]. The new intense proton beam will be used to produce a conventional horn focussed neutrino beam directed at far detectors.

As a continuation of the study that produced the letter of intent, this report will examine several items in more detail. We will compare three possible baselines to understand the physics impact: from BNL to WIPP (or Homestake) at a distance of more than 2500 km, from BNL to locations in upstate NY at a distance of $\sim$ 400 km; and we will also examine the possibility of sending a BNL beam to a large detector placed "off-axis" on the NuMI beamline at Fermilab. Such a detector could be placed in Minnesota or Wisconsin at distance of 1500 to 1800 km from BNL. The detector size, resolution, and background rejection for each of these possibilities are examined. We mainly concentrate on the use of water Cerenkov detectors because of their size, nevertheless we examine magnetized Liquid Argon in the context of the background rejection needed to achieve the ultimate sensitivity with a conventional beam.

The accelerator upgrade will be carried out in phases. We expect the first phase to yield a 0.5 MW proton beam and the second phase to result in a 1.5 MW beam. The details of this upgrade are reported in a companion report. In this report we will assume accelerator intensity of 1 MW for calculating event rates. We will also assume a total experimental duration of 5 years with running time of 10^7 seconds per year.

As part of this report we have also examined the target station and the horn produced neutrino beam with focus on two topics: target and horn design for a 1 MW beam, the broad band spectrum of neutrinos from a 28 GeV proton beam. We have also compared the intensity and off-axis capability of the BNL beam with the Fermilab NuMI beam.

2 Neutrino Oscillations

It is now well known that the strongest evidence for neutrino oscillations so far comes from astrophysical observations of atmospheric neutrinos with $\Delta m^2_{32} = (1.6 - 4.0) \times 10^{-3} eV^2$ and maximal mixing [4] and from solar neutrinos with $\Delta m^2_{21} \sim (2 - 10) \times 10^{-5} eV^2$ and the LMA solution for solar neutrinos [6]. The observation by the LSND experiment [7] will soon be re-tested at Fermilab by the mini-Boone [8] experiment, therefore we will not discuss it further in this document. There are several accelerator based experiments (K2K, MINOS, and CNGS) [9, 10, 11, 12] currently in construction phase or taking data to confirm the atmospheric neutrino signatures for oscillations. There is now a consensus that there are four main goals in the field of neutrino oscillations that should be addressed soon with accelerator neutrino beams:

1. Precise determination of Δm^2_{32} and definitive observation of oscillatory behavior.

2. Detection of $\nu_\mu \to \nu_e$ in the appearance mode. If the measured Δm^2 for this measurement is near Δm^2_{32} then this appearance signal will show that $|U_{e3}|^2 (= \sin^2 \theta_{13})$ from the neutrino mixing matrix in the standard parameterization is non-zero.

3. Detection of the matter enhancement effect in $\nu_\mu \to \nu_e$ in the appearance mode. This effect will also allow us to measure the sign of Δm^2_{32}; i.e. which neutrino is heavier.

4. Detection of CP violation in neutrino physics. The neutrino CP-violation in Standard Model neutrino physics comes from the phase multiplying $\sin \theta_{13}$ in the mixing matrix. This can be detected by observing an asymmetry in the oscillation rates $\nu_\mu \to \nu_e$ versus $\bar{\nu}_\mu \to \bar{\nu}_e$.

In the following we will briefly describe how all of these goals can be achieved under reasonable assumptions for the various parameters using the new intense AGS based beam and the long and very long baselines.

In Section 3 of this report we briefly describe the accelerator upgrade path to achieve a proton source with intensity greater than 1 MW.

In Section 3 we examine the conventional neutrino beam spectrum and the target-horn station. In Sections 4 to 6 we estimate the event rates, backgrounds, and oscillation signals. We also estimate the sensitivity for various oscillation parameters.

3 AGS Upgrade

4 Neutrino Beam Design

The geographic location of BNL on one side of the continent allows us to send beams to a variety of distances including very long baselines of 2000 km or more. This is shown in Fig. 3. The distances from BNL to Lansing NY, Soudan MN, Lead SD(Homestake), and WIPP in NM are 350, 1770, 2540, and 2880 km, respectively. The respective dip angles are 1.7, 7.9, 11.5, and 13.0 degrees. The difficulty of building the beam and the cost increases with the dip angle.

Our preliminary design for a beam to Homestake is shown in figures 1 and 2. This can be adapted to any far location in the western direction. Our design addresses a number of issues. At BNL we are constrained to keep the beam line above the water table which is at a shallow depth ($\sim$ 20 m) on Long Island. Therefore the beam has to be constructed on a hill that is built with the appropriate 11.5 degree slope. Fortunately, it is relatively easy, and inexpensive to build such hills on Long Island because of the flat, sandy geology. It is important to keep the height of the hill low so that the costs are not dominated by the construction of the hill. The proton beam must be elevated to a target station on top of the hill. The cost of the hill can be lowered by bending the proton beam upwards as quickly as possible. We have, however, used the design and bend angle used for the RHIC injection lines for our design because the RHIC injection lines have well known costs.

The new proposed fast extracted proton beam line in the U-line tunnel will be a spur off the line feeding RHIC. It will turn almost due west, a few hundred meters before the horn-target building. In addition to its 90 degree bend, the extracted proton beam will be bent upward through 13.76 degrees to strike the proton target. The downward 11.30 degree angle of the 200 meter meson decay region will then be aimed at the 2500 meter level of the Homestake Laboratory. This will require the construction of a 39 meter hill to support the target-horn building, so as to avoid any penetration of the water table. At its midpoint (about Lake Michigan) the center of the neutrino beam will be roughly 120 km below the Earth's surface.

For a shorter baseline to Lansing NY in approximately the same direction as Homestake, we would not have to build the hill, which would lower the cost by a considerable amount. We are considering a number of strategies for combining the proton transport and the target station for the two different baselines.

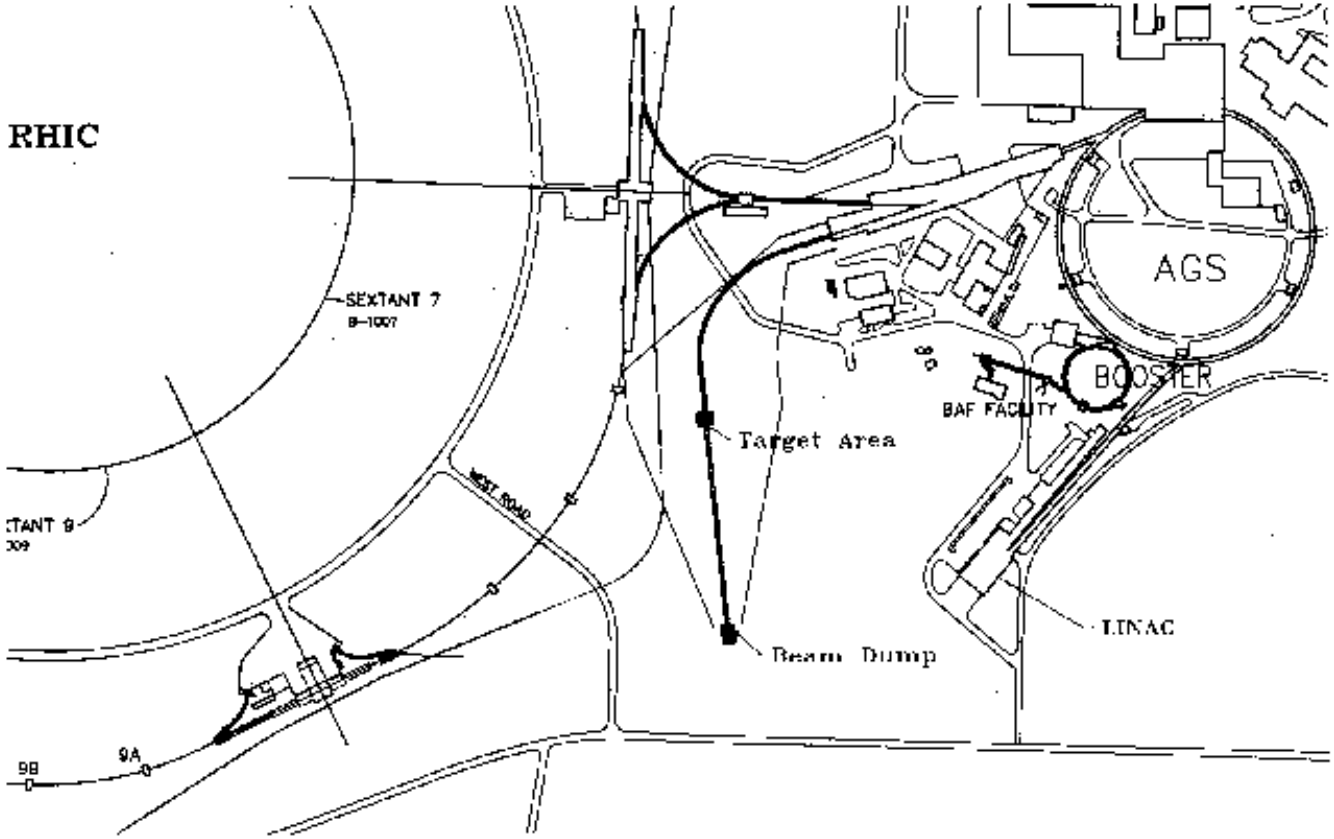

Figure 1: The beam line for sending a neutrino beam to Homestake mine, South Dakota. This same beam line can be adapted for any far location in the Western direction.

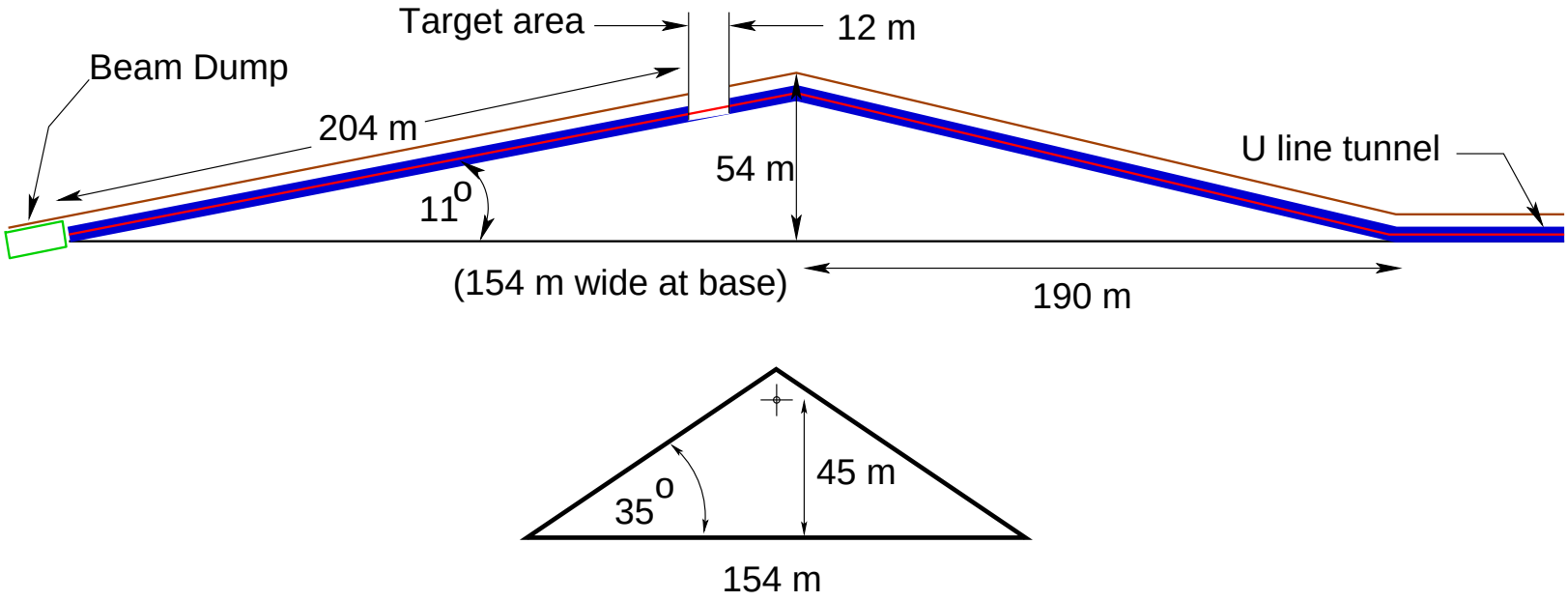

Figure 2: Elevation view of the neutrino beam line to Homestake, South Dakota. For a nearer location a much smaller hill can be constructed. In this beam we assume a decay tunnel length of 200 m. For a shorter tunnel the cost of the hill will reduce as shown in Table 1.

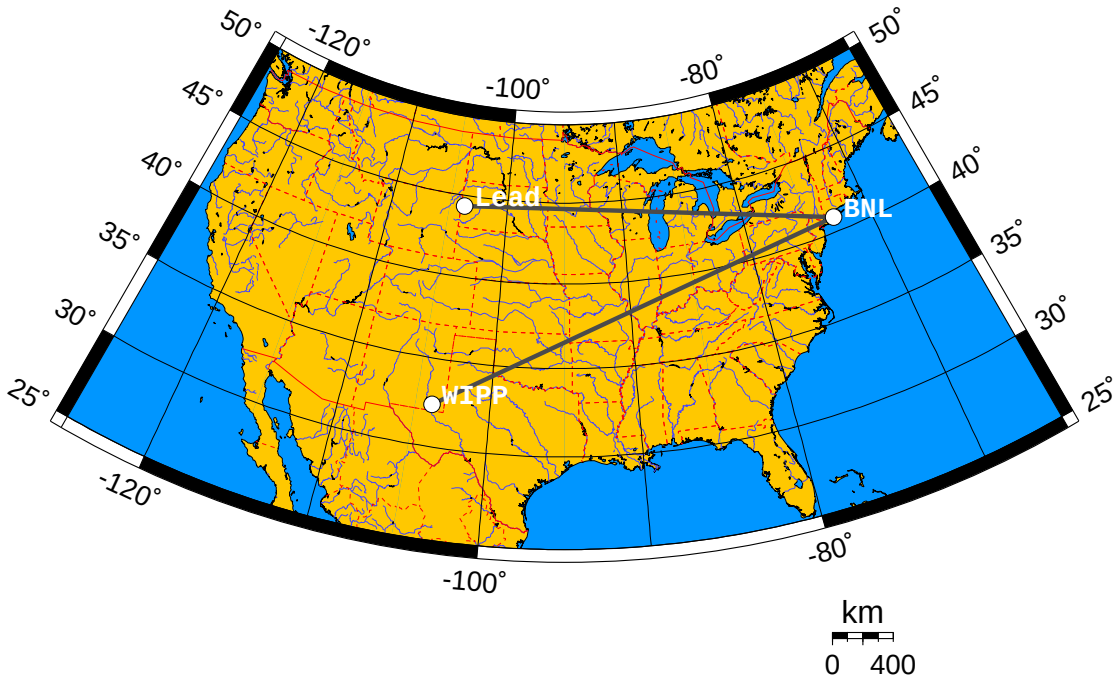

Figure 3: Possibilities for very long baselines from BNL. The distances from BNL to Lead (Homestake), and WIPP are 2540, and 2880 km, respectively.

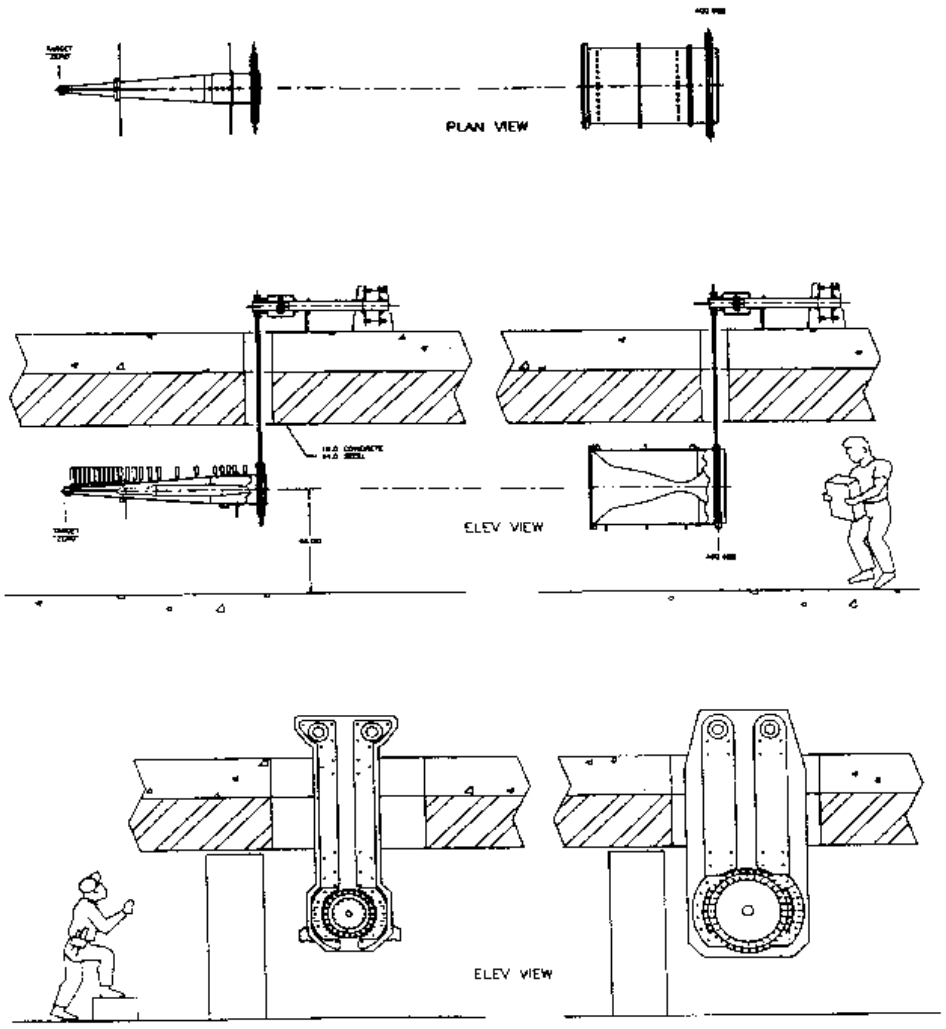

Figure 4: The design of the horn focussing system used for the E734 experiment adapted from the E889 proposal.

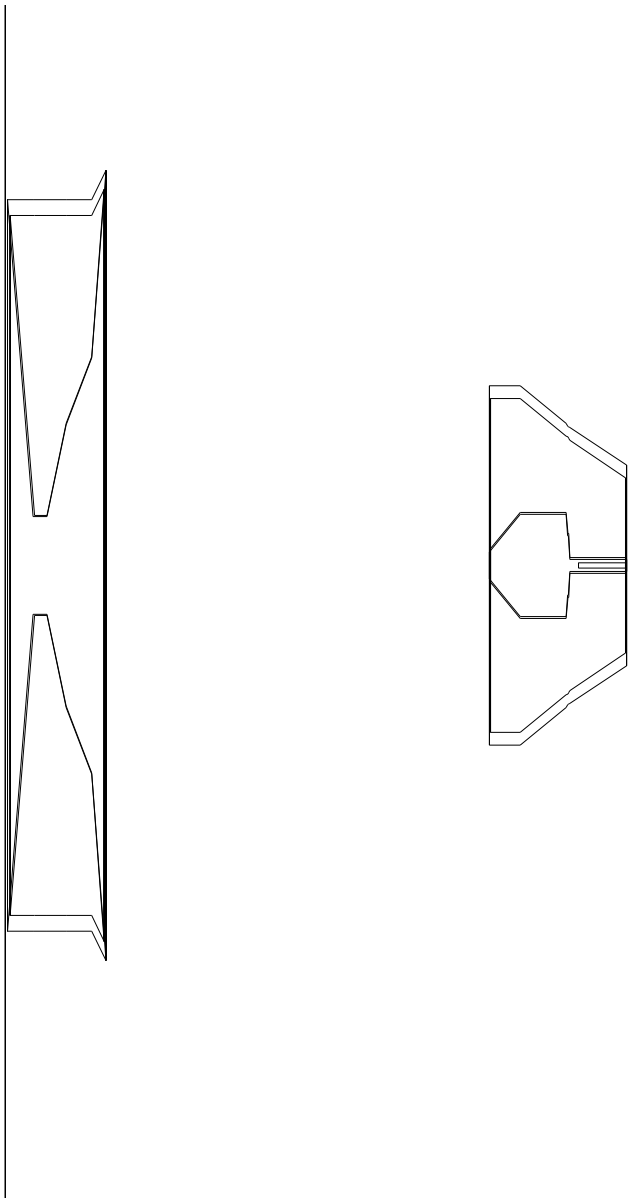

Figure 5: The horn geometry in the GEANT simulation. The vertical and horizontal scales are in the ratio of 1 to 13. The beam is incident from the right.

4.1 Optimization of the wide band spectrum

For this report we have attempted to optimize the beam for the Homestake distance (2540 km). However, our optimization process could be applied to any distance. As explained in later sections, the ideal beam for Homestake should be a broadband beam that covers ~0.5 GeV to ~7.0 GeV range. The $\nu_\mu \to \nu_e$ process through Δm^2_{12} (solar oscillations) could make large effects ($\sim 10\%$) at the lowest energies. The energy range $1-3\ GeV$ could be important for the detection of CP violation. The energy region $3-5$ GeV contains the first matter enhanced (for neutrinos with standard mass hierarchy) $\nu_\mu \to \nu_e$ oscillation maximum. In the following we will argue that the highest energies are important for establishing the existence of $\nu_\mu \to \nu_e$ signature because this region is free from the neutral curernt π^0 background and should have very good efficiency for the signal. Lastly the energy region $6-7$ GeV is important for the $\nu_\mu \to \nu_\mu$ disapearance measurement.

To obtain such a broad band spectrum we have adapted the standard scheme of multiple parabolic horns. Each one focussing a different pion momentum region. The difficulty with this approach is that the lowest energy we need to capture and focus approximately 1-2 GeV pions that come from a long target. Fig. 4 and 5 shows the design of the target and horn geometry for a conventional wide band neutrino beam similar to that used in previous experiments at BNL such as E734. The E734 design uses a water cooled 1.5 interaction length copper target. The calculated energy distributions of a ν_μ beam produced by 28 GeV protons is shown in Fig. 6 [15]. The 0° calculation has been shown consistent with neutrino beam data [16]. The spectrum peaks at about 1 GeV with a total spread at half intensity of about 1 GeV. A copper target will not survive the $\sim$ 1 MW intensity of proton beam that we propose. Therefore both new materials and new focussing geometries must be considered. We discuss the target in much more detail in a later section. The two main issues in the target design are the target material and the space available for cooling the target. If a dense material such as Super-Invar is used then the spectrum will be approximately the same as shown in Fig. 6. The better approach is to use graphite as target material and modify the horn geometry to allow a longer target (Fig. 5). The result of these modifications is shown in Fig. 7. The electron neutrino contamination is shown on the same scale in Fig. 8. We have used a 1.5 interaction length graphite target. As shown in the figures the flux resulting from a graphite target is considerably higher in the 3.5 to 8 GeV region. There is no significant change in the ratio of electron type neutrinos to muon type neutrinos between a graphite and a copper target. We will use the flux from Figs. 7 and 8 for the calculation of event rates and backgrounds in the rest of this report.

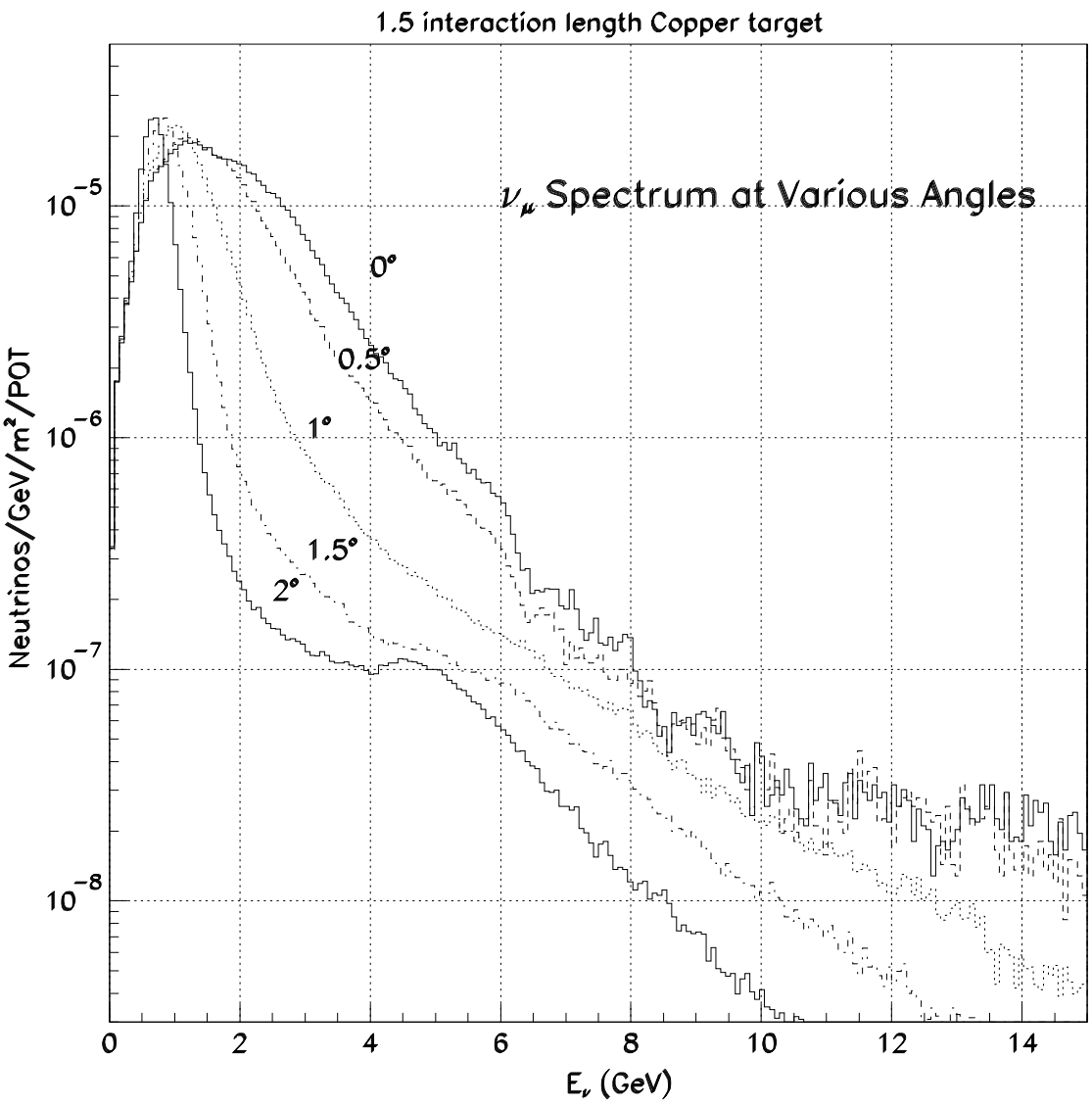

Figure 6: Wide band horn focussed neutrino spectrum for 28 GeV protons on a Copper target. The spectrum is approximately the same if Super-Invar is used as target material. Spectra of neutrinos are calculated at various angles with respect to the 200 m decay tunnel axis at the AGS and at a distance of 1 km from the target.

There is a large ($\sim$ 50%) model dependent uncertainty on the neutrino flux at high energies ($> 4\ GeV$). In particular the hadron production model in MARS gives lower flux than in GEANT.[37] This uncertainty will most likely be resolved by new experiments[29, 31, **?**] in the near future.

Further work on the optimization of this spectrum for the very long baseline experiment is on going. Further optimization focusses on enlarging the horns to accept more lower energy pions so that the flux near 0.5 GeV can be enhanced, as well as using the hadronic hose [18] to capture more higher energy particles. Our design calls for the target to be inside the 2.5 cm diameter aperture of the first horn, where the space is limited. The resulting heat and radiation load on the materials will present a severe challenge for the mechanical construction of this device.

4.2 Target Station

To use the 1 MW proton driver proposed for BNL, serious consideration must be given to the target selection. It is desirable to choose a solid target for generating a high intensity neutrino beam. For pion production with powerful protons beams, target integrity becomes an important issue. Up to now, the production of secondary particles has been limited to proton beams with average beam power on the order of 100 to 200 kW. We now have to consider a target which can survive a 1 MW or greater average power proton beam. For a 28 GeV proton beam, 1 MW beam power implies 2.23×10^{14} proton/sec. For a rep-rate of 2.5 Hz we then must consider nearly 100 TP per spill. The target must be able to withstand a 1 MW proton beam. A number of options have been considered and investigated both in terms of the material selection as well as the feasibility of target configuration. In evaluating the target choices the following concerns are being addressed:

- Heat removal from the target.
- Survivability of the target intercepting energetic, high intensity proton bunches.
- Irradiation issues
- Engineering integration issues
- Heat generation and removal from the horn
- Horn mechanical response

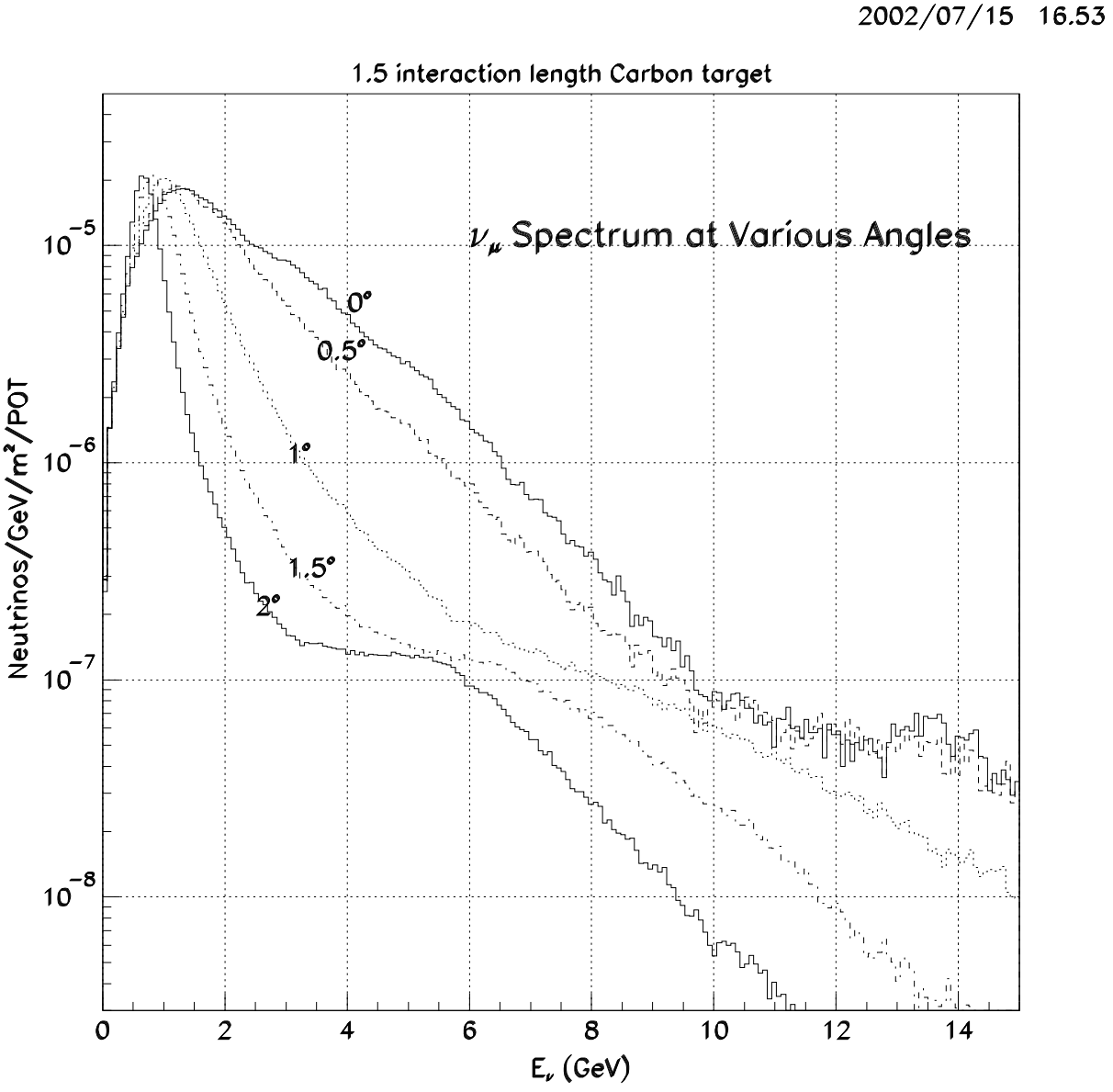

Figure 7: Wide band horn focussed muon neutrino spectrum for 28 GeV protons on a graphite target. The spectra of neutrinos are calculated at various angles with respect to the 200 m decay tunnel axis and at a distance of 1 km from the target.

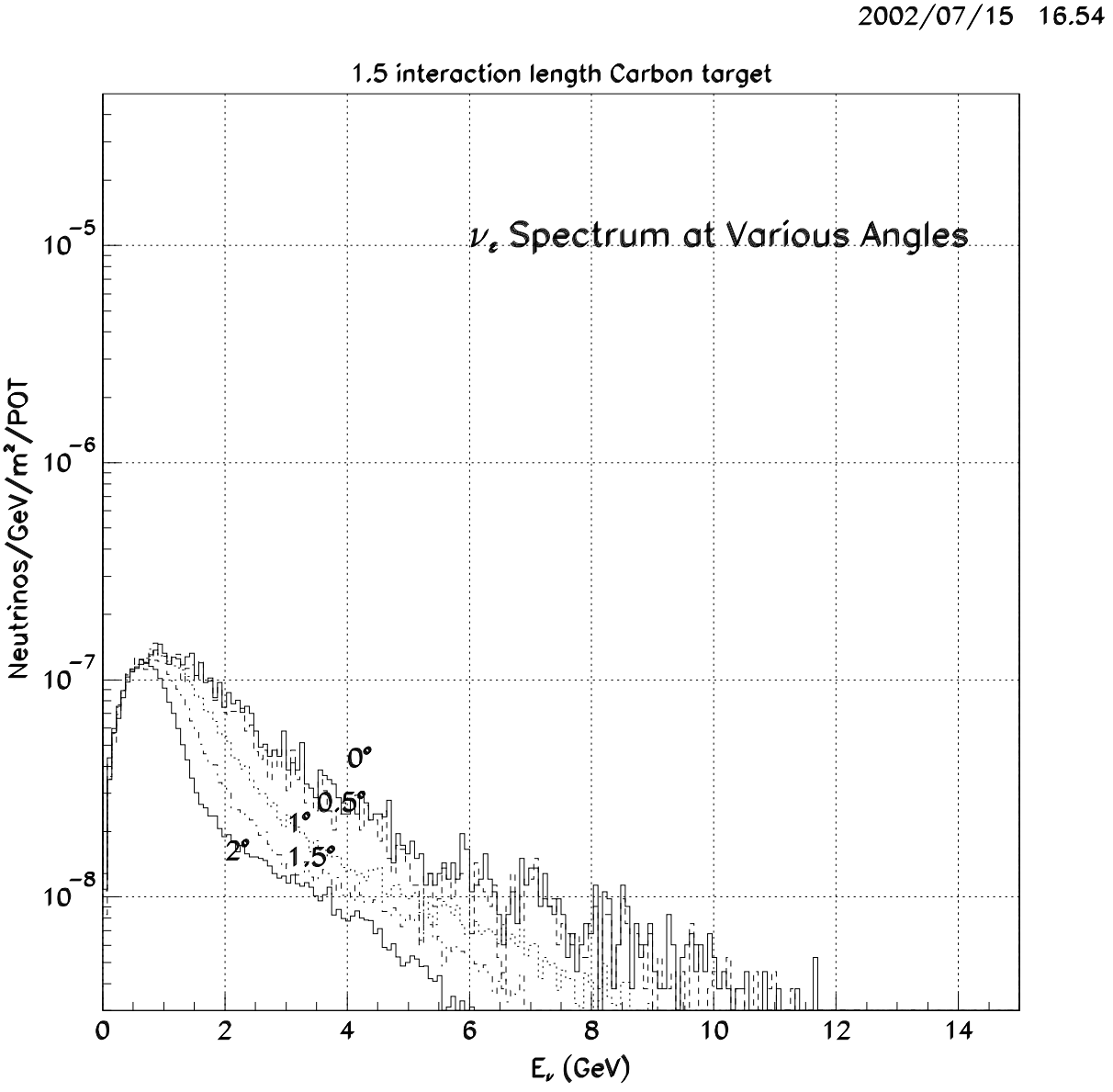

Figure 8: Wide band horn focussed electron neutrino spectrum for 28 GeV protons on a graphite target. Spectra of ν_e are calculated at various angles with respect to the 200 m decay tunnel axis and at a distance of 1 km from the target.

Findings of a number of recent studies [24], including experimental results from E951 [30], on target issues for the muon collider/neutrino factory project are taken into consideration in this effort.

Figs. 10 and 11 show the spectra of π^+ and π^- that are produced from a 2-interaction length target for various materials. For a conventional neutrino beam the useful part of the pion spectrum is in the energy region beyond 2 GeV. For this reason, high-Z targets are no longer advantageous. We find instead that for the production of high-energy pions, lowZ targets are preferred.

In addition to maximizing the flux, the target/horn configuration must survive the thermal shock induced by the beam and the high current. Specifically, the target scheme must (a) ensure the removal of the deposited beam energy within the 400 ms period and (b) survive the thermally induced elastodynamic stresses that are expected to be comparible to the mechanical strength of most common materials. Similar concerns are valid for the horn, itself, which will be subjected to rapid heating and, as a result, high levels of thermal stress that will propagate in its volume. In order to satisfy the first requirement, several cooling scenarios are being investigated such as edge-cooling, forced helium cooling in the space between the target and the horn, and radiation cooling. All of these schemes present challenges stemming from integration with the horn in a limited space. To satisfy the second requirement, materials must be selected such that they can withstand and attenuate the thermal shock and be radiation resistant. To address this, low-Z carbon based materials such as graphite and carbon-carbon composites are being considered. These materials, while they have a lot of promise, present some challenges. Fig. **??** shows the target mounted in the first horn. Also the helium cooling system for the target and the water cooling manifold for the horn are indicated.

Two different forms of carbon, ATJ graphite and a carbon-carbon composite are considered as candidate target materials. These two types have been exposed to the AGS beam in the E951 experiment[30]. The carbon-carbon composite is a 3-D weaved material that exhibits extremely low thermal expansion below 1000^oC and responds like graphite above that. Preliminary studies on the feasibility of using carbon-based targets for this neutrino beam have been conducted. Specifically, utilizing the energy deposition estimates from MARS for 1 mm and 2 mm RMS beam spots (corresponding to 3 mm and 6 mm radii of target), the thermal shock response and the survivability potential of the target were studied. The total energy deposited on the target (and which needs to be removed between pulses) is 5.1 kJ for the 1mm spot and 7.3 kJ for the 2mm spot.

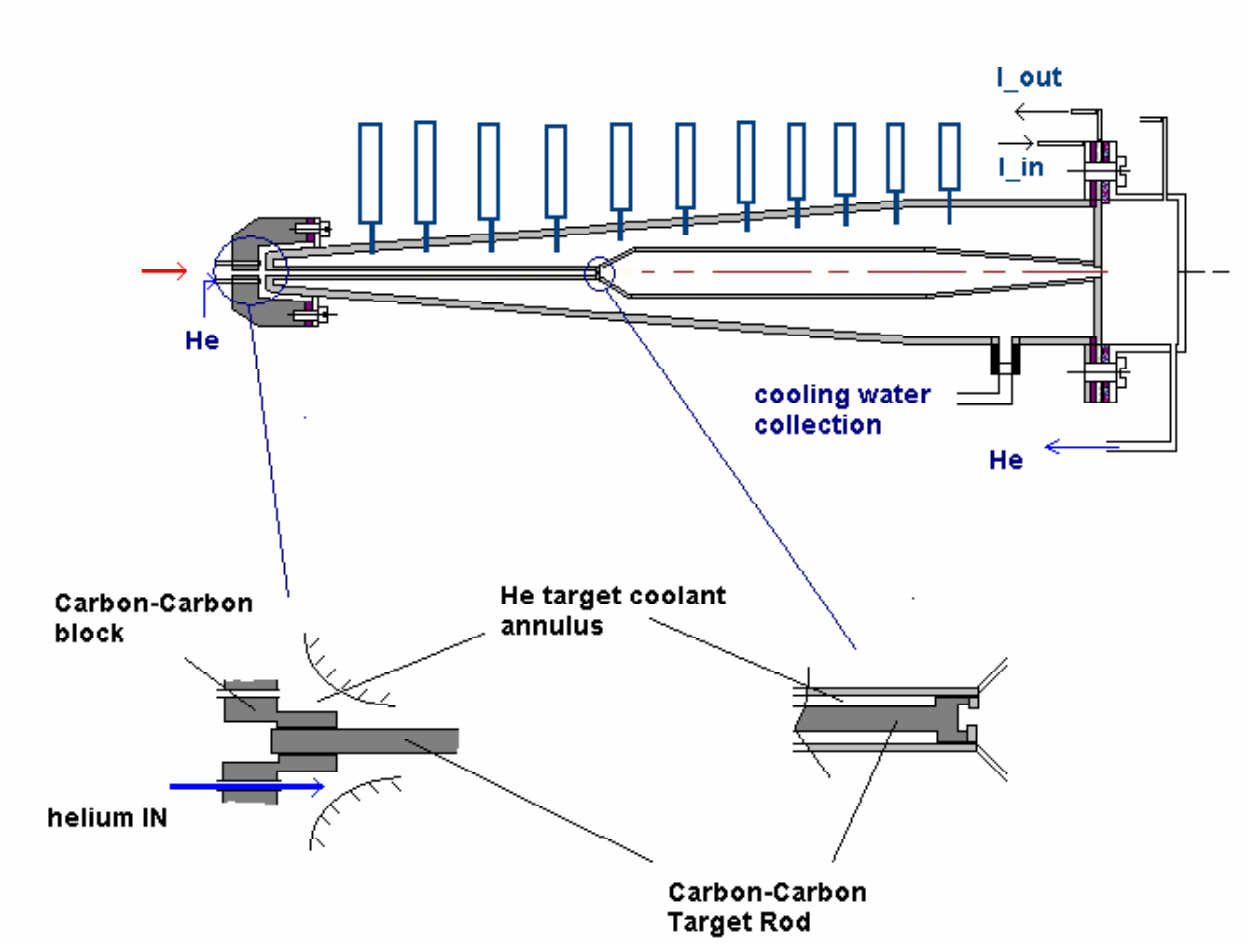

Figure 9: Sketch of the first horn with the graphite target mounted. The target is cooled by helium. The horn is cooled by spraying water on the conducting surface.

Since the 1 mm RMS beam spot is the most serious case, it is examined in detail. For the 100 TP beam the peak energy density is of the order of 720 J/gram. This is expected to lead to instantaneous temperature increases of $\sim 1000°$C. A detailed finite-element analyses that involve both the horn and the target needs to be performed so the heat removal of the system can be optimized and, most importantly, for the thermal shock stresses need to be computed. A material with a small thermal expansion should experience smaller thermal stresses. However, carbon-carbon composite materials exhibit an increaseing thermal expansion at higher temperatures. This behavior of the material needs to be examined further. If the high temperture performance of this material is not satisfactory a larger beam spot size could be used. ¿From energy density considerations a 2 mm rms beam spot would have a peak temperature rise per pulse that is less than a third of the 1 mm rms case. This would ensure that the material will be well within the safe zone. Cooling of the front-end is achieved by maintaining the temperature at the surface of the first 4 cm to 27 ^{o}C.

We examine the optimal geometry for high-energy pion production utilizing a carbon target. In Fig. 12 we see the result of varying the radius of a 1.5 interaction length (60 cm) long carbon target. For this analysis the target radius was constrained to 3 times the proton beam rms radius. We note that although the total secondary pion production increases with radius, the desired high-energy portion of the production spectra is enhanced with smaller beam spot sizes. In Fig. 13 we fix the beam/target radius at (2mm/6mm) and find that the production of 7-9 GeV pions increases with target length up to about 80 cm (2 interaction lengths) and then remains essentially constant up to 2 m.

We now explore the impact of bringing to bear 100 TP proton/spill onto a carbon target. For this analysis we utilize MARS to calculate the energy deposition due to the hadronic showering within the target. We examine the two cases of 3 mm and 6 mm radius targets shown in figure 14. We note the peak energy deposition density occurs near the entrance of the target and has the respective values of 700 and 200 J/g. As a figure of merit, 300 J/g is considered the danger regime where metal targets suffer damage due the propagation of thermal generated pressure waves through the material. There is, however, evidence that carbon can withstand energy depositions in this regime. The best evidence to date comes from experience in the NUMI target development program. The NUMI carbon target is designed to expect 390 J/g peak energy deposition. A NUMI target test, performed in 1999, utilized a specially focussed beam to produce energy depositions in the range of 400 to 1100 J/g without any external evidence of target breakup.

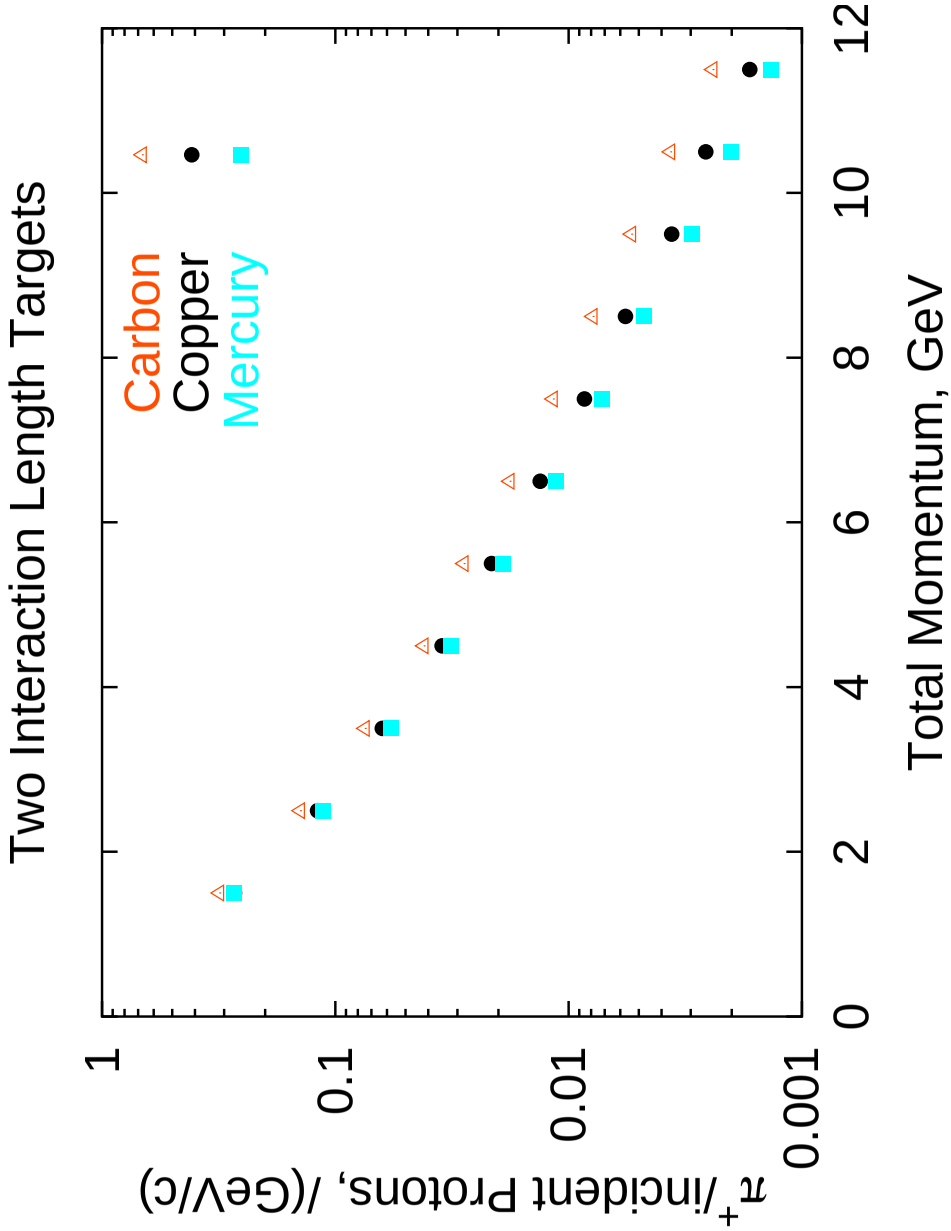

Figure 10: The number of π^+ per incident proton is shown as a function of its momentum for carbon, copper and mercury targets. The target is two interactons lengths long for each material.

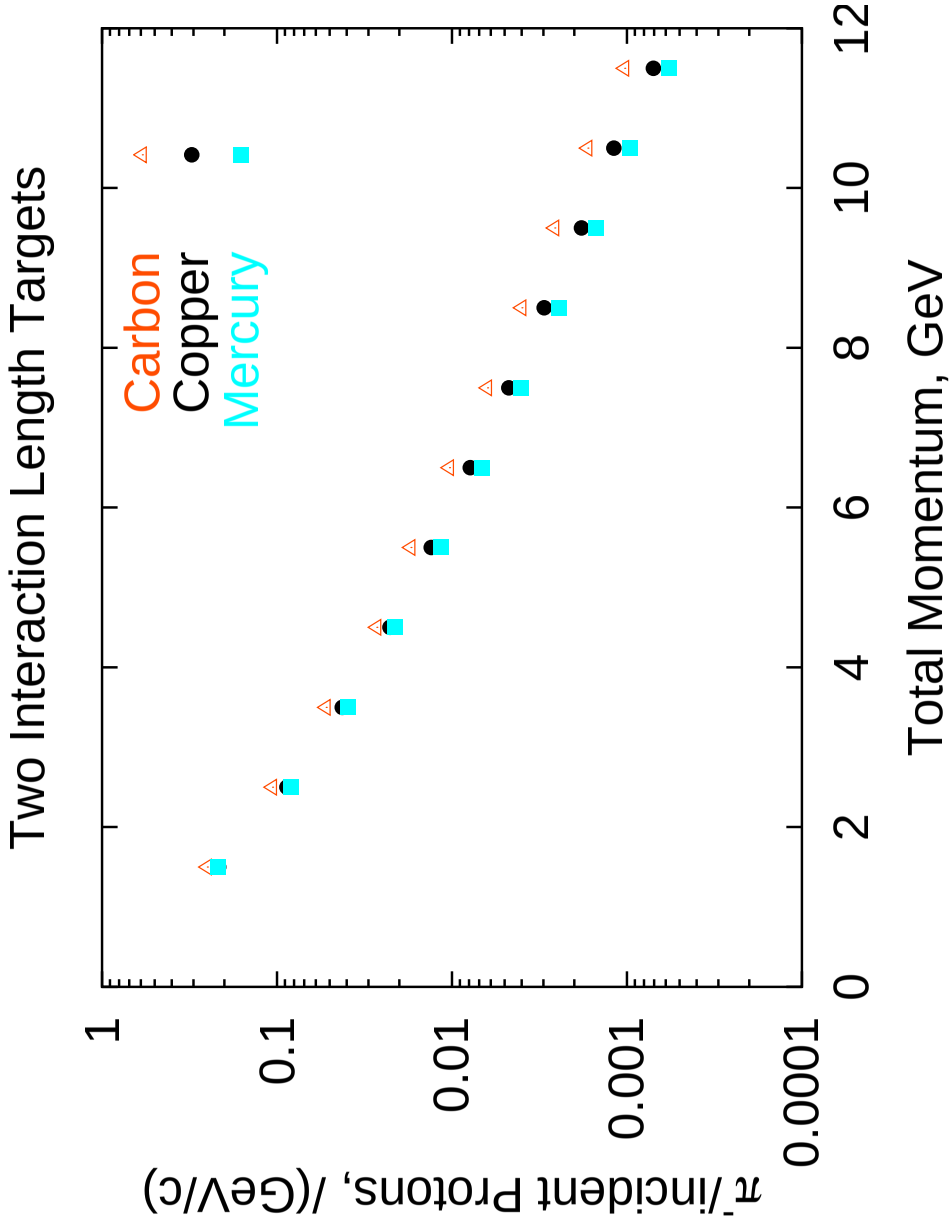

Figure 11: The number of π^- per incident proton is shown as a function of its momentum for carbon, copper and mercury targets. The target is two interactons lengths long for each material.

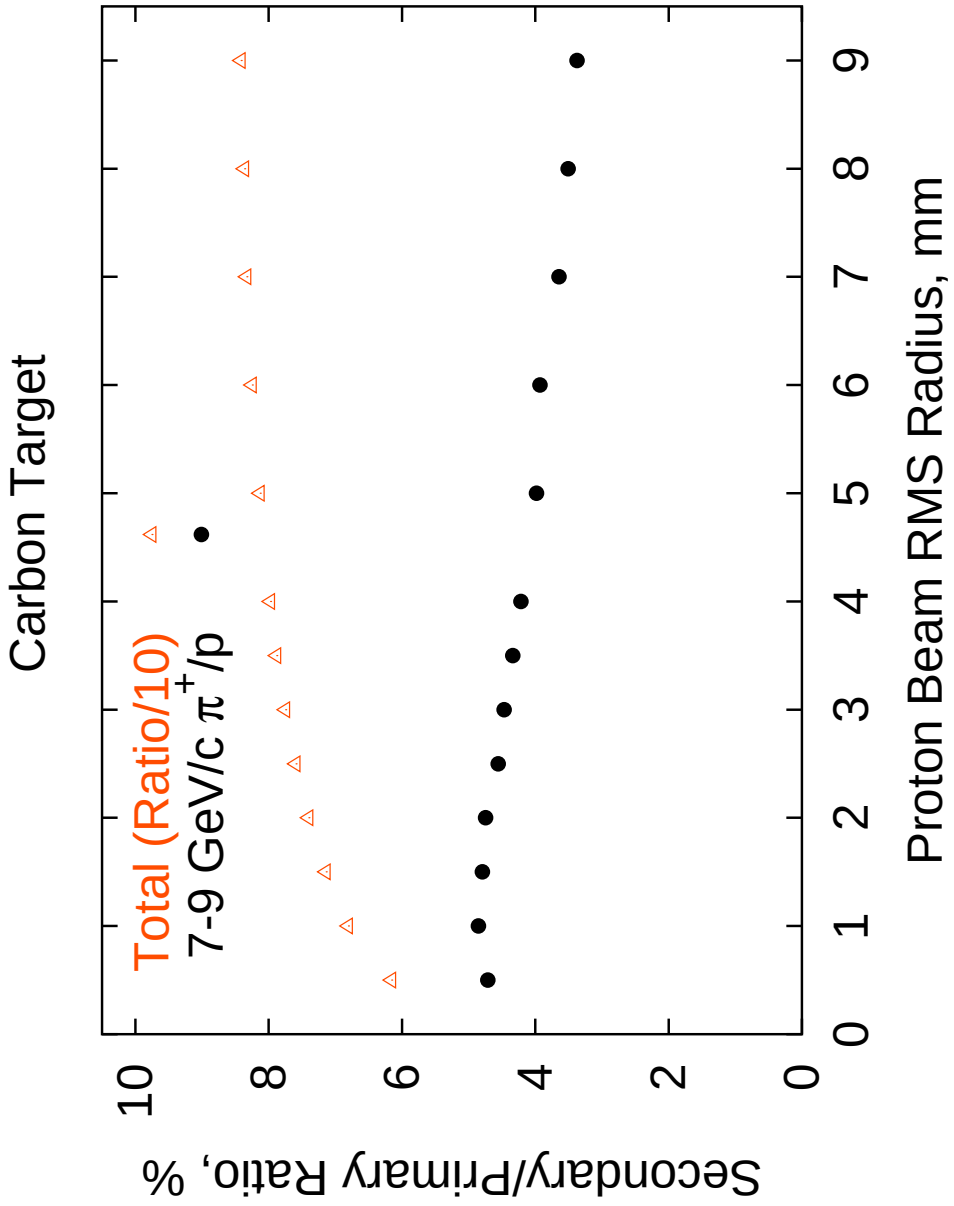

Figure 12: The ratio of the numbers secondaries to the number of primaries is shown as a function of RMS beam radius. The target radius is assumed to be three times the RMS beam radius and the target length is 1.5 interaction lengths.

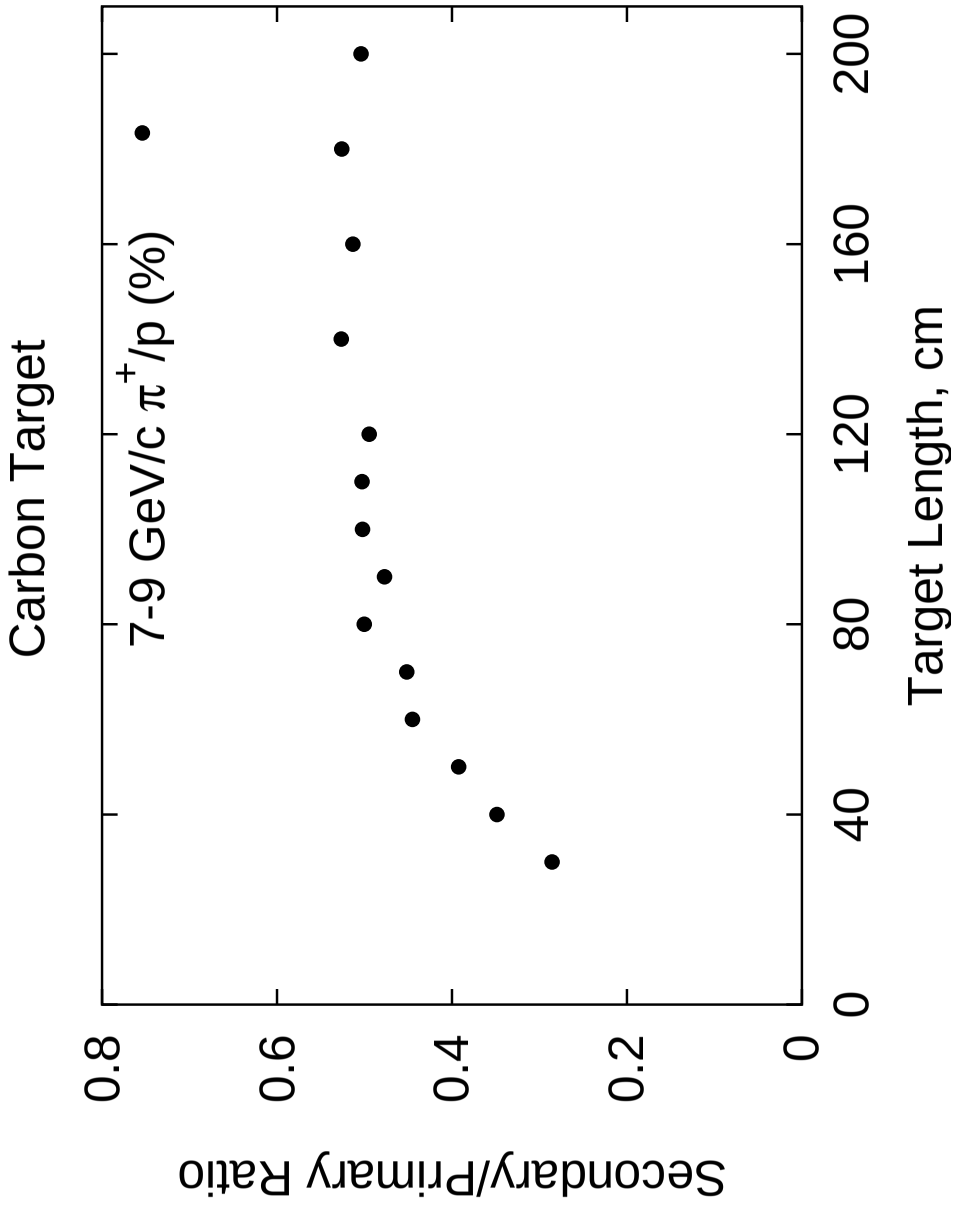

Figure 13: The ratio of the number of secondaries to the number of primaries is shown as a function of the target length for a target radius of 6 mm and a RMS beam size of 2 mm.

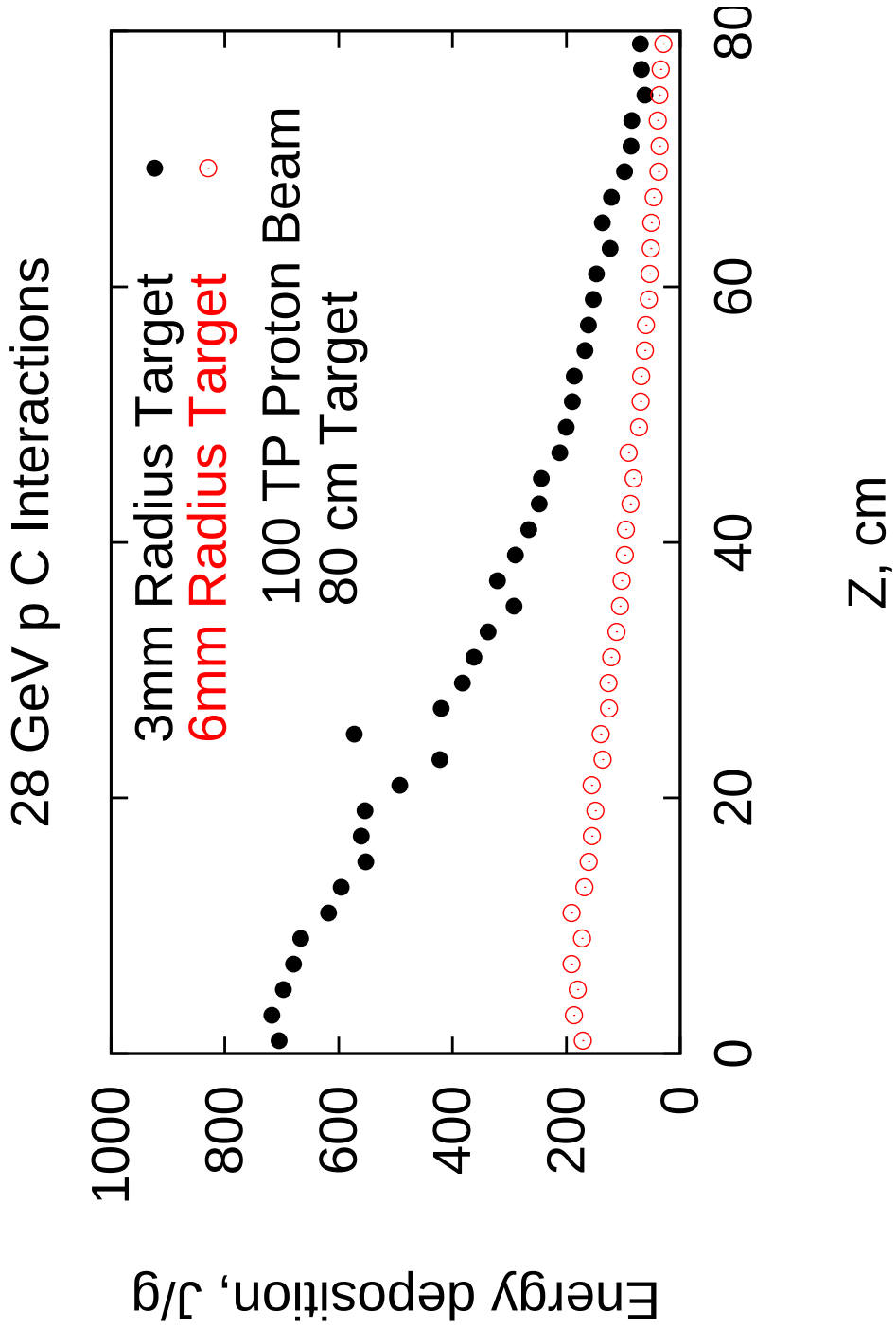

Figure 14: The energy deposition is shown as a function of target axial position for a 28 GeV 100 TP beam.

The secondary particle shower resulting from the interaction of primary protons with the low-Z target will add to the transient heat load of the horn. This shower will be less significant for low-Z targets than for high-Z targets. However, its effect will be examined, and added to the electric resistance heat load estimated above.

The resulting activation of the target and horn structure due to secondary and primary particles will be estimated. This activation will be primarily due to spallation products and activation due to neutrons generated in the secondary shower. The survival of the primary target in the radiation field needs to be examined. This can only be carried out experimentally using a prototypic proton beam on samples of the appropriate target material. The change in physical properties including, thermal expansion coefficient, elastic modulus, and yield strength need to be examined as a function of proton fluence.

4.3 Cost of the beam

A preliminary estimate of the cost without any of the customary burdens is shown in Table 1. The costs are based on the the RHIC injector work, as well as the E889 proposal and the neutrino factory study. The conventional construction costs are dominated by the size of the hill which is approximately proportional to the third power of the decay tunnel length. In our cost estimate we assume that we will bury the beam dump underground to reduce the height of the hill. It is assumed that the target station shielding can be retrieved from existing resources. We have also estimated the cost assuming a 200 m long decay tunnel. Shortening the decay tunnel to 150 m would only save \$ 3 M and would reduce the high energy ($E_\nu > 2$ GeV) flux by $\sim 25\%$. We will study this optimization further in future updates of this proposal. The spectra shown in Fig. 6 are based on a 200 m long tunnel.

5 Very Long Baseline Experiment

We calculate the event rate without oscillations assuming a 1.0 MW proton beam power with 28 GeV protons (1.1×10^{14} ppp), a 0.5 MT fiducial mass water Cerenkov detector and 5 years of running. Because the AGS can run in a parasitic mode to RHIC, we expect to get beam for as much as 1.8×10^7 sec per year. However, we conservatively assume only 1.0×10^7 sec of AGS running per year here. Using these parameters, the flux from figures 7 and 8 and the relevant cross section, we calculate that the number of quasi-elastic charged

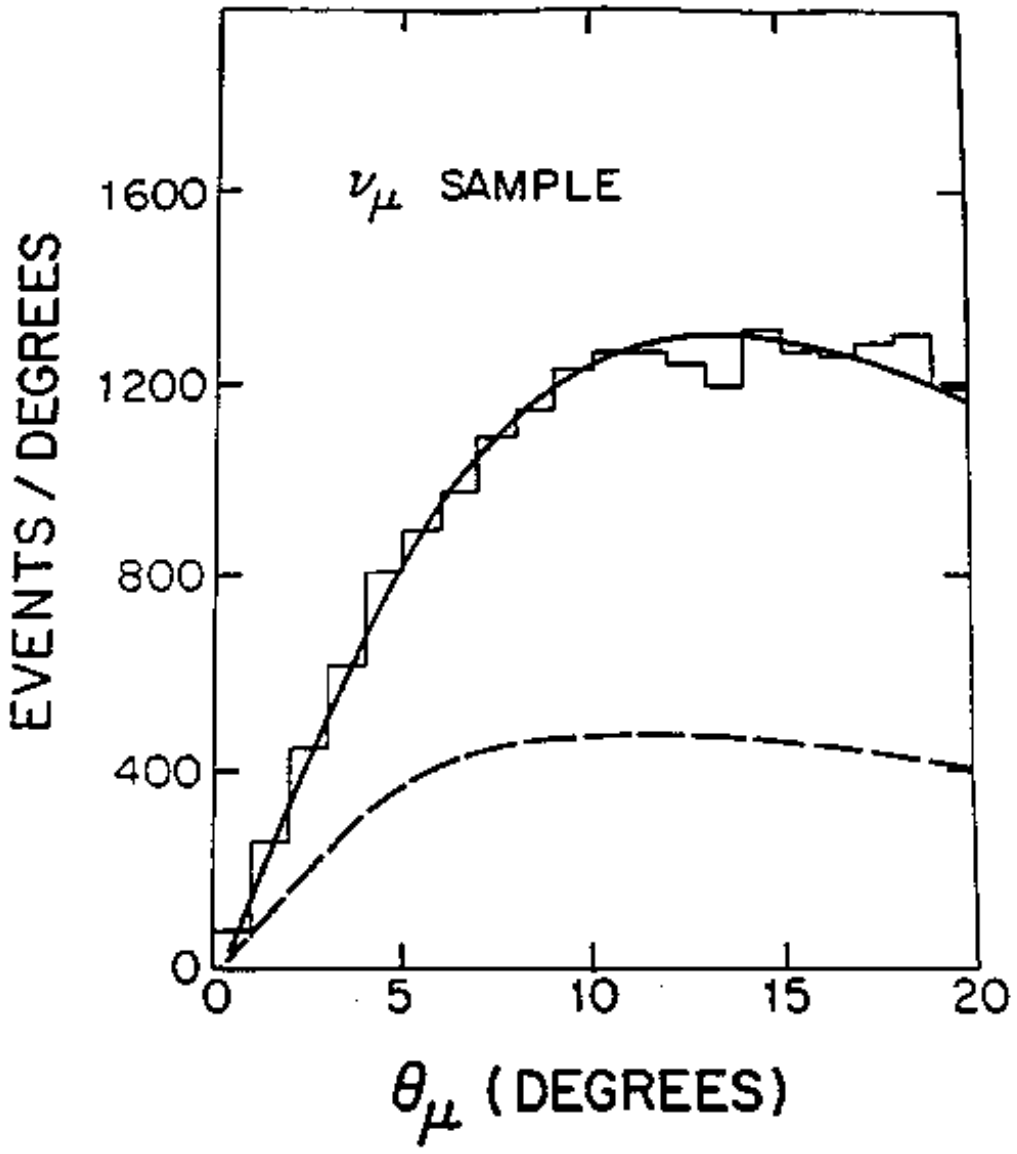

Fig. 10a

Figure 15: Angular distribution of muons from the process $\nu_\mu n \to \mu^- p$ (top curve) and background from $\nu_\mu N \to \mu^- N' \pi$ (bottom curve). The histogram is data from E734 and lines are Monte Carlo.

Item	basis	cost
Proton transport	RHIC injector	\$11.85 M
Target/horn	E889	\$3.0 M
Installation/Beam Dump	New	\$2.67 M
Decay Tunnel	E889	\$0.45 M
Conventional const. (hill)	New	\$8.0 M
Conventional const. (other)	E889	\$9.1 M
Total		\$35.19

Table 1: Preliminary cost of building the neutrino beam with 200 meter decay tunnel. If the tunnel length were reduced to 150 meters a savings of \$3 M could be realized at a cost of losing 25% of the neutrino flux with $E_\nu > 2$ GeV.

current muon neutrino events in a detector located at 2540 km will be $\sim$ 12000 in five years running. Table 2 shows the number of different kinds of events we expect in the absence of oscillations. This large statistics combined with the long baseline makes many of the following important measurements possible.

5.1 ν_μ disappearance

The angular distribution of the muons from the quasi-elastic process $\nu_\mu + n \rightarrow \mu^- + p$ produced by the 0^o beam in Fig. 6 was measured in experiment E734 at BNL; it is shown in Fig. 15; the principal background, $\nu_\mu + N \rightarrow \mu^- + N + \pi$ is also shown [17]. A variety of strategies are possible to reduce this background further in a water Cerenkov detector. Knowing the direction of an incident ν_μ accurately and measuring the angle of the observed muon allows the energy of the ν_μ to be calculated, up to Fermi momentum effects. This method is used by the currently running K2K experiment [9]. The known capability of large water Cerenkov detectors indicates that at energies lower than 1 GeV the ν_μ energy resolution will be dominated by Fermi motion and nuclear effects[14]. The contribution to the resolution from water Cerenkov track reconstruction depends on the photo-multiplier tube coverage. With coverage greater than $\sim$ 10%, we expect that the reconstruction resolution should be more that adequate for our purposes [15]. In the following discussion we assume a 10% resolution on the ν_μ energy. This is consistent with the resolution achieved by the K2K experiment.

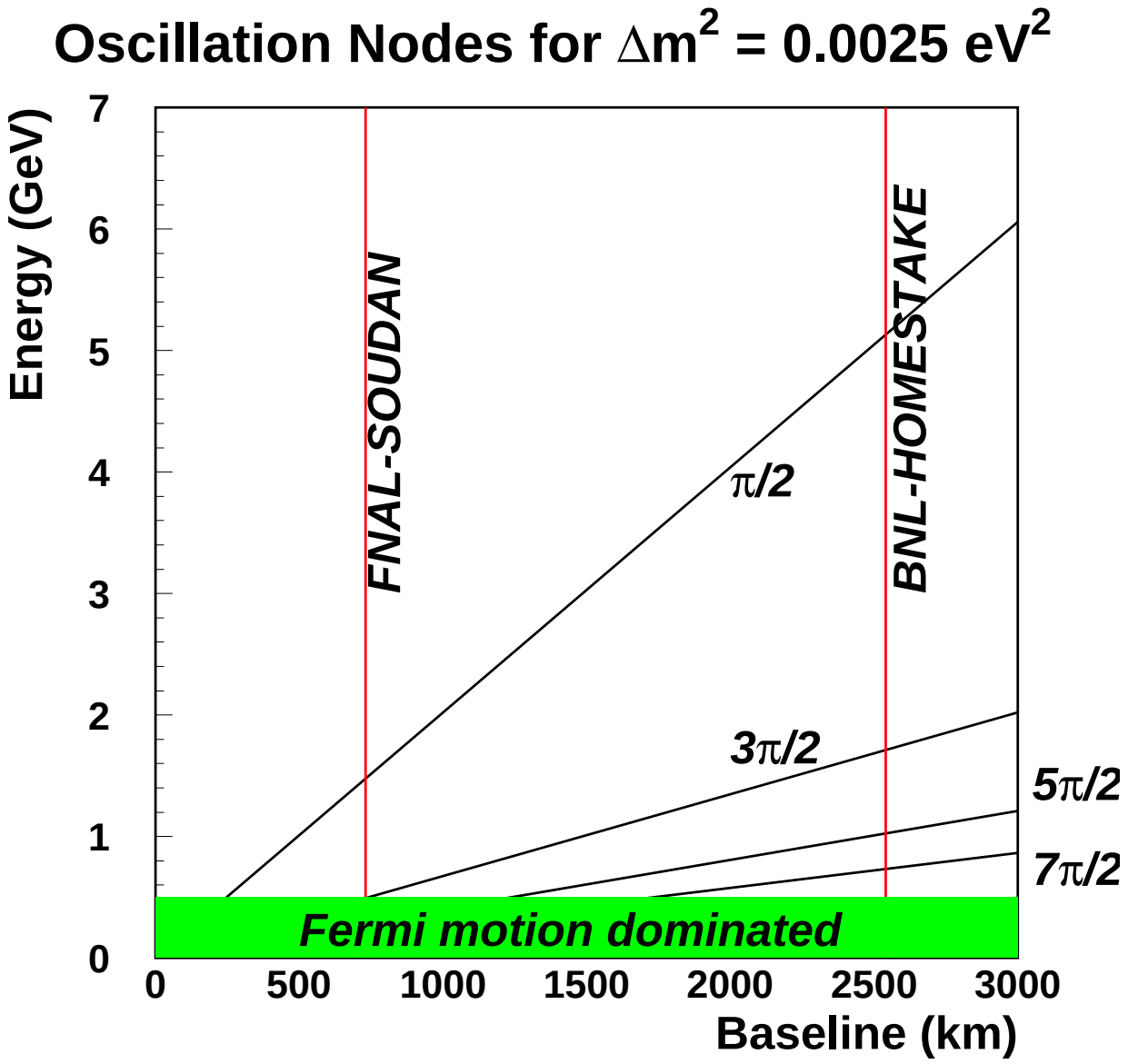

Figure 16: Nodes of neutrino oscillations for disappearance (Not affected by matter effects) as a function of oscillation length and energy for $\Delta m^2_{32} = 0.0025 eV^2$. The distance from FNAL to Soudan (The distance from BNL to Morton salt works is approximately the same[5]) and from BNL to Homestake is shown by the vertical lines.

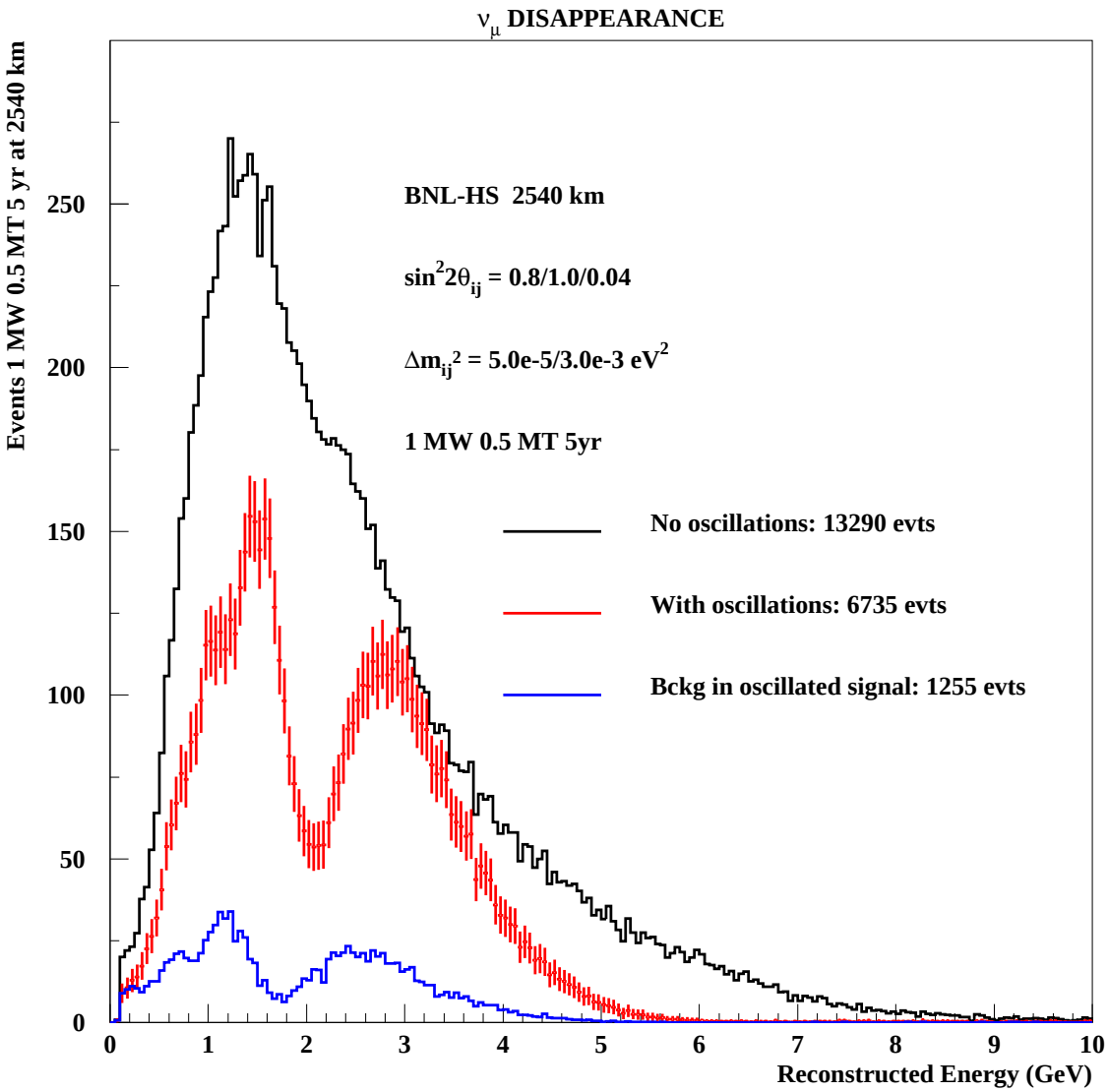

Figure 17: Spectrum of detected events in a 0.5 MT detector at 2540 km from BNL including quasielastic signal and CC-single pion background. We have assumed 1.0 MW of beam power and 5 years of running. The top data points are without oscillations; the middle points are with oscillations and the bottom are the contribution of the background to the oscillated signal only. This plot is for $\Delta m^2_{32} = 0.003 e\mathrm{V}^2$. The error bars correspond to the statistical error expected in the bin. A 10 % detector energy resolution is assumed. At low energies the Fermi movement, which is included in simulation, will dominate the resolution.

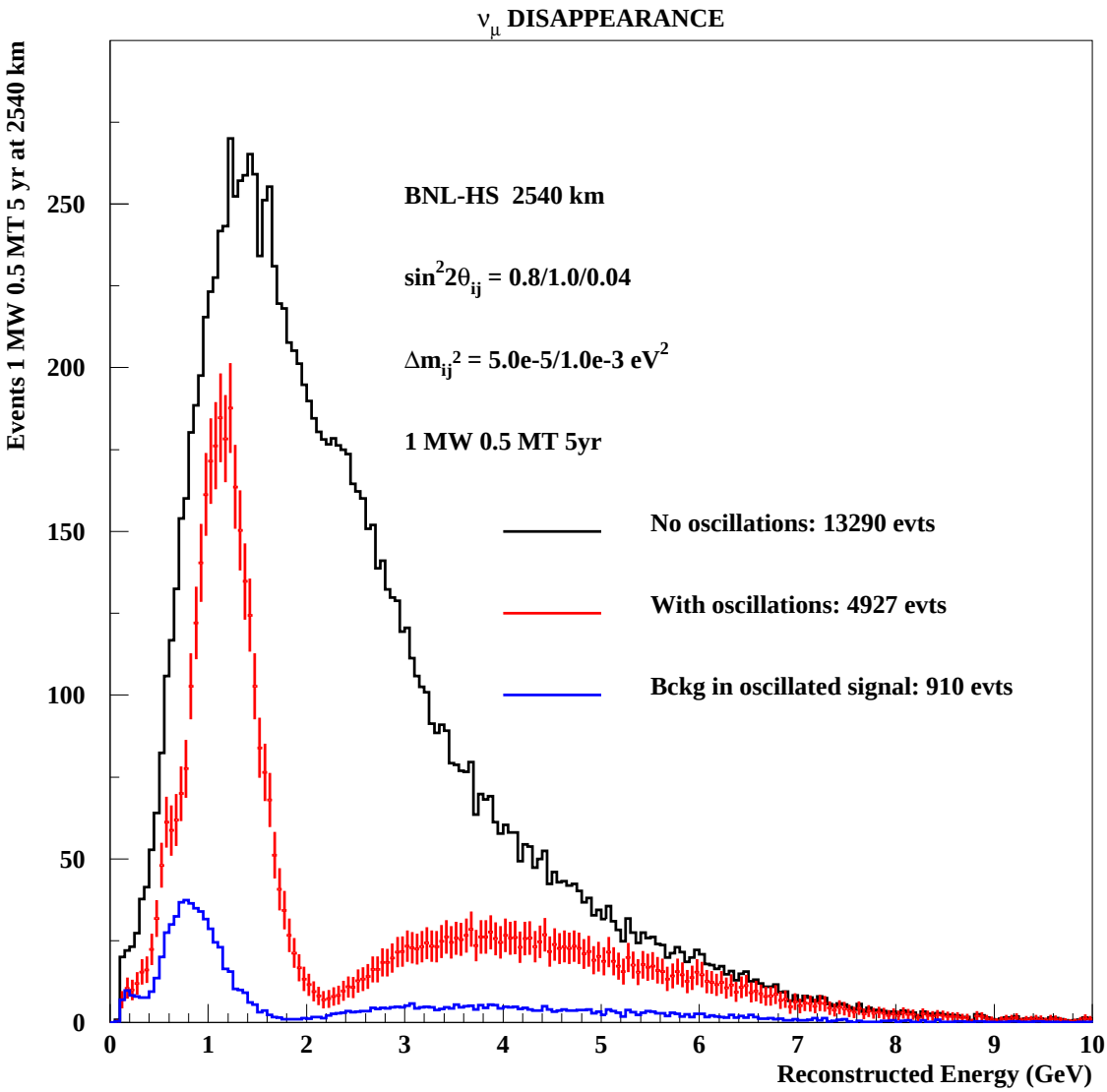

Figure 18: Spectrum of detected events in a 0.5 MT detector at 2540 km from BNL including quasielastic signal and CC-single pion background. We have assumed 1.0 MW of beam power and 5 years of running. The top data points are without oscillations; the middle points are with oscillations and the bottom are the contribution of the background to the oscillated signal only. This plot is for $\Delta m^2_{32} = 0.001 e\mathrm{V}^2$. The error bars correspond to the statistical error expected in the bin. A 10 % detector energy resolution is assumed. At low energies the Fermi movement, which is included in simulation, will dominate the resolution.

Reaction	Number
CC $\nu_\mu + N \to \mu^- + X$	51800
NC $\nu_\mu + N \to \nu_\mu + X$	16908
CC $\nu_e + N \to e^- + X$	380
QE $\nu_\mu + n \to \mu^- + p$	11767
QE $\nu_e + n \to e^- + p$	84
CC $\nu_\mu + N \to \mu^- + \pi^+ + N$	14574
NC $\nu_\mu + N \to \nu_\mu + N + \pi^0$	3178
NC $\nu_\mu + O^{16} \to \nu_\mu + O^{16} + \pi^0$	574
CC $\nu_\tau + N \to \tau^- + X$ (if all $\nu_\mu \to \nu_\tau$)	319

Table 2: Number of events of different types for the very long baseline experiment. The parameters are 1 MW of beam, 0.5 MT of fiducial mass, and 5 years of running with 10^7 seconds of live time each year. As usual, CC, NC, QE, stands for charged current, neutral current, and quasielastic, respectively. The ν_e interaction rate is from the electron neutrino contamination in the beam.

The range of $\Delta m^2_{32} \sim 1.24 \frac{E_\nu[\mathrm{GeV}]}{L[\mathrm{km}]}$ covered by the proposed experiment using the beam in Fig. 7 extends to the low value of about 5×10^{-4} $e\mathrm{V}^2$. The lower end of this extensive range of values is considerably below the corresponding values for other long baseline terrestrial experiments [11, 12]. If the value of Δm^2_{32} turns out to be towards the lower end ($\sim 10^{-3}$) of its current range, or if the value of Δm^2_{21} turns out to be towards its high end ($\sim 10^{-4} e\mathrm{V}^2$), then large and very interesting interference effects in the very long baseline experiment will be possible.

Extra-long neutrino flight paths open the possibility of observing multiple nodes (minimum intensity points) of the neutrino oscillation probability in the disappearance experiment. Observation of one such pattern will for the first time directly demonstrate the oscillatory nature of the flavor changing phenomenon. The nodes occur at distances $L_n = 1.24(2n-1)E_\nu/\Delta m^2_{32}$, $n = 1, 2, 3, \ldots$. In Fig. 16, as an example, we show the flight path L versus E_ν relationship of the nodes for $\Delta m^2 = 0.003\ eV^2$, a value close to the value measured in atmospheric neutrino experiments [4]. An advantage of having a very long baseline is that the multiple node pattern is detectable over a broad range of Δm^2. For Δm^2_{32} as small as 0.001 $e\mathrm{V}^2$, the oscillation effects will be very large.

The two single charged pion reactions $\nu_\mu + p \to \mu^- + p + \pi^+$ and $\nu_\mu + n \to \mu^- + n + \pi^+$

produce a signal which is somewhat larger than the quasi-elastic total in Table 2. For these events, if both the muon and the pion produce more than 50 photoelectrons each, the event can be easily identified as a two ring event in a water Cherenkov detector and rejected. 50 photoelectrons corresponds to about 170 MeV/c (250 MeV/c) for muons (pions) for a detector with 10% photo-multiplier coverage. An additional cut to require the muon to be within 60^o of the neutrino direction reduces the background further. With such a cut, we find that 18% of the events will show one ring (principally the μ^-). The detection of two muon decays, one from the μ^- the other from the decay chain $\pi \to \mu \to e$, could be used to further suppress this background by approximately a factor of 2. More importantly, background events can be tagged by the two muon decays to determine the shape of the background from the data itself. This will greatly increase the confidence in the systematic error due to this background. The reaction $\nu_\mu + n \to \mu^- + p + \pi^0$ (the only allowed CC-π^0 reaction) is $\sim$15% of the total quasi-elastic rate. The momentum distribution of μ^- and π^0 are essentially the same as those for CC-charged pion production. Only 0.5% of the CC-π^0 events will look like quasi-elastic muon events because at least one of the gamma rays from the π^0 decay is usually visible. Thus this background is negligible in the quasi-elastic sample.

The expected plot of signal and background is demonstrated in Figs. 17 and 18, which show the disappearance of muon type neutrino events as a function of neutrino energy measured in quasi-elastic events. The background, which will be mainly charged current, will also oscillate, but the neutrino energy reconstruction will be systematically lower for the background. Nevertheless, the main effect will be to slightly broaden the large dips due to disappearing muon neutrinos.

In figure 19 we show the statistical precision which is expected on the measurement of Δm^2_{12} and $\sin^2 2\theta_{23}$ for several different points in the parameter space. It is clear that since the signal and the statistics are large, the systematic error in fitting the spectrum will dominate the final error. We have listed various effect that must be considered for the measurement with brief comments about each.

- The determination of Δm^2 has a statistical uncertainty of approximately $\pm 0.7\%$ at $\Delta m^2 = 0.0026\ eV^2$ at maximum mixing. It is about $\pm 1.0\%$ when $\sin^2 2\theta_{23} = 0.75$. Clearly the knowledge of the energy scale will be very important in measuring this number. If the energy scale uncertainty is $\delta E/E$ then the final error will be given by

$$(\frac{\sigma(\Delta m^2)}{\Delta m^2})^2 = (\frac{\sigma_{stat}}{\Delta m^2})^2 + (\frac{\delta E}{E})^2$$

  Therefore it will be very important to understand the energy calibration of the detector

to about 1 % for muon energy of $\sim$ 1 GeV. One solution could be a magnetic spectrometer to measure the momentum of cosmic ray muons entering the detector. This consideration could affect the depth at which this detector should be mounted. Another option could be a small linear accelerator that could provide protons or electrons at a rate of few Hz at $\sim$ 100 MeV.

- Even if the overall energy scale is known well, the energy calibration could fluctuate over the entire spectrum. The worst effects of this will be where the spectrum has the maximum slope. This effect will cause additional smearing of the spectrum and reduce the resolution on Δm^2. We assume a 5% fluctuation of the energy calibration over the entire range.

  It should be pointed out that the oscillation minima should be at energies that are in precisely known ratios of integers: 3, 5, 3/5, etc. This could be used to determine the relative energy scale precisely. On the other hand these ratios could be important to determine the presence of new physics (non-sinusoidal depletion of muon neutrinos) in the oscillations.

- The model of Fermi motion and reconstruction resolution will affect both the shape of the signal and the background used in the fit. The consequences of this effect are probably the same as the previous one in terms of the resolution of fitted parameters.

  It was pointed out earlier that some of the the CC-$\pi^{\pm}$ background could be tagged by two muon decays. This sample of events can be used in separate fits to put more constraints on the detector simulations. The large number of charged current events ($\sim$ 52000) that are not quasielastic could also be used in the same manner.

- The statistical uncertainty in the determination of $\sin^2 2\theta_{23}$ is ± 0.016 at $\sin^2 2\theta_{23} = 0.75$ and $\Delta m^2_{23} = 0.0026\ eV^2$. This determination is somewhat better at smaller Δm^2. At maximum mixing Fig. 19 shows that we can determine $\sin^2 2\theta_{23} > 0.99$ at 90% confidence level.

  We expect this error to be even better if proper background subtraction is performed on the data. Normally the determination of this quantity is dependent on the systematic error on the normalization of the flux. However, in the case of very long baseline, the largest part of the sensitivity comes from the shape of the spectrum or how deep the valleys are compared to the peaks (see Fig. 17). Therefore this determination is not affected greatly by the systematic error on the overall normalization. This is demostrated as follows: for $\Delta m^2_{23} = 0.003\ eV^2$, even without background subtraction,

the valleys at $\pi/2$ and $3\pi/2$ have only 2% and 30% of the un-oscillated event rate (see Fig. 17). If will assume the flux normalization error to be 5%, which is consistent with what has been achieved by the K2K experiment[19], then the expected error due to flux normalization on $\sin^2 2\theta_{23}$ is $0.02 \times 0.05 = 0.001$.

- We note that within the paremeter region of interest these should be very little correlation in the determination of Δm^2_{23} and $\sin^2 2\theta_{23}$.

With the assumption on the systematic errors as above we obtain Fig. 20. The systematic errors introduce a small correlation in the Δm^2_{23} vs. $\sin^2 2\theta_{23}$ measurement. The error on the determination of Δm^2_{23} at 0.0026 eV^2 increases to about $\pm 1.2\%$ at maximum mixing, but there is only a small effect on the determination of $\sin^2 2\theta_{23}$. As mentioned before, the energy scale uncertainty must be added in quadrature to the calculated uncertainty on Δm^2_{23}. The precision of this experiment can be compared with the precision expected from MINOS (Fig. 21) and the precision obtained so far from the K2K experiment (Fig. 22. It is expected that K2K will obtain twice as much data; therefore we could naively estimate that the precision on the parameter determination will improve as $1/\sqrt{2}$.

Finally, we note that the flux normalization is usually obtained by placing a detector close to the neutrino source. For example, both K2K and MINOS have large near detectors to determine the flux. Since absolute flux determination is not very important for parameter determination in our case, we can argue that the requirements on a near detector need not be very severe for this measurement. It may not be necessary to build a near detector until sufficient statistics are obtain in the far detector.

5.2 $\nu_\mu \to \nu_e$ appearance

The oscillation of $\nu_\mu \to \nu_e$ is discussed is several recent papers [20, 21, 22]. This oscillation in vacuum is described fully by the following equation:

$$\begin{aligned} P(\nu_\mu \to \nu_e) &= 4(s_2^2 s_3^2 c_3^2 + J_{CP} \sin\Delta_{21}) \sin^2 \frac{\Delta_{31}}{2} \\ &\quad +2(s_1 s_2 s_3 c_1 c_2 c_3^2 \cos\delta - s_1^2 s_2^2 s_3^2 c_3^2) \sin\Delta_{31} \sin\Delta_{21} \\ &\quad +4(s_1^2 c_1^2 c_2^2 c_3^2 + s_1^4 s_2^2 s_3^2 c_3^2 - 2 s_1^3 s_2 s_3 c_1 c_2 c_3^2 \cos\delta - J_{CP} \sin\Delta_{31}) \sin^2 \frac{\Delta_{21}}{2} \\ &\quad +8(s_1 s_2 s_3 c_1 c_2 c_3^2 \cos\delta - s_1^2 s_2^2 s_3^2 c_3^2) \sin^2 \frac{\Delta_{31}}{2} \sin^2 \frac{\Delta_{21}}{2} \end{aligned} \quad (1)$$

where

$$J_{CP} \equiv s_1 s_2 s_3 c_1 c_2 c_3^2 \sin\delta \quad (2)$$

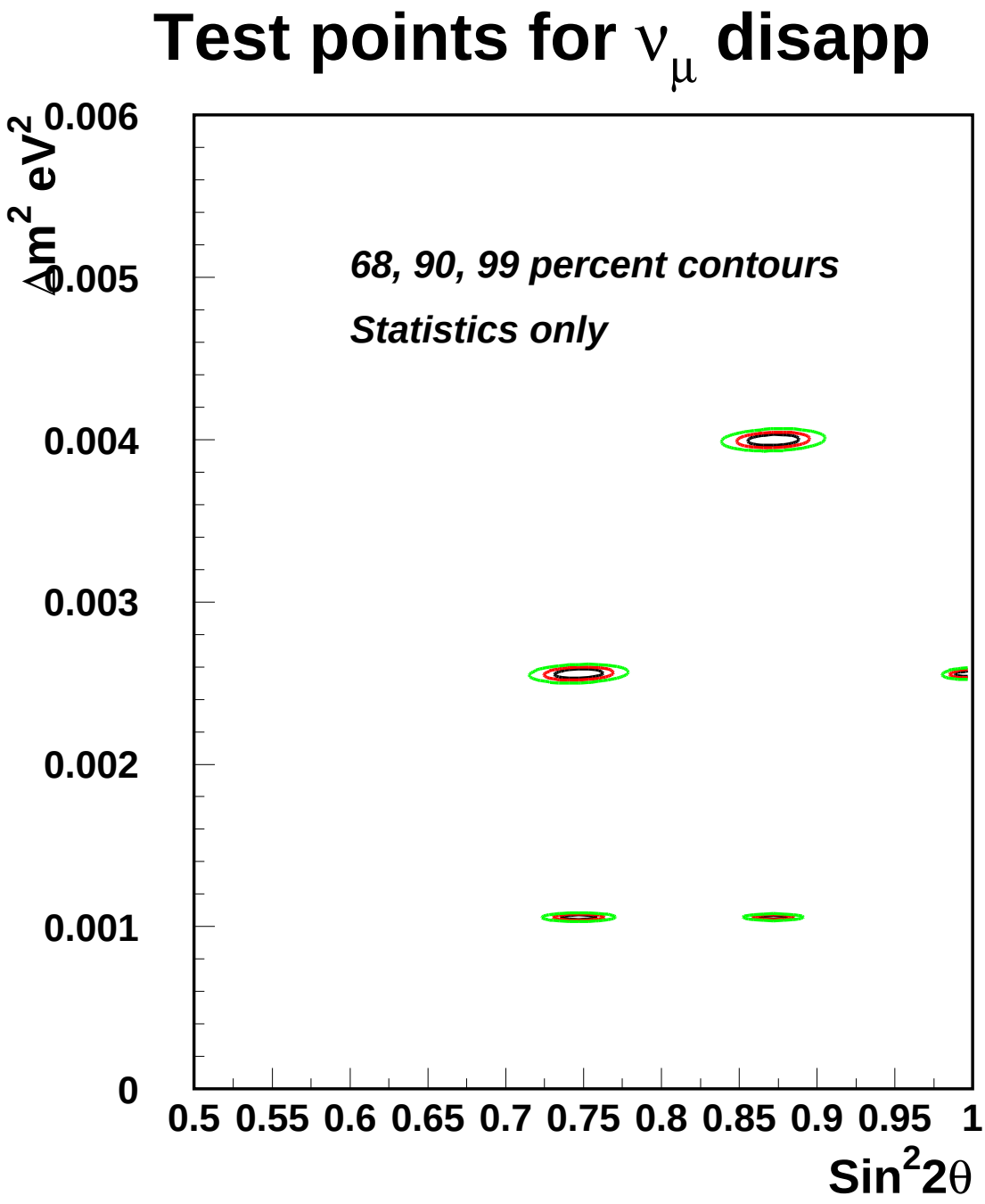

Figure 19: Statistical resolution at 68%, 90% and 99% confidence level on Δm^2_{23} and $\sin^2 2\theta_{23}$ for the 2540 baseline experiment; assuming 1 MW, 0.5 MT, and 5 years of exposure.

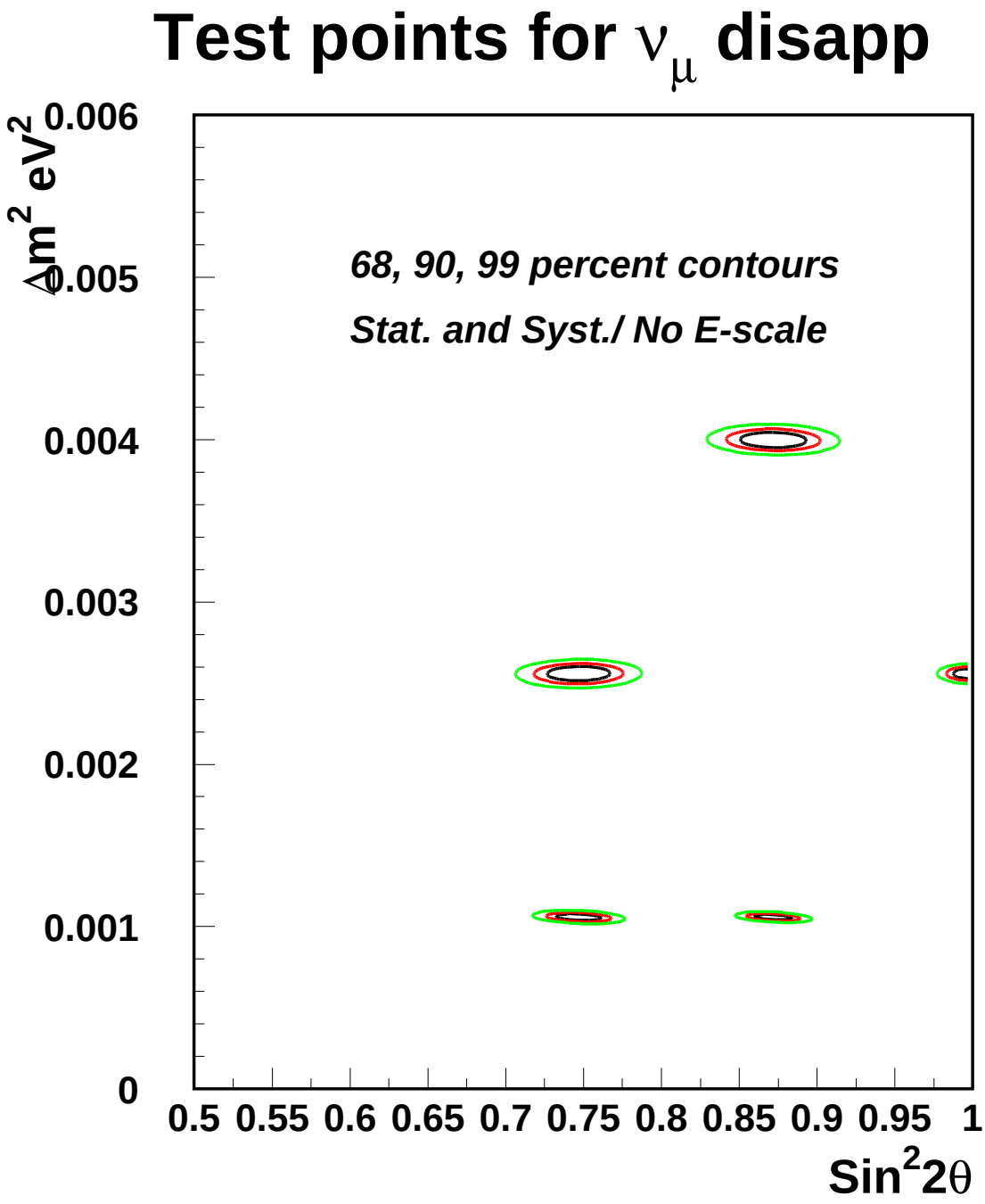

Figure 20: Resolution including statistical and systematic effects at 68%, 90% and 99% confidence level on Δm^2_{23} and $\sin^2 2\theta_{23}$ for the 2540 baseline experiment; assuming 1 MW, 0.5 MT, and 5 years of exposure. We have included a 5% bin-to-bin systematic uncertainty in the energy calibration as well as a 5% systematic uncertainty in the normalization.

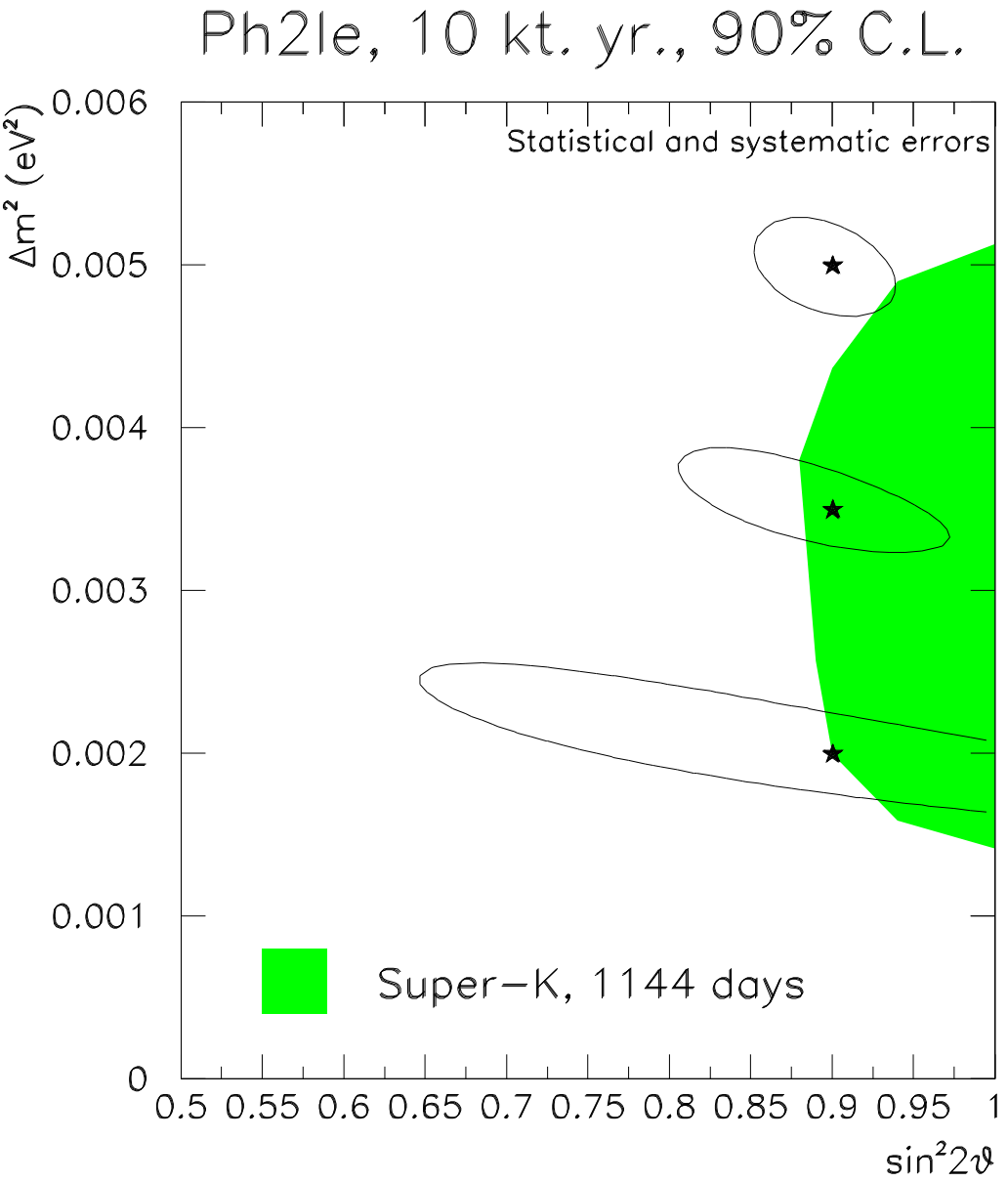

Figure 21: The expected resolution from the MINOS experiment at Fermilab using a low energy beam from the main injector superimposed on the allowed region from Super Kamiokande data.

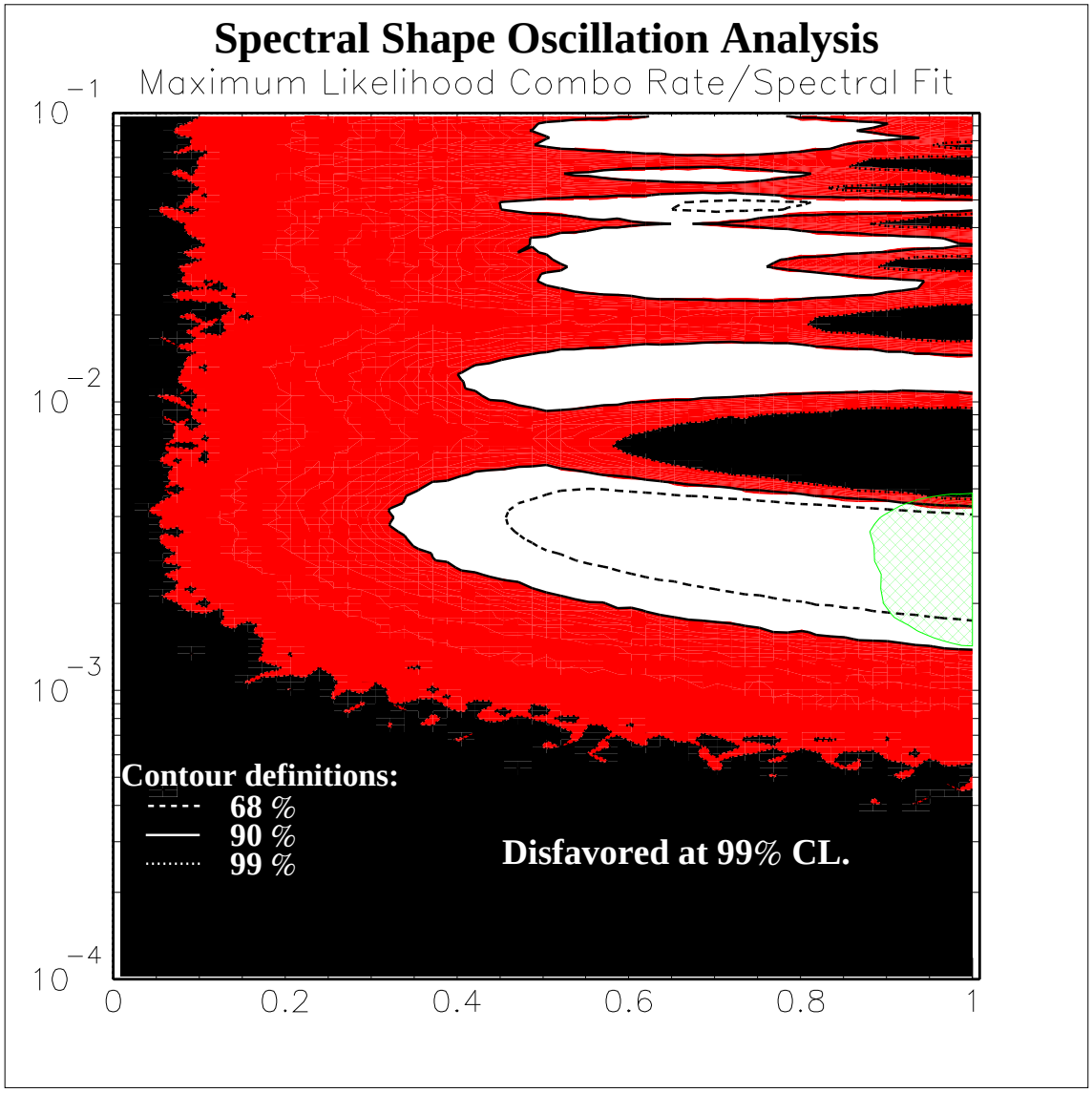

Figure 22: The allowed region from the K2K experiment. From thesis by Eric Sharkey, SUNY at Stony Brook.

J_{CP} is an invariant that quantifies CP violation in the neutrino sector. The formula for $P(\bar{\nu}_\mu \rightarrow \bar{\nu}_e)$ is the same as above except that the J_{CP} terms have opposite sign. Please see attached appendix (hep-ph/0108181) for definitions of symbols but note that Δ_{31} is the atmospheric term and Δ_{21} is the solar term. The vacuum oscillations for a baseline of 2540 km are illustrated in Fig. 23 as a function of energy for both muon and anti-muon neutrinos. The main feature of the oscillation is due to the term linear in $\sin^2 \frac{\Delta_{31}}{2}$. The oscillation probability rises for lower energies due to the terms linear in $\sin^2 \frac{\Delta_{21}}{2}$. The interference terms involve CP violation and they create an asymmetry between neutrinos and anti-neutrinos. The vacuum oscillation formula (Eq.1) and Fig. 23 (The parameters listed in the figure are $\sin^2 2\theta_{12} = 0.8$, $\sin^2 2\theta_{23} = 1.0$, and $\sin^2 2\theta_{13} = 0.04$ and $\Delta m^2_{21} = 5.0 \times 10^{-5} eV^2$, $\Delta m^2_{32} = 0.0026 eV^2$. Similar notation for parameters will be followed in the following plots.) show that the CP asymmetry also grows as $1/E$ in the 0.5-3.0 GeV region. Because of this effect it is argued that the figure of merit for measuring CP violation is independent of the baseline. For very long baselines the statistics for a given size detector at a given energy are poorer by one over the square of the distance, but the CP asymmetry grows linearly in distance [21].

The vacuum oscillation formulation must be modified to include the effect of matter [22]. The $\nu_\mu \rightarrow \nu_e$ probability in the presence of matter is shown in Figs. 24 and 25. When compared to Fig. 23 we can see that matter will enhance (suppress) neutrino (anti-neutrino) conversion at high energies and will also lower (increase) the energy at which the oscillation maximum occurs. The effect is opposite (enhancement for anti-neutrinos and suppression for neutrinos) if the sign of Δm^2_{32} is negative. The matter enhancement effect in neutrino oscillations has been postulated for a long time without experimental confirmation [23]. Detection of such an effect by measuring a large asymmetry between neutrino and anti-neutrino oscillations or by measuring the spectrum of electron neutrinos is a major goal for neutrino physics. This measurement will also yield the sign of Δm^2_{32}.

The Figs. 23 to 25 gives us hints about possible strategies in understanding neutrino oscillation parameters.

In the low energy region from 0 to 1.0 GeV, the probablity for $\nu_\mu \rightarrow \nu_e$ is dominated by the effects of Δm^2_{21} if the solution to the Solar neutrino deficit is the large mixing angle (LMA) solution. An excess of electron like events in this region would be sensitive to Δm^2_{21} and $\sin^2 2\theta_{12}$.

In the intermediate energy region from 1.0 to 3.0 GeV, we see that the CP violating phase δ_{CP} has a large effect on the oscillation probability and the effects of matter are relatively small. Therefore this energy region could be used to measure the CP violating phase δ_{CP}

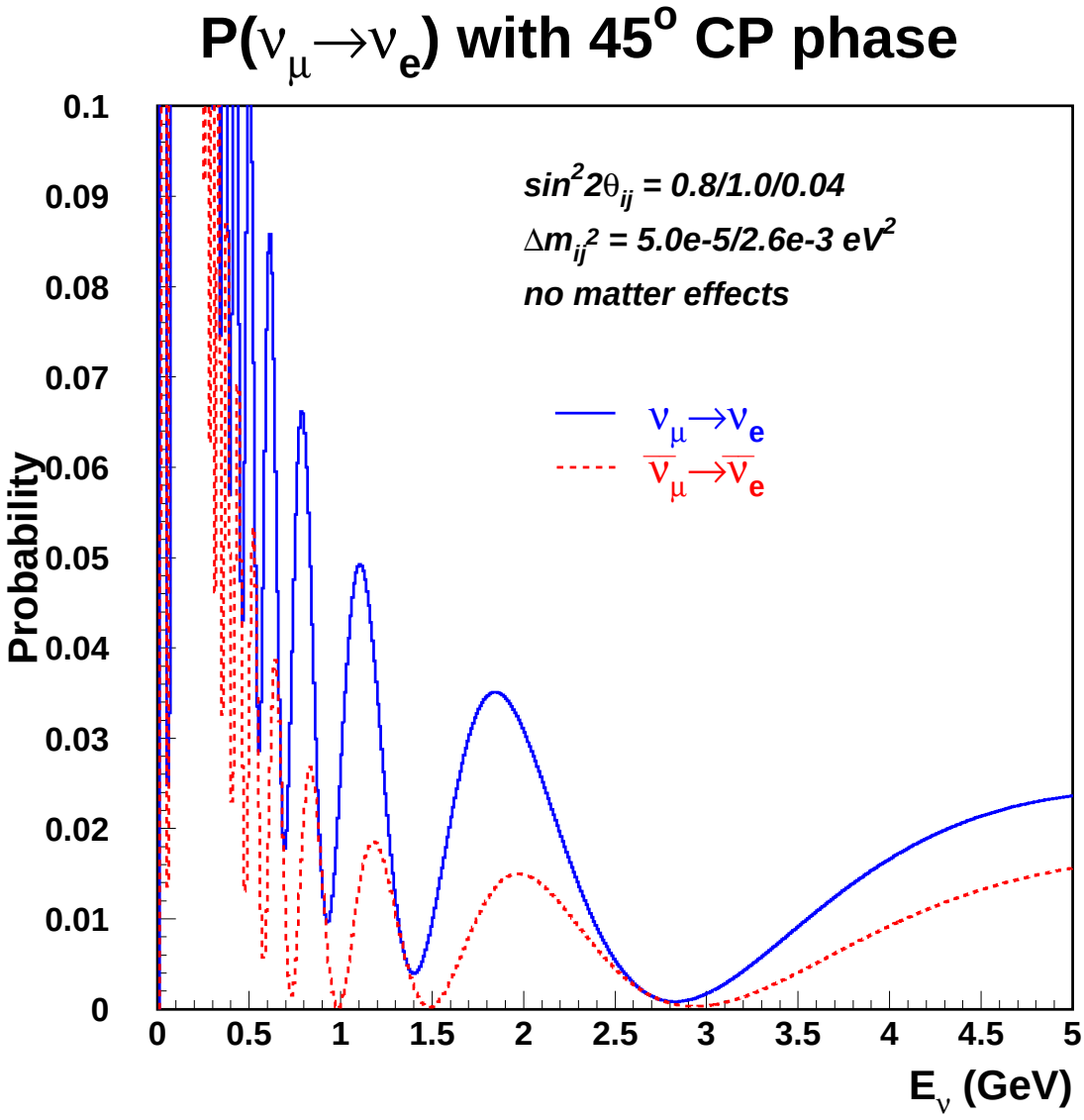

Figure 23: Probability of $\nu_\mu \to \nu_e$ and $\bar{\nu}_\mu \to \bar{\nu}_e$ oscillations at 2540 km in vacuum. assuming a $\delta_{CP} = 45^o$ CP violation phase. It can be seen that the CP asymmetry between ν_μ and $\bar{\nu}_\mu$ increases for lower energies because the CP asymmetry is proportional to $\Delta m^2_{21} L/E$ which increases for lower energies. The parameters listed in the figure are $\sin^2 2\theta_{12} = 0.8$, $\sin^2 2\theta_{23} = 1.0$, and $\sin^2 2\theta_{13} = 0.04$ and $\Delta m^2_{21} = 5.0 \times 10^{-5} eV^2$, $\Delta m^2_{32} = 0.0026 eV^2$.

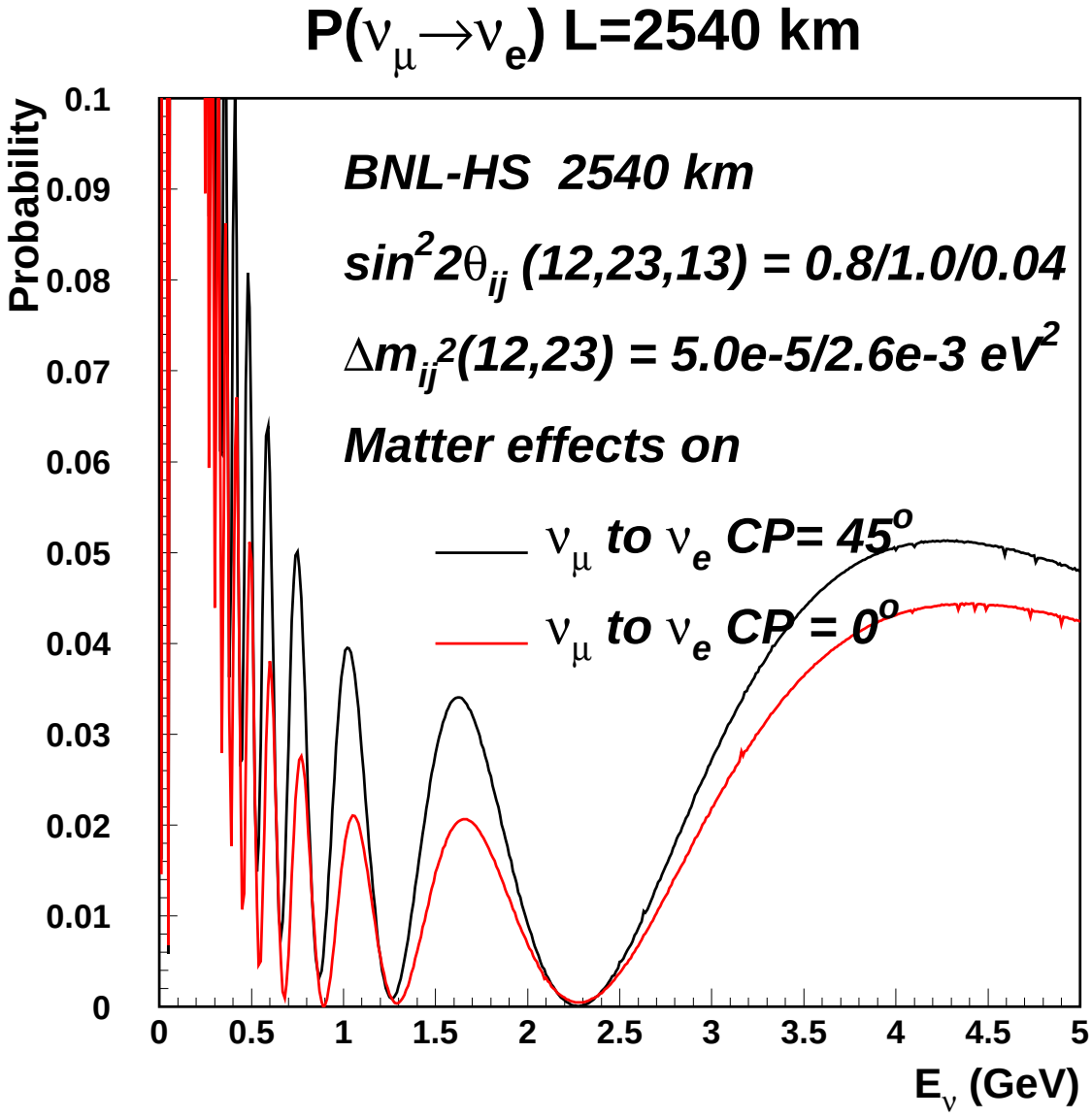

Figure 24: Probability of ν_μ oscillating into ν_e after 2540 km. The parameters assumed are listed in the figures. The upper and lower curves correspond to CP phase angle of 45^o and 0^o respectively. We point out that the effect of CP phase increases for lower energies.

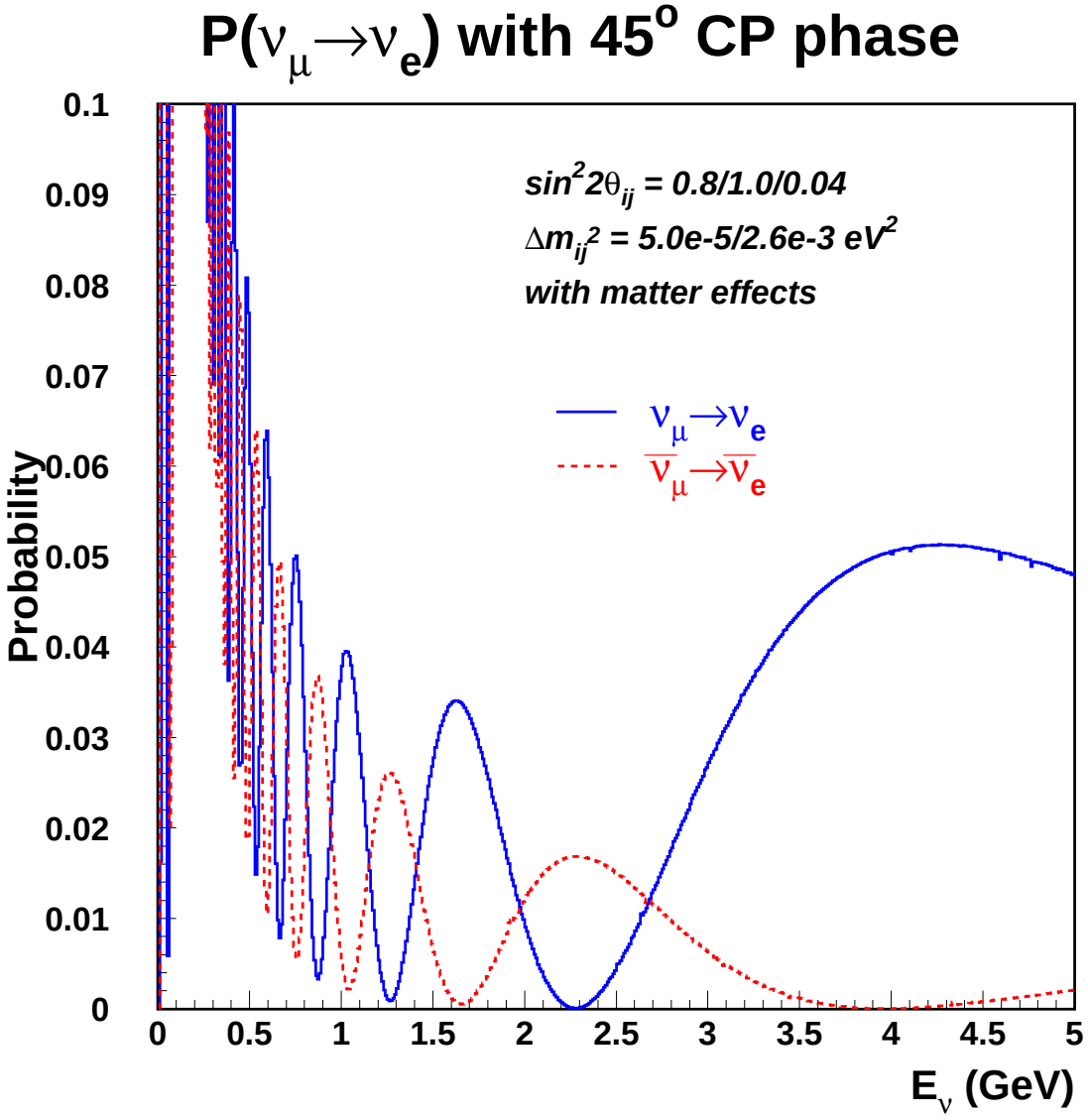

Figure 25: Probability of ν_μ oscillating into ν_e after 2540 km. The parameters assumed are listed in the figures. This plot assumes a CP violation phase of 45^o. The upper and lower curves are for neutrinos and anti-neutrinos, respectively. We see that for distance of 2540 the matter effects will be large and will lead to almost complete reversal of nodes and anti-nodes for neutrinos and anti-neutrinos. The probablity for neutrinos with reversed mass hierarchy will be similar (but not exactly) to anti-neutrinos.

from the observed spectrum of electron like events.

Finally, the higher energy region with energy greater than 3.0 GeV is clearly the region of discovery for $\nu_\mu \to \nu_e$ oscillations as well as the sign of Δm^2_{32}. In the case of the normal mass hierarchy ($m_3 > m_2 > m_1$) the oscillation signal in the high energy region for neutrinos will be enhanced by more than a factor of 2. Moreover, as we will discuss below the backgrounds from both neutral currents and intrinsic ν_e will be falling in this region. Therefore the appearance signal will have a distinctive shape to distinguish it from the background. In the case of the reversed mass hierarchy ($m_2 > m_1 > m_3$) the oscillation signal in the high energy region will be almost completely suppressed. However, there will be a peak between 2 and 3 GeV. If $\sin^2 2\theta_{13}$ is sufficiently large, this will be a clear signature for a reversed mass hierarchy, a very important result in particle physics.

5.3 Backgrounds

While the ν_μ disappearance result will be affected by systematic errors, the $\nu_\mu \to \nu_e$ appearance result will be affected mainly by the backgrounds to the ν_e reactions in the detector. The signal we are looking for a clean single electron events in the detector. The signal will mainly result from the quasielastic reaction $\nu_e + n \to e^- + p$. The main backgrounds will be from neutral current reactions and the intrinsic electron neutrino background. Most of the $\sim$ 17000 neutral current reactions from Tab. 2 are either elaxtic scattering off nuclei or single pion production channels. Out of these the channels that produce single π^0 will be the major source of backgrounds. We estimate that approximately 2000 events will have multiple pions in the final state. We expect that these can be rejected much more effectively than the single π^0 production channels which will have $\sim$ 3700 events (see Tab. 2). This number includes the coherent production channel of $\nu_\mu + O^{16} \to \nu_\mu + O^{16} + \pi^0$. The charged current background channel $\nu_\mu + n \to \mu^- + p + \pi^0$ in which the muon remains invisible was shown to be small in the E889 proposal [15].

For a baseline of 2540 km the matter enhanced oscillation signal will be above 3 GeV. Our strategy for obtaining a unique, clear signal therefore depends on the observation that neutral current background will peak at low energies and fall rapidly as a function of observed energy. This is demonstrated in figures 26 and 27 for the neutral current single pion production channel. In figure 26 we see that the q^2 distribution peaks at low energies and is independent of the neutrino energy. The neutrino energy only determines the physical cutoff of the q^2 distribution. This behavior leads most neutral current events to be at low energies. Fig. 27

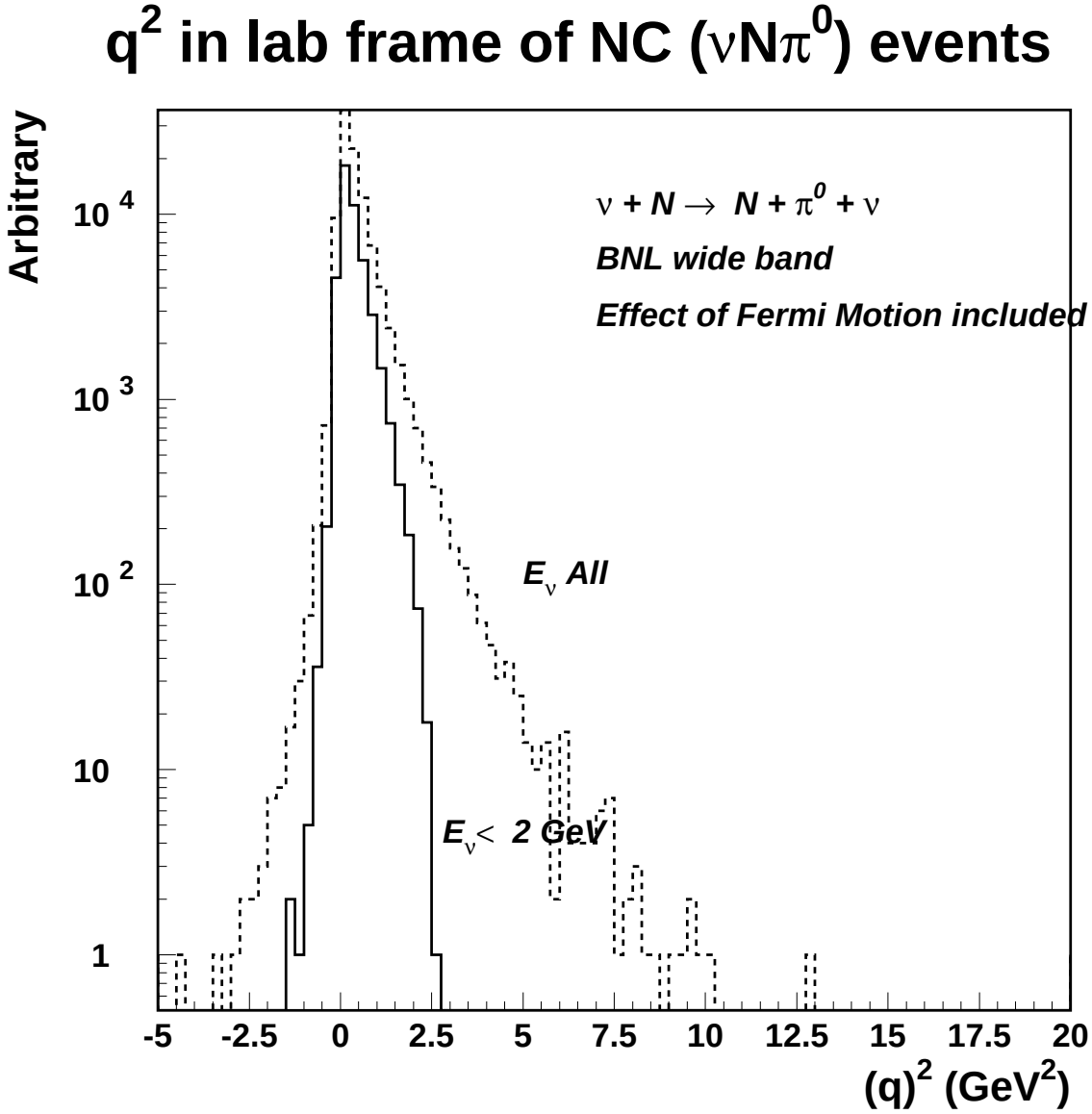

Figure 26: The q^2 distribution of $\nu_\mu + N \to \nu_\mu + N + \pi^0$ channels. Here $q^2 = (p'_N + p'_\pi) - p_N$. p_N is the initial 4 momentum of the target nucleon (assumed to be at rest in the lab frame). p'_N and p'_π are the 4-momenta of the final state nucleaon and pion, respectively. We point out the peak of the distribution is independent of neutrino energy. The neutrino energy only determines the physical cutoff of the q^2 distribution. The slightly negative behaviour of the distribution is caused by the Fermi motion of the target nucleus which was assumed to be at rest in the above formula.

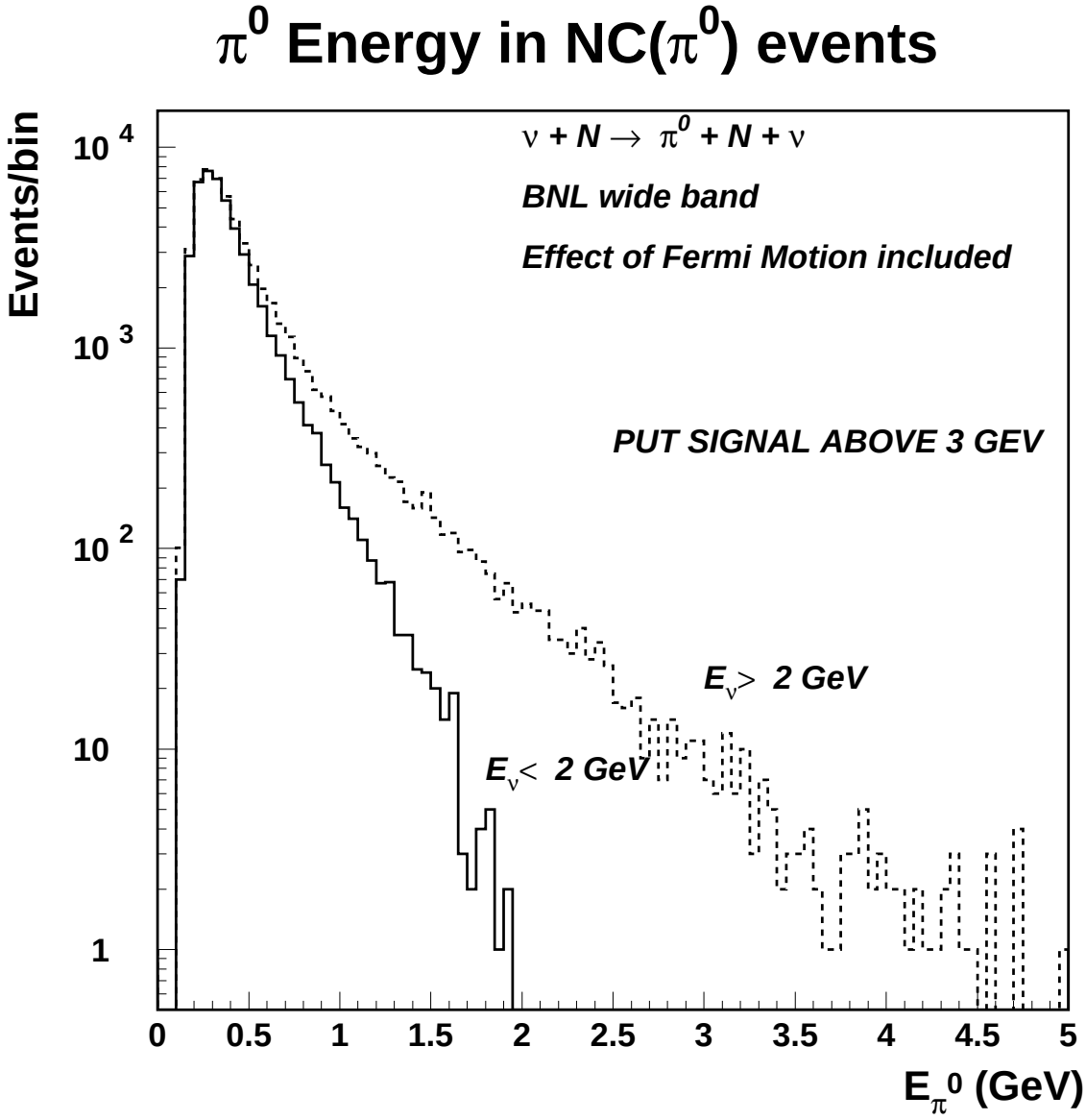

Figure 27: The π^0 energy distribution of $\nu_\mu + N \rightarrow \nu_\mu + N + \pi^0$ channels with no cuts. The peak of the distribution is independent of neutrino energy. The neutrino energy determines the high energy cutoff of the distribution. The distribution is more than 3 orders of magnitude suppressed above 2.5 GeV where we expect the signal from $\nu_\mu \rightarrow \nu_e$ appearance.

shows the distribution of total π^0 energy for single pion production events with no detector cuts. We see that the distribution is more than 3 orders of magnitude suppressed above 2.5 GeV where we expect the signal from $\nu_\mu \rightarrow \nu_e$ appearance (see Fig. 24). Therefore, we propose that even a modest rejection of neutral current background above 2.5 GeV is sufficient to provide us with good sensitivity for $\nu_\mu \rightarrow \nu_e$ appearance. This modest rejection can be obtained by first cutting all events with visible energy less than 500 MeV. Further rejection is obtained by getting rid of events with two showers with energy greated than 150 MeV separated by more than 9 degrees in angle and by cutting events with angle between the shower and the neutrino direction of greater than 60 degrees; this was calculated using a fast Monte Carlo with appropriate angle and energy resolution corresponding to a Water Cerenkov detector. At high energies above 3 GeV a full simulation of a large Water Cerekov detector showed us that it is possible to obtain about a 50% rejection based on the shower shape. The overall rate of π^0 misidentification is shown in figure 28. It should be noted that the advantage of the very long baseline is in applying a simple cut on the total visble energy to eliminate most of the background. The rate of π^0 misidentification for neutral current events (Fig. 27) above 500 MeV is 6%. The efficiency for electrons is shown on the right hand side of Fig. 28. The electron efficiency for quasielatic electron neutrino events is 64% at energy less than 1.5 GeV. Above 1.5 GeV the efficiency is 90%. Using appropriate resolution and efficiency factors we obtain the predicted background spectrum of electron like showering events in Fig. 29. The reconstructed electron energy and the angle of the electron with respect to the neutrino direction is used to recontruct the neutrino energy assuming a quasielastic scattering event. This figure includes backgrounds from the neutral current single π^0 production off nucleaon as well as coherent π^0 production off O^{16}, which has much more energetic spectrum. The spectrum also includes the background from instrinsic beam-ν_e contamination in the beam.

The predicted number of total background events is 146 with the intrinsic beam-ν_e contamination accounting for 70 events. It should be remarked that above 2 GeV the background is dominated by the beam-ν_e contamination: there are 35 ν_e events versus 17 π^0 events. This is despite the rather poor rejection of NCπ^0 events at high energies. Below 2 GeV the background will be dominated by the NCπ^0 events: with 35 ν_e events and 59 π^0 events. Therefore any error in determination of the NCπ^0 background including contamination from other neutral current background channels (which will have similar energy dependence) will not significantly affect the high energy region above 2 GeV where we expect to see a distinct signal for electron enutrino appearance.

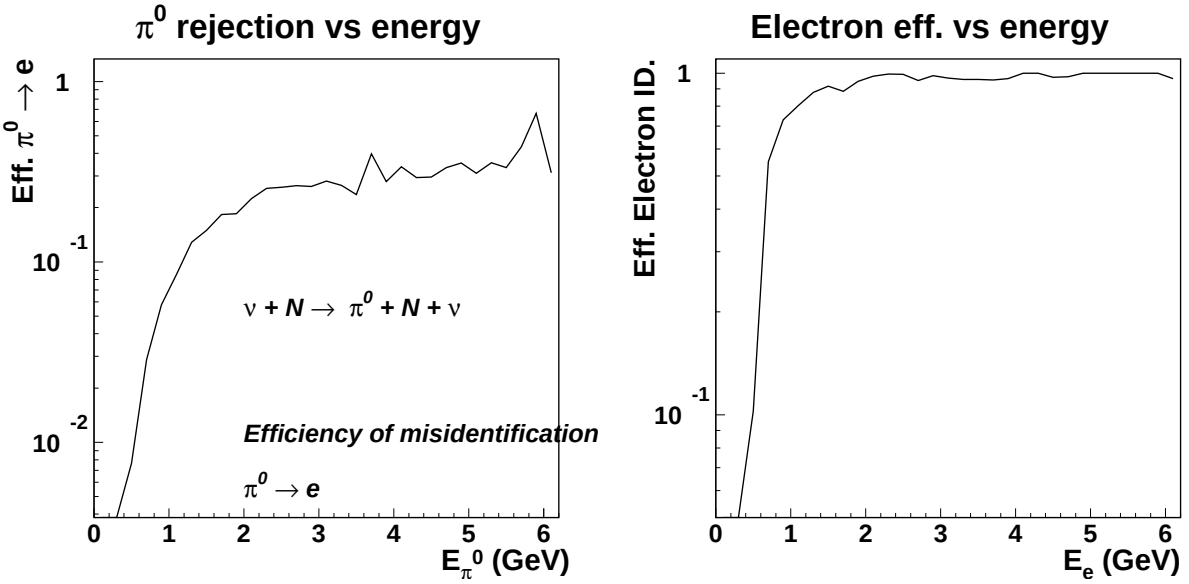

Figure 28: On the left: the rate of misidentification of π^0 events as electrons versus total π^0 energy for the calculations in this paper. On the right: electron efficiency used in this calcualation.

5.4 Sensitivity to $\sin^2 2\theta_{13}$

Figures **??**, **??** and **??** show the spectrum of electron type neutrinos that will be detected at 2540 km. The signal for $\sin^2 2\theta_{13} \sim 0.04$ will be about 100 events. The background for this signal will come from the intrinsic contamination of ν_e particles in the beam as well as neutral current events producing π^0s. This background will be examined in detail in a future update to this proposal. From past experience using this beam, we expect that the total background in the signal region can be reduced to about 0.5% of the charged current muon neutrino events. The advantages of the very long baseline are in obtaining a large enhancement at higher energies and creating a nodal pattern in the appearance spectrum. Both of these can be used to further improve the sensitivity of the experiment. The very long baseline experiment has a great advantage if Δm^2_{21} is found to be somewhat larger within its allowed range $(2-10)\times 10^{-5} e\mathrm{V}^2$. This is shown in Fig. **??**. The differences in the electron neutrino spectra are striking within Figs. **??** and **??**,**??**.

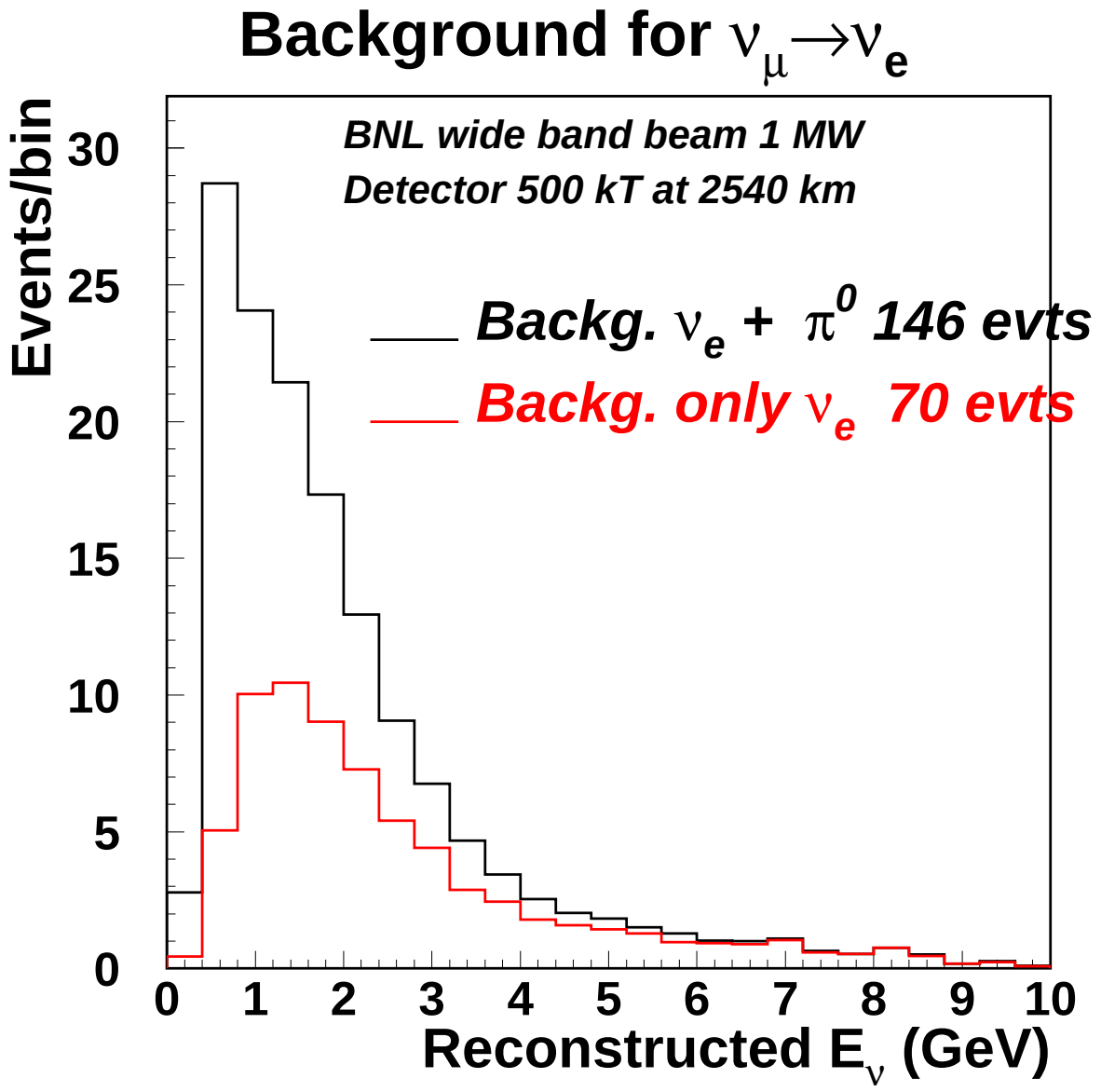

Figure 29: Spectrum in reconstructed electron neutrino energy (assuming quasielastic events) of the background for $\nu_\mu \rightarrow \nu_e$ search. This is for 1 MW beam power, 0.5 MT detectors mass and 5×10^7 sec of running. The top histogram includes both the NC-π^0 and electron contamination backgrounds. The electron neutrino contamination is also shown separately.

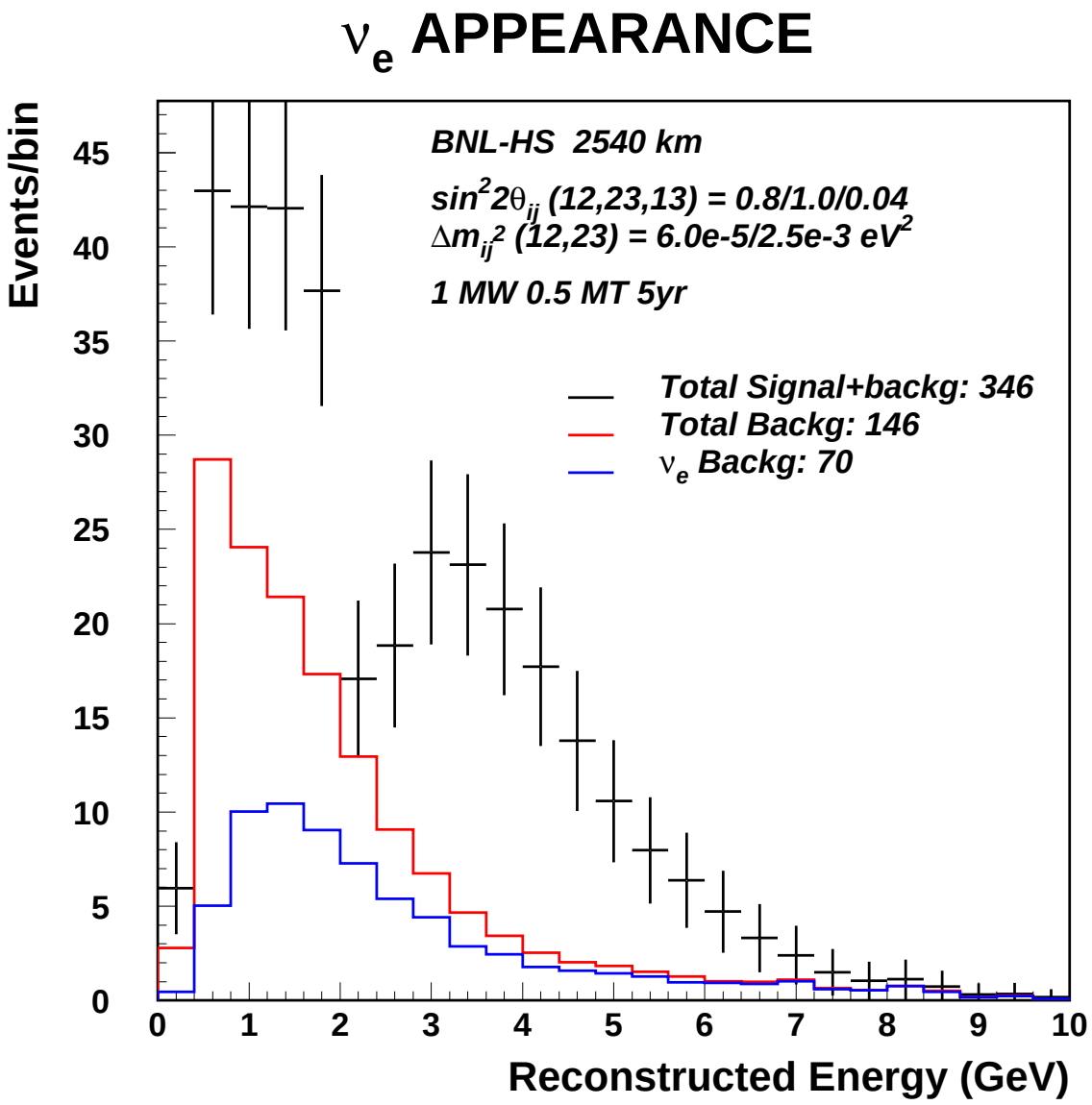

Figure 30: Spectrum of detected quasi-elastic electron neutrino charged current events in a 0.5 MT detector at 2540 km from BNL. We have assumed 0.5 MW of beam power and 5 years of running. This plot is for $\Delta m^2_{32} = 0.0026 eV^2$. We have assumed $\sin^2 2\theta_{13} = 0.04$ and $\Delta m^2_{21} = 5 \times 10^{-5} eV^2$. The error bars correspond to the statistical error expected in the bin. A 10 % energy resolution is assumed; this corresponds to the expected resolution due to both nuclear effects and the electron momentum reconstruction in the detector.

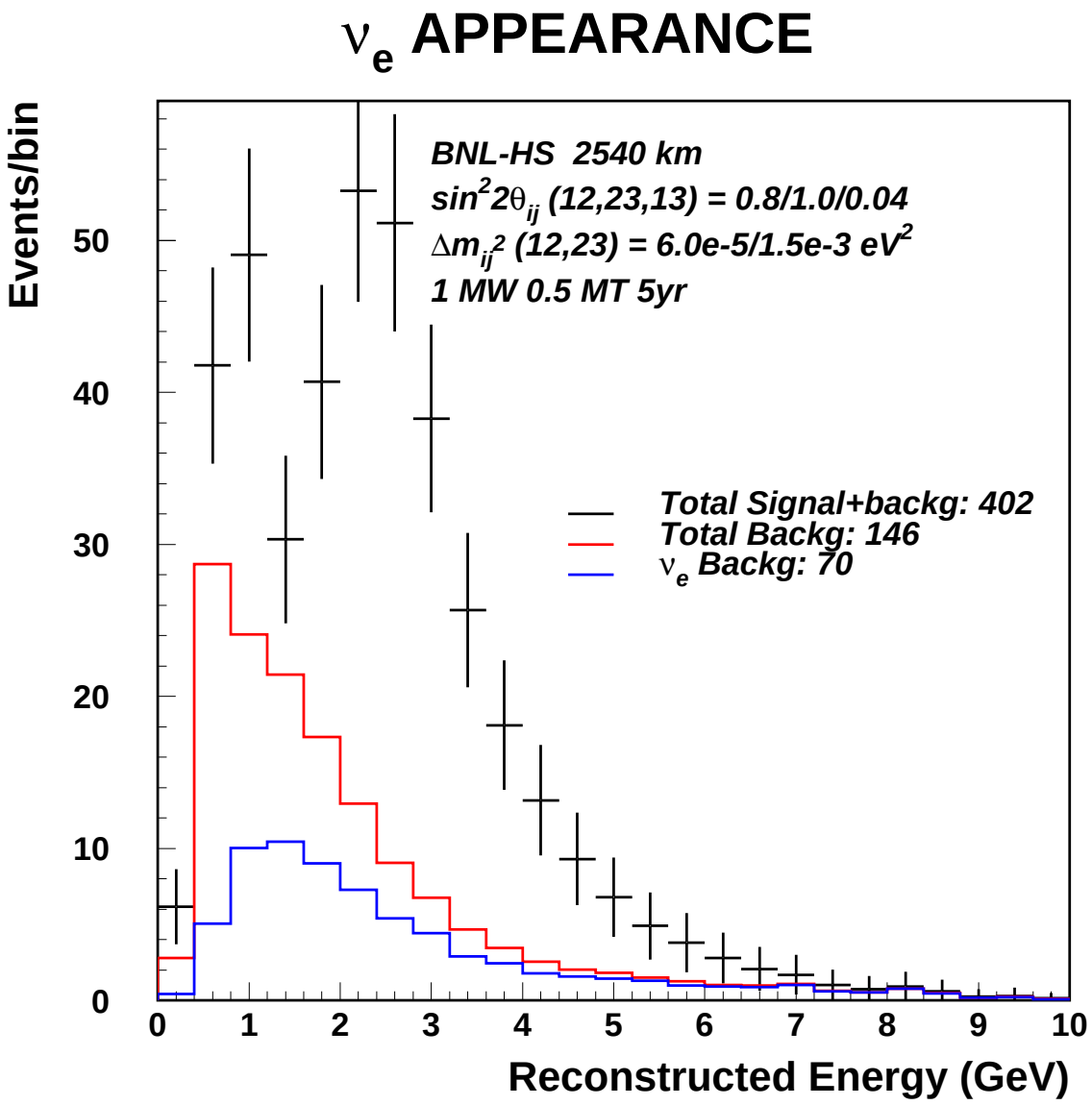

Figure 31: Spectrum of detected quasi-elastic electron neutrino charged current events in a 0.5 MT detector at 2540 km from BNL. We have assumed 0.5 MW of beam power and 5 years of running. This plot is for $\Delta m^2_{32} = 0.0015 e\mathrm{V}^2$. We have assumed $\sin^2 2\theta_{13} = 0.04$ and $\Delta m^2_{21} = 5 \times 10^{-5} e\mathrm{V}^2$. The error bars correspond to the statistical error expected in the bin. A 10 % energy resolution is assumed; this corresponds to the expected resolution due to both nuclear effects and the electron momentum reconstruction in the detector.

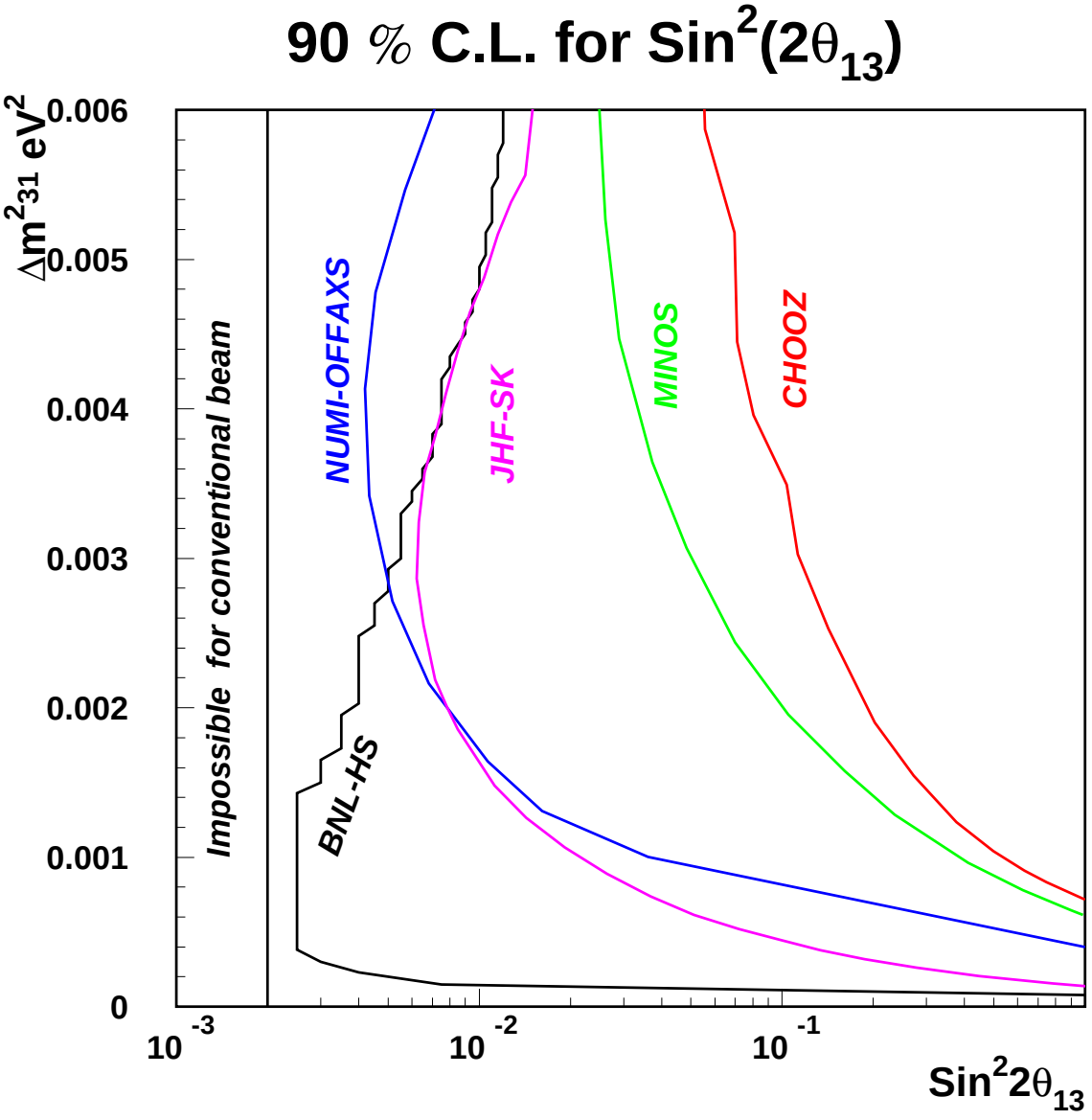

Figure 32: something

5.5 Sensitivity to mass hierarchy

5.6 Sensitivity to CP violation parameter

To understand CP violation, the effect of matter enhancement must be clearly understood and subtracted from any observation. If CP violation is large and the signal to $\nu_\mu \rightarrow \nu_e$ is also large then it is possible to measure CP violation with just the (ν_μ) neutrino beam. As shown in Fig. 23 the effects of CP violation grow linearly as energy is decreased (or the baseline increased). For a very long baseline experiment it is possible to compare the signal strength in the $\pi/2$ node versus the $3\pi/2$ or higher nodes. Such a comparison will yield a measurement of CP violation. Any such measurement of CP must be augmented by data using a muon anti-neutrino beam. Such a program of measurements will require large statistics. This proposal has the flexibility to obtain much larger data sets because the detector will eventually be upgraded to its final configuration with 1 MT of mass and the AGS accelerator complex can be upgraded up to 2.5 MW of beam power. It is also possible that the conventional neutrino beam which we propose here will be replaced by a neutrino factory based on a muon storage ring [24].

5.7 Sensitivity to Δm^2_{21}

5.8 Experimental program

5.9 Detectors for the very long baseline experiment

The conversion of Homestake Gold Mine in Lead, South Dakota, into the National Underground Science Laboratory (NUSL), tentatively to take place in 2002, will provide a unique opportunity for a program of extra-long baseline neutrino oscillation experiments. As explained above these will be possible because of the length of the baseline, 2540 km from the Brookhaven National Laboratory (BNL) to Lead, South Dakota. It is proposed that the NUSL facility will accommodate an array of detectors with total mass approaching 1 Megaton. Most of these will be water Cerenkov detectors that can observe neutrino interactions in the desired energy range with sufficient energy and time resolution [39]. Details of underground construction of these detectors is in Appendix II.

An alternative to Homestake also exists at the Waste Isolation Pilot Plant (WIPP) located in an ancient salt bed at a depth of $\sim 700m$ near Carlsbad, New Mexico. One advantage

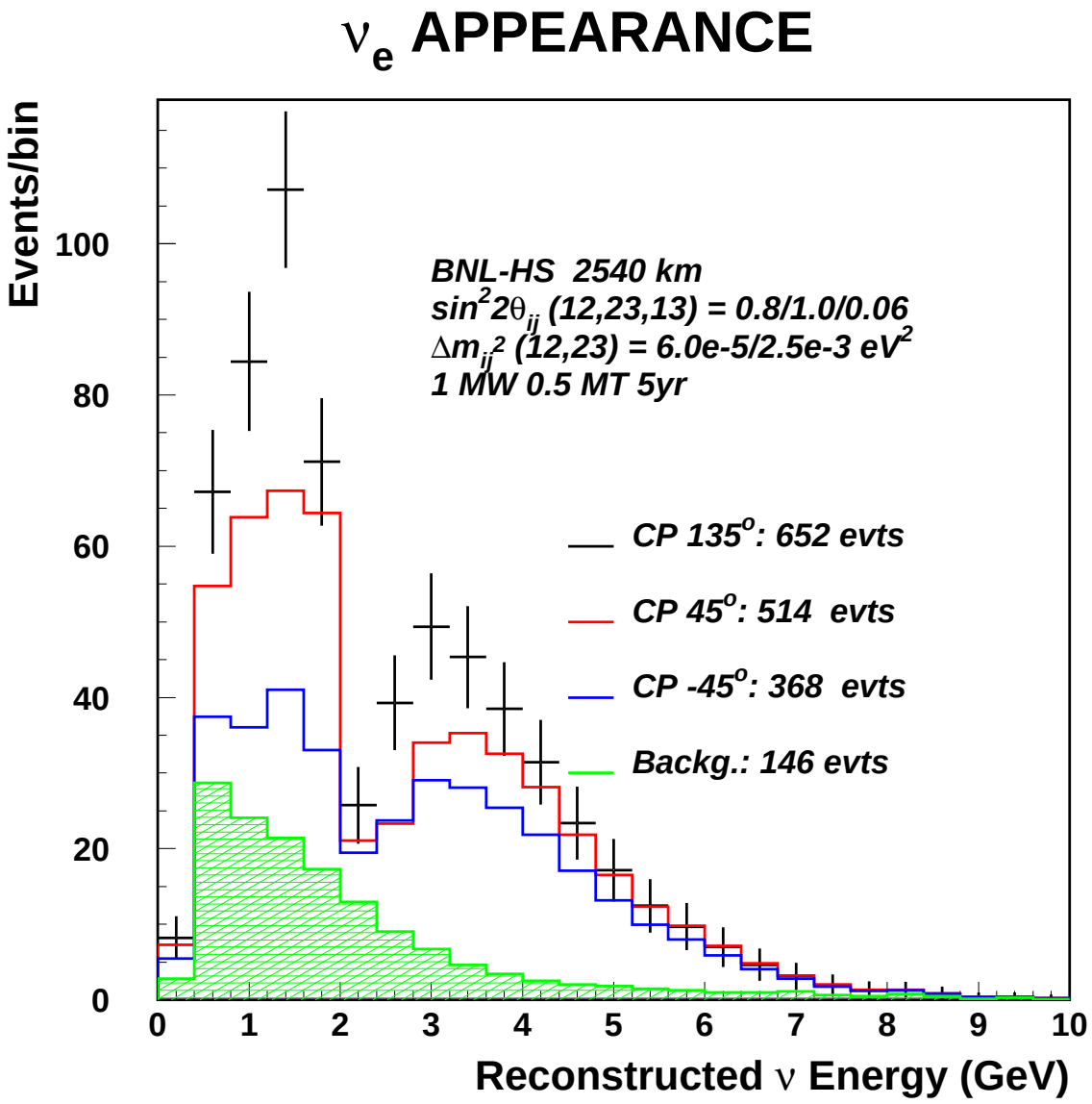

Figure 33: something

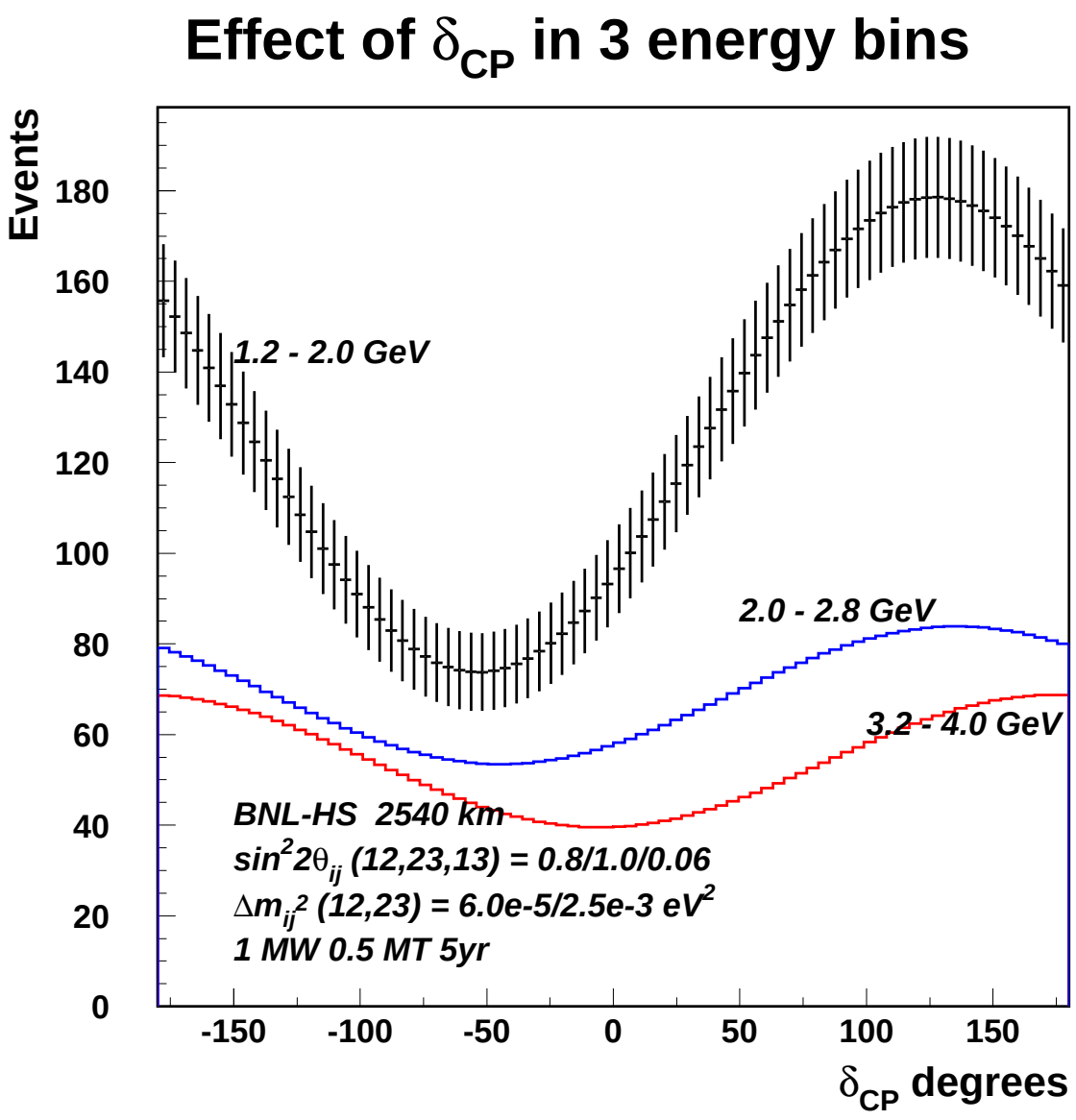

Figure 34: something

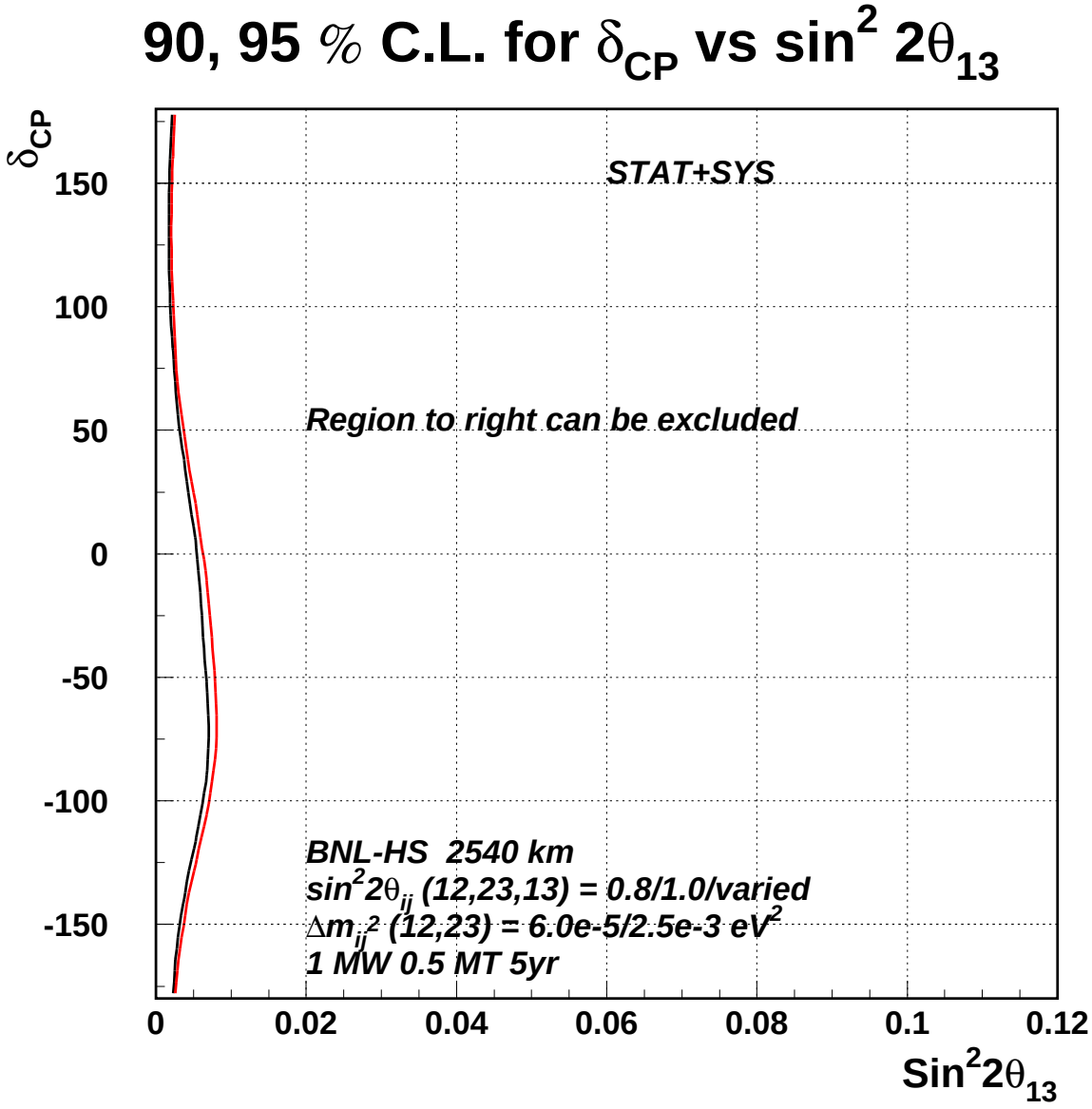

Figure 35: something

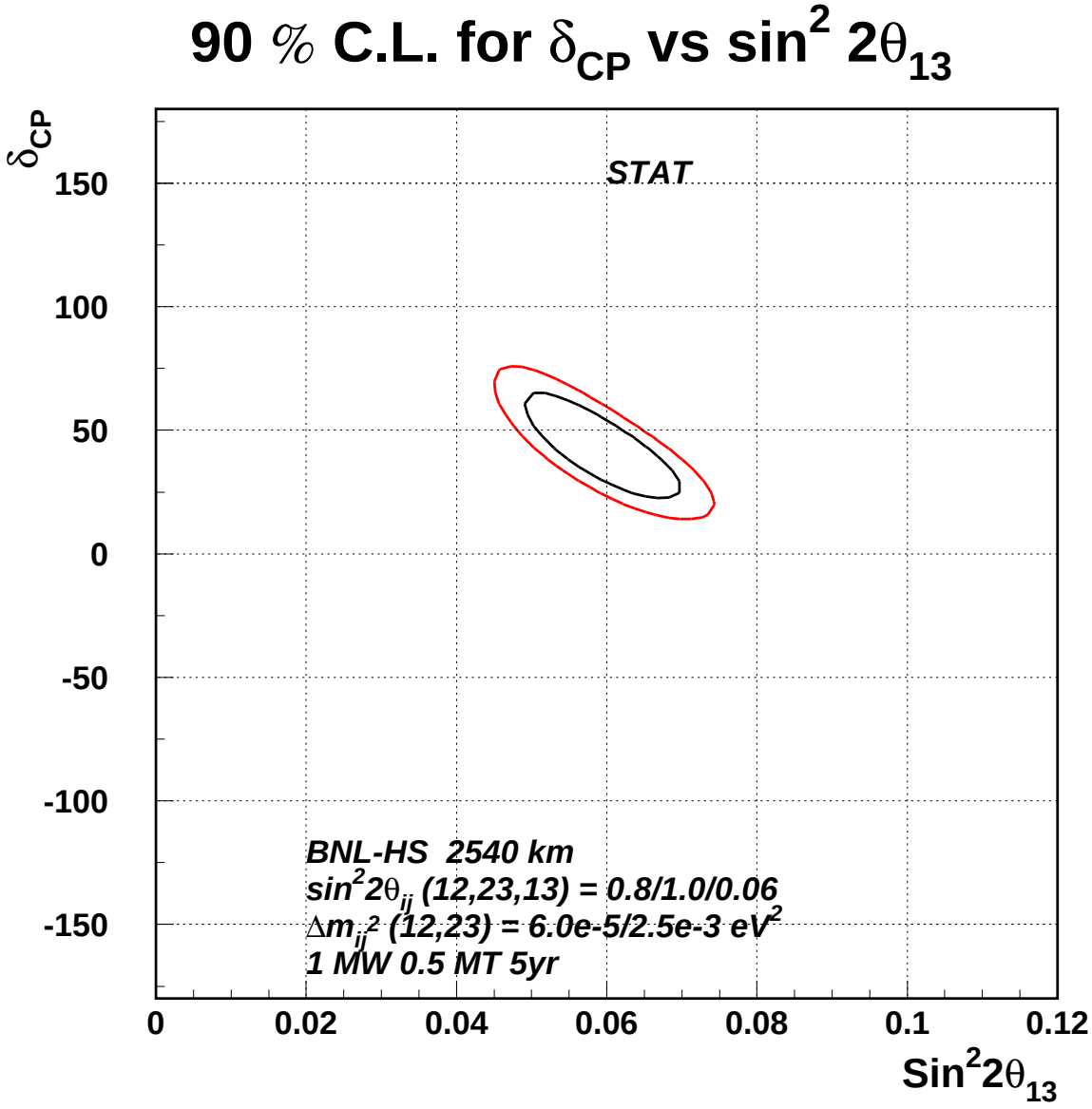

Figure 36: something

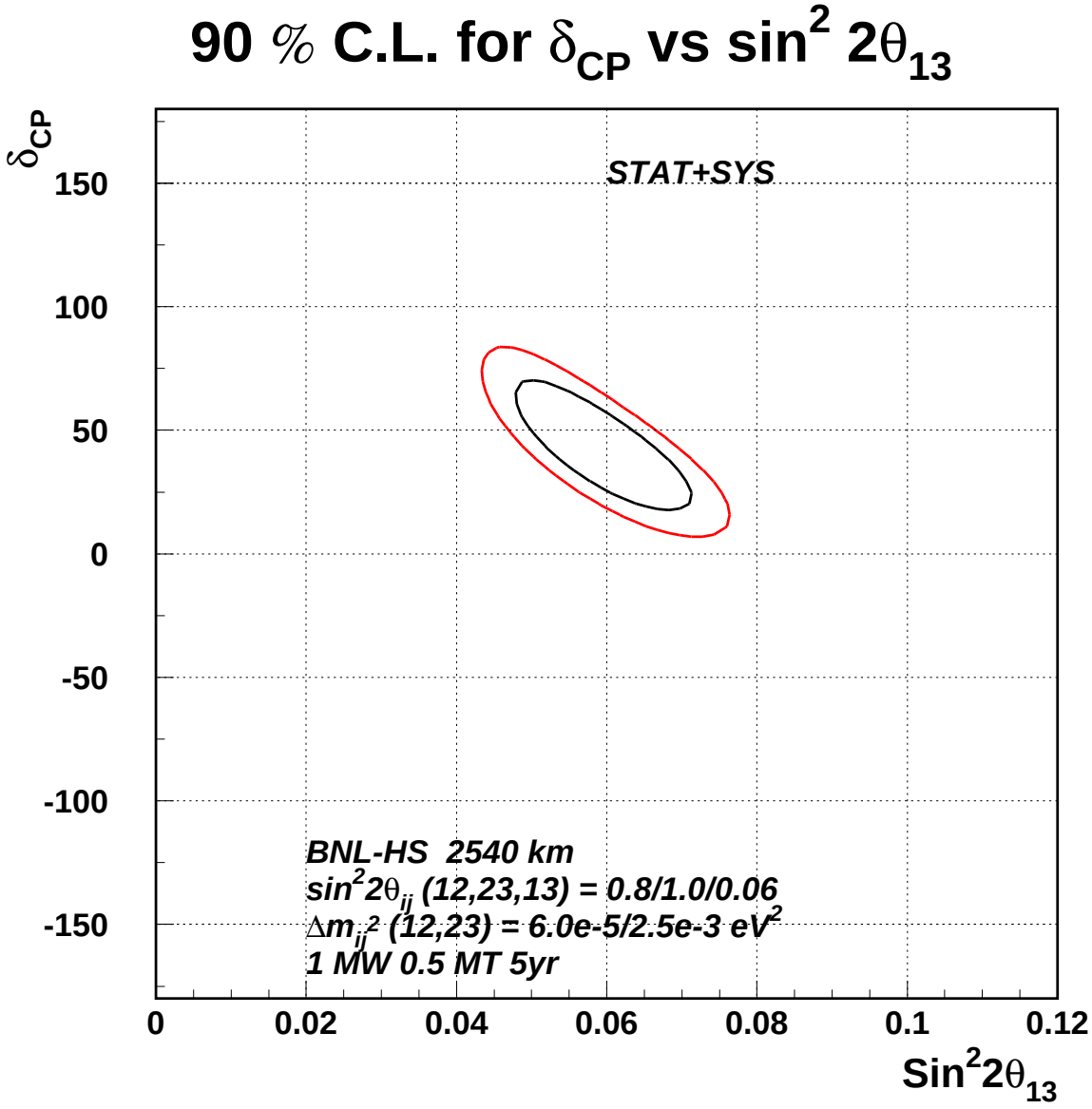

Figure 37: something

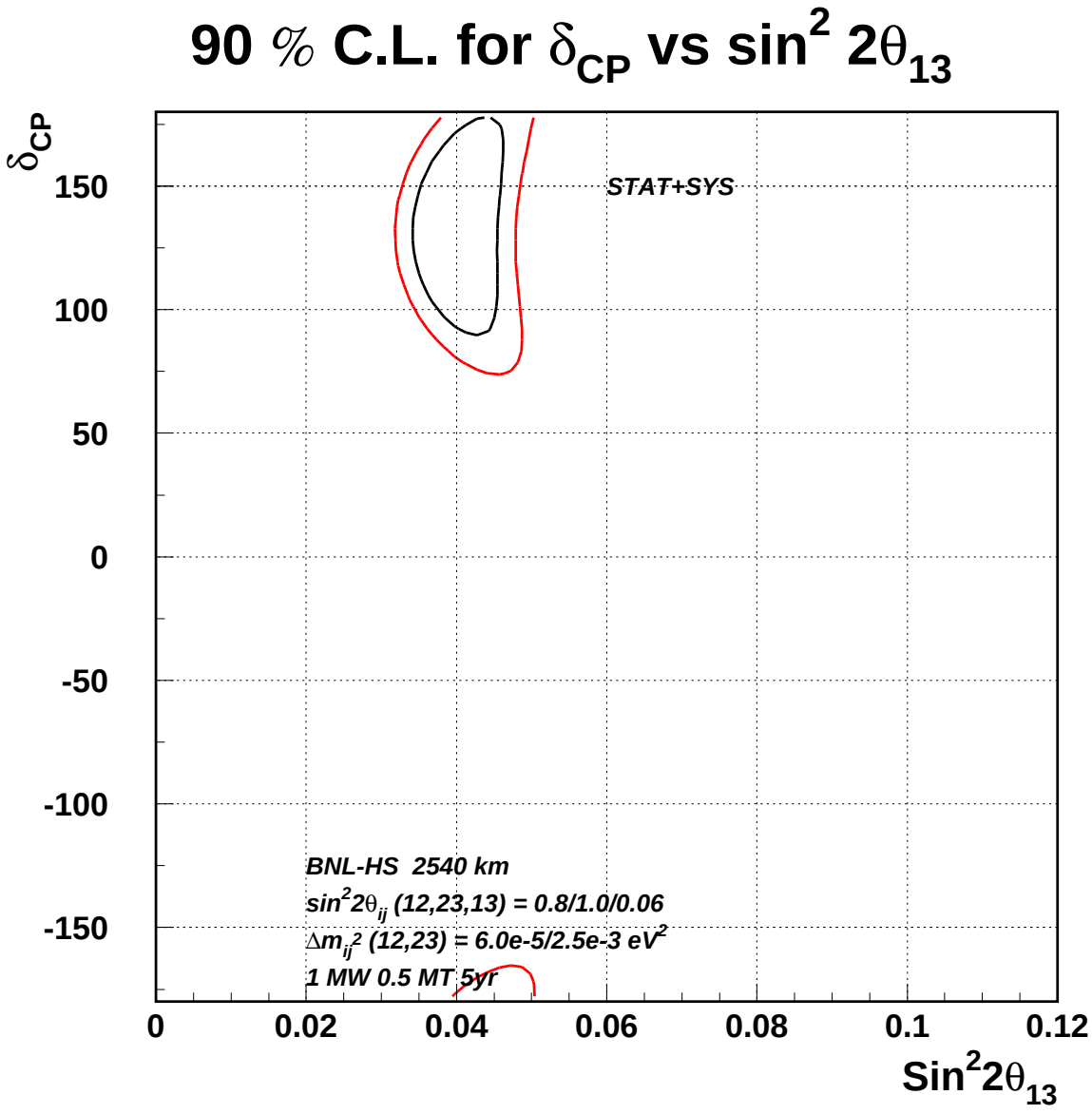

Figure 38: something

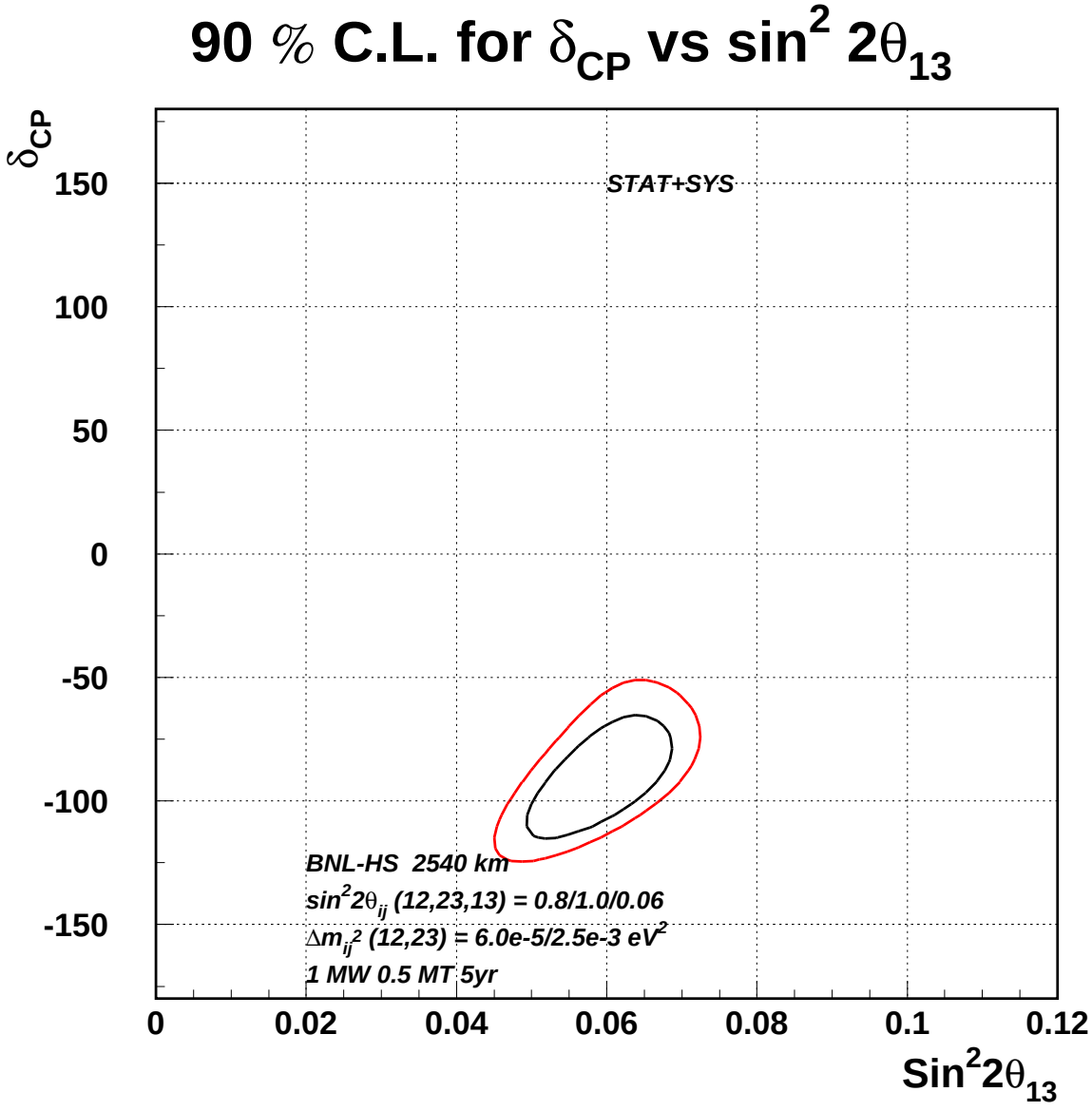

Figure 39: something

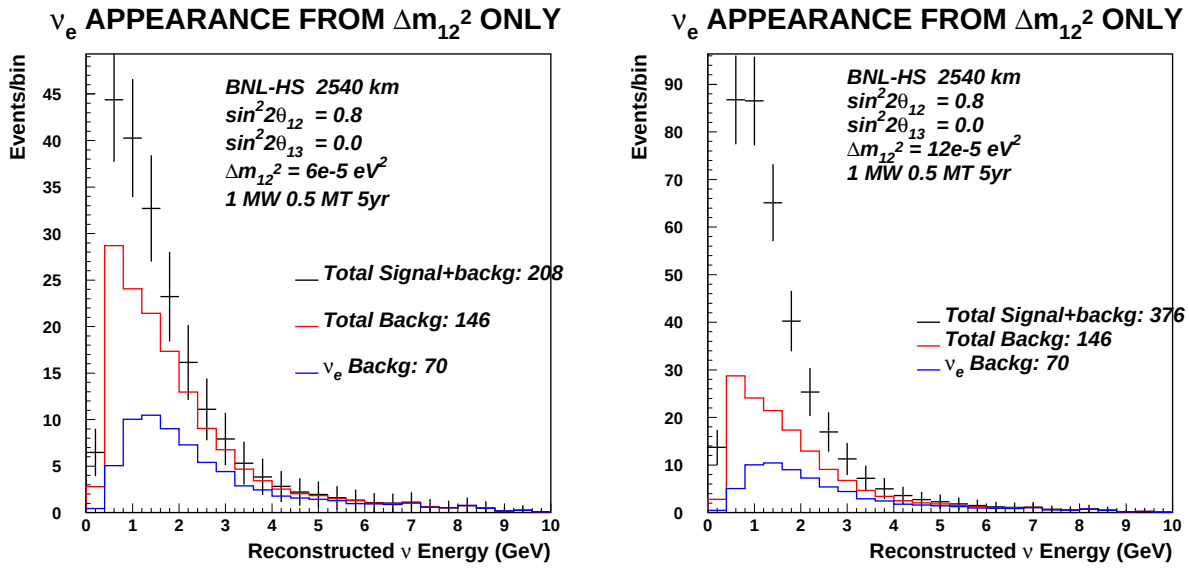

Figure 40: something

of the WIPP site is that, it is owned by the DOE and now has a program of underground science. We note that the recent Neutrino Factory Study [24] at BNL identified the WIPP site as one possible location for a far detector, and the current BNL neutrino beam could use the same concept. The distance from BNL to WIPP is about 2880 km. The cosmic ray background will be higher at WIPP because the facility is not as deep as Homestake which has levels as deep as $\sim 2500m$. The increased background, although undesirable, is not an insurmountable problem. However, the mechanical design of a large cavity in a salt bed has to be very different because of the slow movement of salt that causes a cavity to slowly collapse in a salt mine. In this report we will not address the detailed issues of detector design and cost. A more detailed study of a very large water Cerenkov detector has been done by the UNO collaboration [40]. The mechanical design for Photo-Multiplier tube mounting developed by the E889 collaboration [15] could be used for the new detectors in Homestake. Figures 43 and 44 show the mechanical arrangement for photo-multiplier mounting.

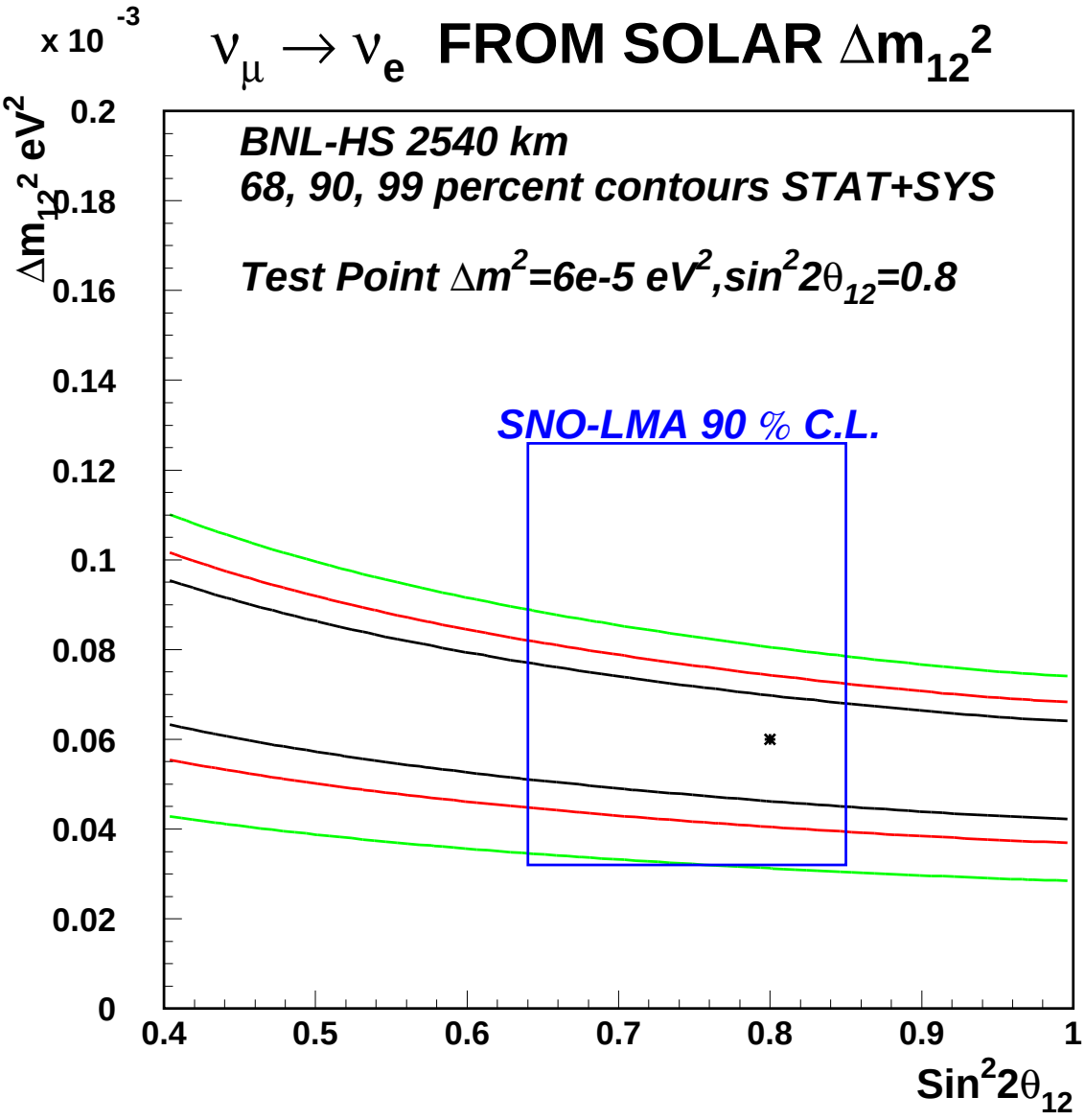

Figure 41: something

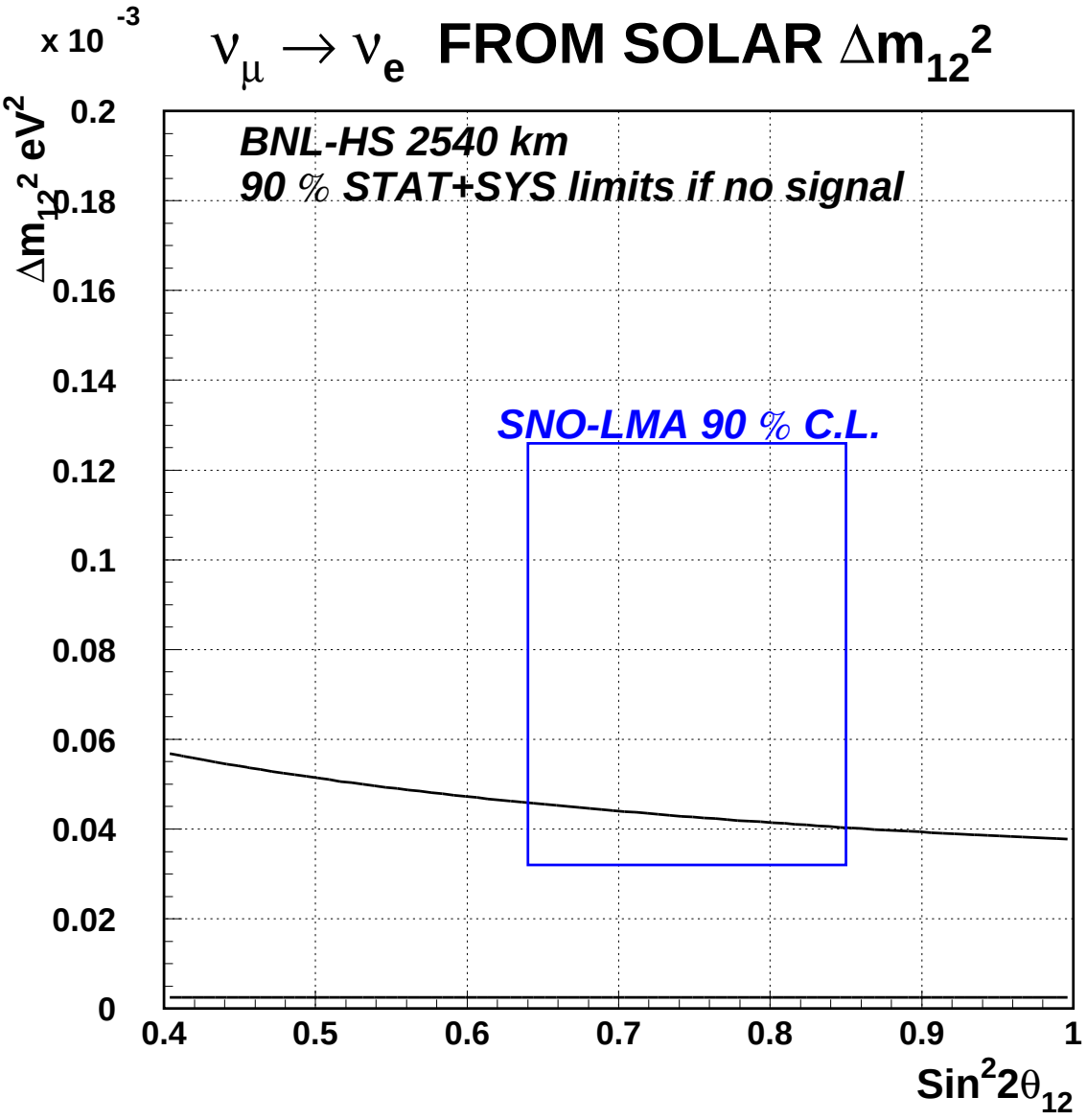

Figure 42: something

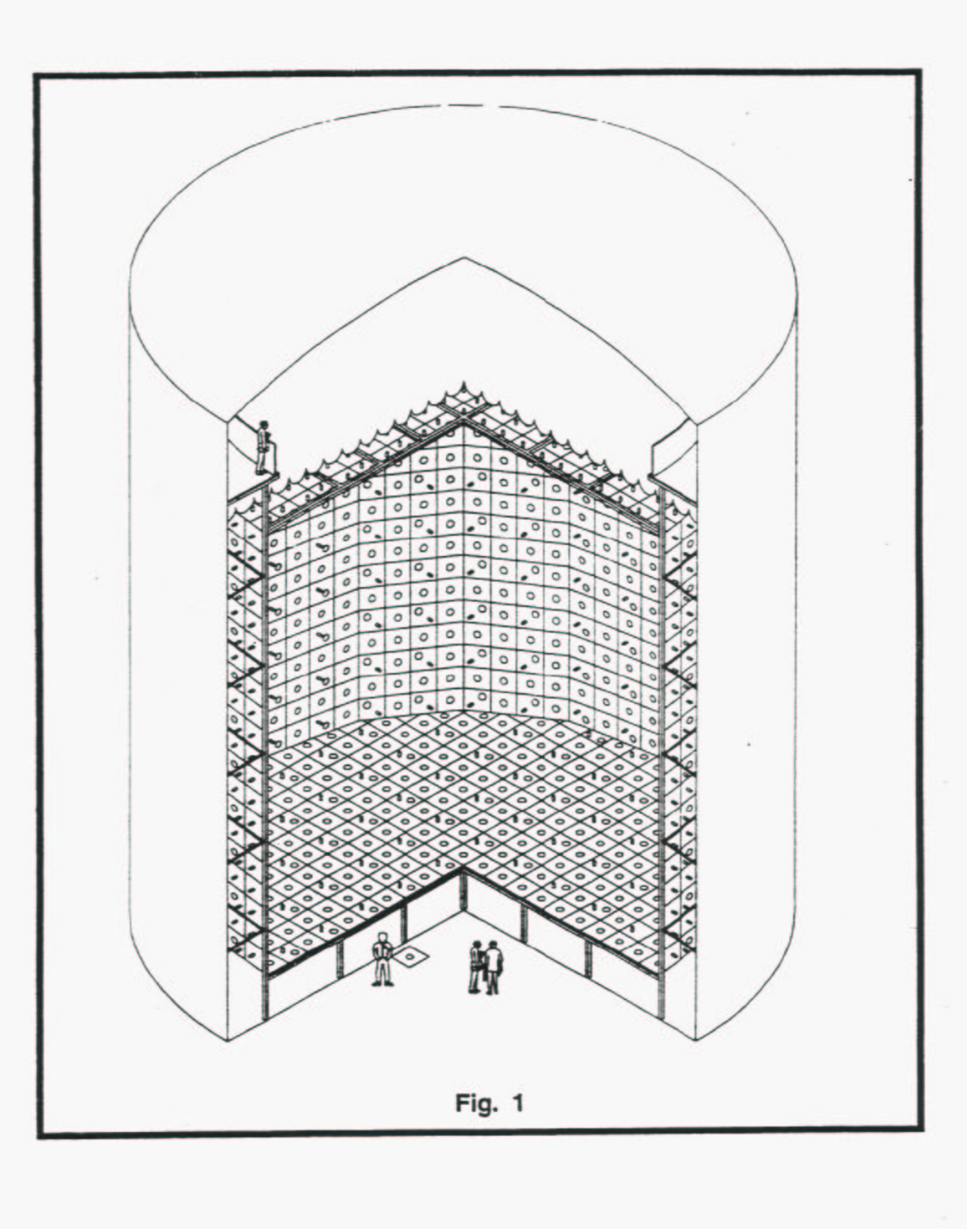

Figure 43: Mechanical assembly of the photo-multiplier tubes inside one of the 100 kT tanks. This figure is not to scale.

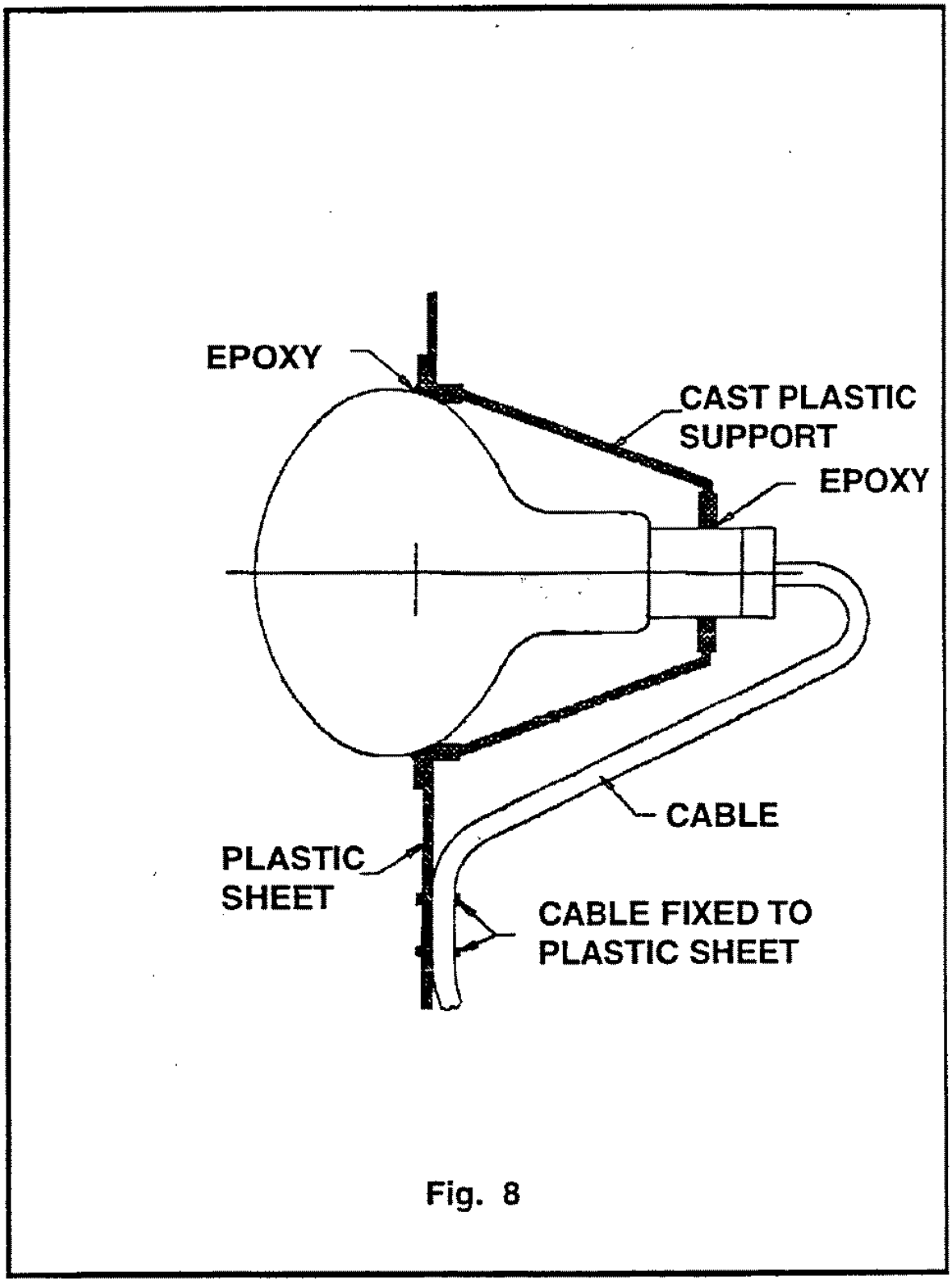

Figure 44: Individual photo-multiplier tubes assembly.

6 Conclusion

We have outlined the neutrino physics program for an intense new neutrino beam from the Brookhaven AGS. The four goals of accelerator neutrino physics: precise determination of Δm^2_{32}, detection of $\nu_\mu \to \nu_e$ appearance, measurement of the matter effect, and detection of CP asymmetries in the neutrino section are all possible for the proposed complex for reasonable values of the oscillation and mixing parameters, some of which are not yet known. Further surprises in neutrino physics should not be discounted, therefore any new facility must have sufficient flexibility to address new challenges. Our proposal allows such flexibility because of the possibility to mount both very long (over 2500 km) and intermediate (400 km) baseline experiments with beam intensity that can be increased in stages.

The AGS complex is unique because it can be upgraded simply by increasing the repetition rate of the machine. This ability allows us the flexibility to continuously upgrade the facility to as much as 2.5 MW [13]. In this proposal we have examined upgrades up to 1.3 MW. The estimated cost of the first phase of the AGS upgrades to reach 0.53 MW, plus the new neutrino beam directed to Homestake is approximately \$100M. With a 30 percent contingency, the total cost is \$130M. It is probable that the first three modules of the detector array will be produced in about five years, so that construction of the AGS upgrades and neutrino beam would be planned for that period and involve an average expenditure of approximately \$30M/yr. For a detector at intermediate baseline the costs will be less. The total yearly cost to the AGS department to provide protons for and maintain the neutrino beam would be about \$9M, approximately equal to the operations expense at present for HEP experiments. Neither the duration of the construction period nor the anticipated cost of the improvements to the BNL AGS complex is large in relation to plans and expenditures now usual for major apparatus in high energy and elementary particle physics. Moreover, the improvements to the AGS and the new beam line will be available for carefully chosen other physics (for example, rare muon and kaon decays as well as muon EDM measurements) in addition to providing important advances in our understanding of this exciting new frontier of elementary particle physics.

7 Appendix I

Director's Office

Building 510F
P.O. Box 5000
Upton, NY 11973-5000
Phone 631 344-5414
Fax 631 344-5820
tkirk@bnl.gov

date: December 1, 2001
to: S. Aronson, M. Harrison, D. Lowenstein, R. Palmer, V. Radeka
W. Marciano, M. Diwan and W.T. Weng
from: T. Kirk Associate Laboratory Director, HENP
subject: Neutrino R&D Working Group Charge and Assignments

Attached, please find the Charge to the Neutrino R&D Working Group that we have discussed. As agreed, Bill Marciano will be the Neutrino Team Leader, Milind Diwan will be the Physics Goals and Detector Team Leader and Bill Weng will be the Accelerator and Beam Systems Team Leader. The recruitment of working participants on the teams will be the responsibility of the team leaders, aided by the department heads and myself. The composition of the R&D teams will not be limited to BNL employees. In fact, the participation of outside physicists in the study will have obvious benefits for the next stage of the work which is expected to be the establishment of a formal collaboration and the creation of a formal proposal to the funding agency or agencies to build and operate a neutrino beam and detector system and carry out an experimental neutrino physics program. If the work gets off to a promising start and the physics prospects appear to be sufficiently compelling, it is possible that the initiation of the collaboration and the start of a related proposal may overlap the R&D study in time. Such an outcome could also have benefits for the timely advance of neutrino physics.

We are initiating neutrino R&D work without explicit funding for this purpose.

Accordingly, the R&D work should be regarded as part of the participants research activity, work that is generally supported by the Laboratory research mission in high energy and nuclear physics. I expect that the department heads will help and support the teams to carry out the work within their capabilities. This has already been discussed and agreed to. If conflicts arise about the allocation of internal resources and priorities between the needs of the R&D study and other activities of the departments that cannot be settled between the team leaders and the department heads, I will establish a forum for reconciliation of the conflict. I believe we are all aware of the importance to the Laboratory of a successful outcome for this work and we will expend our efforts accordingly.

Attachment (1)

Cc: P. Paul

Charge to the BNL Neutrino R&D Working Group

December 1, 2001

BNL intends to initiate an R&D study to refine the technical basis for a future proposal to employ the BNL AGS as the source of a 1MW (or possibly greater), ~1GeV neutrino beam for the continuing exploration of neutrino physics, including CP-violation in the neutrino sector. We also expect as the second element of this R&D study, to be key organizers of an experimental physics and detector design effort that will engage interested physicists in the U.S. and other countries in the preparation of the conceptual basis for a formal proposal to design and build a neutrino detector system to exploit the BNL neutrino beam and to carry out the associated neutrino physics program.

To this end, the Laboratory will designate three R&D leaders for these efforts: the Neutrino Team Leader; the Accelerator and Beam Systems Team Leader; and the Physics Goals and Detector Design Team Leader. These three leaders will, in turn, be responsible for organizing the technical work that will enable a good scientific proposal to be written to the funding agencies that are identified as potential sponsors of this new U.S. particle physics effort. The three team leaders will serve until this R&D study is complete and documented in a written report. It is intended that the written R&D report should be completed no later than June 1, 2002.

The specific roles of the three Team Leaders comprise:

Neutrino Team Leader: The Neutrino Team Leader (NTL) will have responsibility for ensuring that the overall goals of a successful neutrino physics program have been covered by appropriate R&D studies in each of the important contributing technical systems and that there is a coherent overall time evolution plan that is consistent with preparing a compelling proposal that addresses the goals of neutrino physics in a timely manner. This role should be understood as primarily a guidance and oversight role rather than a detailed management role. The balance and completeness of the study is the primary

responsibility of the NTL.

Accelerator and Beam Systems Team Leader: The Accelerator and Beam Systems Team Leader (ABSTL) is the person primarily responsible for planning, staffing, carrying out and reporting on the accelerator and neutrino beam forming systems that are relevant for the preparation of a credible proposal to construct and operate a 1MW or greater proton target and associated useful neutrino beam(s) using the AGS (suitably upgraded) as the proton driver. To accomplish this mission, the ABSTL will be helped by the relevant BNL department heads to identify sufficient and appropriate technical staff to carry out the needed studies. The ABSTL is also expected to create an appropriate discussion and reporting forum(s) where the ongoing progress in this R&D effort can be reported and discussed for the general benefit of interested parties and participants. The ABSTL role is understood to be the principal management role for accomplishing the desired R&D studies in the accelerator and beam forming elements of the overall R&D program.

Physics Goals and Detector Team Leader: The Physics Goals and Detector Team Leader (PGDTL) is the person primarily responsible for planning, staffing, carrying out and reporting on the physics goals and detector strategies that are relevant for the preparation of a credible proposal to construct and operate a detector array that can exploit the 1MW or greater neutrino beams from the AGS proton driver. To accomplish this mission, the PGDTL will be helped by the BNL Physics Department head and (hopefully) by neutrino community scientists and engineers in other institutions to find sufficient and appropriate scientific staff to carry out the needed studies. The PGDTL is also expected to create appropriate discussion and reporting forums where the ongoing progress in this R&D effort can be reported and discussed for the general benefit of interested parties and participants. The PGDTL role is understood to be the principal management role for accomplishing the desired R&D physics and detector studies for the overall neutrino R&D program.

8 Appendix II Underground Detector Construction at Homestake

Plans for the construction of a multiple module megaton Cerenkov detector at the Homestake Mine have gone through a number of essential evaluation and design stages consisting of rock strength and stability evaluation, chamber design and layout, construction planning and sequencing and development of budget and timetable. Here is a summary of these steps.

8.1 Determination of Excavation Stability

The Rock Stability Group at the Spokane Research Laboratory of NIOSH (National Institute of Occupational Safety and Health) carried out an evaluation of the stability of large excavations as a function of depth in the Yates rock formation in the Homestake Mine. This involved a three-dimensional finite difference evaluation using the FLAC3D program. These results were compared with the empirical prediction charts of Barton and Grimstad and Barton. The conclusions were that 50 meter diameter by 50 meter high chambers could be safely excavated and would be stable for long term occupancy at 2150 meter depth and probably somewhat deeper.

The Yates rock quality was determined by direct measurement of samples taken from the accessible edges of this formation. Before excavation begins, it is essential that core samples from various internal sections of the proposed rock formation are measured and the excavation reevaluated.

8.2 Construction of Multiple 100 kiloton Modules in the Homestake Mine

Using the results of the stability evaluation a group of ex-Homestake mining engineers, (Mark Laurenti - former Chief Mine Engineer, Mike Stahl - former Mine Production Engineer and John Marks - former Chief Ventilation Engineer) designed an array of ten 100 kiloton water Cerenkov chambers. The chambers are located along the circumference of a 250 meter radius circle that is centered on the Winze 6 shaft. The top of each chamber is connected to the 6950 ft station of the shaft via a horizontal, radial tunnel. A similar tunnel connects the bottom of each chamber to the 7100 ft shaft station. Fresh air will be sent to each chamber via the

top tunnel and exhaust air removed via the bottom tunnel, thus providing independent air supplies to each chamber.

Figure 45: Schematic design of the detector cavities at Homestake

During chamber construction, waste rock will be removed via the bottom tunnel. This will prevent rock dust from one chamber contaminating the fresh air supply of another chamber. Once construction is completed, the bottom chamber to tunnel connection will be sealed. A spiral ramp that surrounds each chamber and is used for access during construction will then complete the ventilation loop between top and bottom tunnels.

Each chamber will have a concrete liner. The inner surface of the liner provides a smooth surface for the water tight plastic liner that will separate the Cerenkov counter fill from the chamber walls. The liner also provides additional mechanical stability for the excavation. If necessary, drainage can be provided between the concrete liner and the surrounding rock.

8.3 Construction Timetable and Cost

Marc Laurenti has worked out a detailed timetable and budget for the construction of these modules including initial rock evaluation coring, construction of both top and bottom access tunnels, removal of waste rock, maintenance of mining equipment, etc.

The excavation process consists of continuous repetition of three separate tasks, (1) drilling and blasting of rock, (2) removal of the rock rubble, and (3) installation of rock and cable bolts to stabilize the freshly exposed rock walls. Each excavation cycle is about 10 weeks with 3 weeks for each of the above three steps. There is a considerable cost savings in excavating three chambers at the same time, with a three week phase shift between steps in each module. This arrangement permits each of the three specialized crews to move from one excavation to the next every three weeks or so and continue using the same equipment and carry out their specialized tasks. In contrast, using one crew to sequentially do three different tasks will result in idle equipment for 2/3 of the time and inefficiency as they switch from one task to another.

For the three module mode, the cost of excavating each chamber is \$14.7M. This includes \$3.25M for the concrete liner and a 15

Assuming three shifts/day and 5 days/week operation, it will take 208 weeks or 4 years to excavate each 3 module group. This time could be reduced by going to a 6 or 7 day week.

The Homestake Company frequently operated on 6 or 7 day per week basis.

8.4 Rock Removal

Each 100 kiloton module (105 m3) involves the removal of about 416,000 tons of rock including access tunnels, domed roof, etc. For three chambers this results in 1,248,000 tons of rock in 4 years or 312,000 tons of rock per year. Since the hoisting capacity of the Winze 6 - Ross shaft system is 750,000 tons per year, the simultaneous construction of three modules utilizes only 40

8.5 Equipment Cost

Since all mining equipment has now been removed, new mining equipment will have to be purchased or leased. The required equipment, one Face Drill, two LHD loaders, 2 Bolters, 2 Underground Support Vehicles, 2 Lift Trucks, 1 LH Drill and 2 ITH Drills, costs about $4.2M. It may be possible to arrange for leases instead of purchasing these items. Normal equipment maintenance has been included in the construction cost. It is unclear whether the cost of this equipment should be assigned to this specific task or should be part of the general facility budget.

8.6 Choice of Depth and Depth Dependent Cost

There has been considerable discussion of depth necessary for very large detectors and the costs associated with deep detector locations. It is clear that the deeper the detector, the lower the cosmic ray muon and associated particle background. It is always preferable to have lower background. We can quantify the background limit by specifying that there be less than one cosmic ray related event per year within the megaton detector during the time that the accelerator neutrino beam is on. If we assume the accelerator beam is on for one microsecond per second, this requirement specifies an upper limit of $1.6x10^{-6} mu/m^2/sec$, essentially the cosmic ray flux at about 7000 ft depth. The effect of this specification is that every event observed in the detector during the beam-on time is due to a neutrino from the accelerator without any cuts whatsoever.

The question then is one of access and rock strength, namely, does a specific facility have ready access to a deep location and is the local rock structure capable of supporting large

chambers. For Homestake the answer to both of these questions is YES. The present mine extends to 8000 ft, about 1000 ft deeper than the proposed detector location, and the rock seems strong enough to readily permit the excavation of large chambers.

In the appendix we provide a comparison of costs of building the megaton Cerenkov detector at 6950 ft depth vs at the 4850 ft depth. As indicated there, the maximum additional cost for putting the megaton Cerenkov array at 6950 ft versus at 4850 ft is 5-6% of excavation cost or less than 2% of total detector cost.

8.7 What Lessons About Depth Can be Learned from Previous Experience?

Detectors are located underground to reduce background in the detector due to cosmic rays. The deeper the detector, the lower the cosmic ray background. We have yet to have a detector that claimed to be "too deep". The only issues are: (1) is there a substantial additional cost associated with depth, and (2) are there technical limits associated with rock strength, etc. that limit depth at a given location? For many existing laboratories, depth is specified by what is available at that facility. Only two locations, the Sudbury mine, SNO, and the Homestake Mine, chlorine, have multiple levels available. SNO chose to be at 6800 ft, essentially the same as the proposed megaton detector. Since chlorine was the first underground neutrino detector, there were no precedents and so it might be instructive to review the sequence of events that led to its location.

In 1962, Ray Davis tested a small perchloroethylene detector in a limestone mine in Barberton, Ohio at a depth of 2200 ft. The 37Ar production was completely dominated by cosmic rays. That started a search for a much deeper site. There were two possibilities in the U.S., with Homestake the preferable one. At that time, in 1965, 4850 ft was the deepest level that the Company would agree to. At the time the prediction for the solar neutrino signal was larger than now, there was no thought about signal depression because of neutrino flavor conversion and no one expected a final measurement with a 5

The final result was that the cosmic ray induced signal is 10

A detailed construction plan for the construction of three 100 kiloton modules in four years at the 7000 ft depth in the Homestake Mine has been developed. The total construction cost of these three modules is about $44 M or $11M/year. In addition, there must be a one time purchase of about $4.2 M worth of mechanized mining equipment. The lead time in delivery of the mining equipment can be used to carry out coring of the rock region in which

the detector array is to be constructed.

8.8 Comparison of Costs at 4850 ft versus 6950 ft

There are two depth dependent costs, the cost of hoisting rock and the cost of rock and cable bolting. To estimate this effect, we determine the difference in costs between identical chambers built at the 4850 ft level (the bottom level of the Ross shaft, the upper hoist system, and the beginning of the Winze 6, the lower hoist system) and the 6950 ft level. The direct manpower costs for hoisting the extra 700 meters in the Winze 6 are about \$0.30/ton. The power costs add another \$0.20/ton for a total of \$0.50/ton or \$208,000 per 100 kiloton module, where shaft maintenance costs have not been included.

The incremental rock support costs are more difficult to determine. The cable bolting planned and budgeted for these modules is far greater than required. This was done to insure that the chambers would have a minimum 50 year occupancy. A similar approach to corresponding excavations at the 4850 ft level might result in exactly the same bolting pattern and thus the same cost. Another approach would scale the bolting cost by the difference in rock stress between the two levels. The rock stress in the Homestake and Poorman formations, the formations that have been extensively studied in mine, are rather surprising. The measured vertical stress $S_v = 28.3 \times DkPa$, where D is the depth in meters, is exactly what is expected for a fluid of density 2.9 (the rock density). The horizontal stress is very direction dependent. Along the high stress axis $S_{h1} = 14,328 + 12.4 \times DkPa$, while along the low stress axis, $S_{h2} = 834 + 12 \times DkPa$. Presumably, the high horizontal stress results from the rock folding that resulted in the upbringing of the gold ore deposit to the surface and thus its discovery.

We assume that the effective stress at 6950 ft is about 35% greater than the corresponding one at the 4850 ft level. Since the total cost of the cable and rock bolts is \$910,000 and the related labor, including benefits, is about the same, we assign a depth dependent cost increase of \$630,000 for rock support. Combining this with the increase in hoisting costs gives a total of \$838,000 or 6% of the total construction cost. Note that this is less than 2% of the complete detector cost.

However, there are three offsetting costs that reduce the cost of constructing the Cerenkov detector array at 6950 ft vs. at 4850 ft. The first of these is the water fill. The total water fill for the megaton detector is 250 million gallons. Removing that much water from the local streams would be quite significant, especially given the present drought conditions in the

area. Instead, we plan to use the water that is being pumped from the bottom of the mine at the 8000 ft level. This water will be purified to remove any light scattering or absorbing material and any radioactive contaminants. Since the mine now pumps out about 350 gallons per minute, we will require about 1.4 years worth of water distributed over the construction time of the entire detector. For a detector at the 6950 ft level, this water is only pumped up 1000 ft while for a detector at 4850 ft, the water must be pumped up about 3100 ft. The cost savings here is about 1/4 of the increase in rock hoist cost or about $50,000.

The second offsetting cost is that of cooling the Cerenkov detector. Operating the detector at 10^oC gives 1/4 the photomultiplier noise of operation at 20^oC. Since the rock temperature at the 4850 ft level is over 35^oC and still higher at 6950 ft, cooling will be necessary at either depth. The mine has an enormous refrigeration plant (2400 ton capacity) at the 6950 ft level, with a fairly short path for the coolant from the refrigeration plant to the detector. A detector at the 4850 ft level will either require a new refrigeration plant at that level or the installation of 2000 ft of vertical coolant piping in the mine shaft. We have not estimated the cost of either of these steps, but they are clearly very substantial.

The third offsetting cost is that the level structure at 4850 ft does not readily lend itself to the construction and ventilation system described above. If the upper detector access is at 4850 ft then the lower, rock removal tunnel is at 5000 ft. Unfortunately, there is no ventilation exhaust system at that level and waste rock would have to be raised in order to get it into the hoist system. The alternate approach, putting the top access at 4700 ft, would require additional excavation in order to provide the necessary tunnels for the upper access.

The material in this section was assembled and compiled by Kenneth Lande based on work done by a number of senior mining engineers who previously were in charge of mining operations at the Homestake Mine.

References

[1] "Neutrino Oscillation Experiments for Precise Measurements of Oscillation Parameters and Search for $\nu_\mu \rightarrow \nu_e$ Appearance and CP Violation. LETTER OF INTENT to Brookhaven National Laboratory.", D. Beavis, et al., hep-ex/0205040.

[2] National Underground Science Laboratory at Homestake, Lead, SD, http://mocha.phys.washington.edu/NUSL/

[3] Waste Isolation Pilot Plant, Carlsbad, NM,
http://www.wipp.carlsbad.nm,us/

[4] S. Fukuda et al., Phys. Rev. Lett. **86** 5656, 2001; E.W. Beier, Phys. Lett. **B283**, 446 (1992); T. Kajita and Y. Totsuka, Rev. Mod. Phys. **73**, 85 (2001).

[5] C. McGrew *et al.*, Phys. Rev. D **59**, 052004 (1999).

[6] Q. R. Ahmad et al., Phys. Rev. Lett. **87** 071301 (2001). S. Fukuda et al., Phys. Rev. Lett., **86** 5651 (2001).

[7] C. Athanassopoulos et al., Phys. Rev. Lett. **77** 3082 (1996); C. Athanassopoulos et al., Phys. Rev. Lett. **81** 1774 (1998)

[8] Booster Neutrino Experiment, Fermi National Laboratory,
http:/www-boone.fnal.gov/

[9] S. H. Ahn et al., Phys. Lett. **B 511** 178 (2001).

[10] The JHF-Kamioka neutrino project, Y. Itow et al., arXiv:hep-ex/0106019, June 2001.

[11] Numi MINOS project at Fermi National Accelerator Laboratory,
http:/www-numi.fnal.gov/

[12] CERN Neutrinos to Gran Sasso,
http://proj-cngs.web.cern.ch/proj-cngs/

[13] M.J. Brennan et al., , *1 MW AGS proton driver*, presented by T. Roser at Snowmass'01 (June 2001),

[14] S. Kasuga *et al.*, Phys Lett. **B374**, 238 (1996).

[15] E889 Collaboration, Physics Design Report, BNL No. 52459, April, 1995.
http://minos.phy.bnl.gov/nwg/papers/E889/

[16] L. A. Ahrens et al., Phys. Rev. **D 34**, 75 (1986).

[17] L. A. Ahrens et al., Phys. Rev. **D 41**, 3297 (1990).

[18] "Effects of beam plugs and hadronic hose", B. Viren, NUMI-0719, 2001-07-06. "Neutrino Fluxes, Hadron Production and the Hadronic Hose", M. Messier, et al., NUMI-070, 2000-12-01.

[19] Ph.D. thesis, Eric Sharkey, State University of New York at Stony Brook, May 2002.

[20] Jiro Arafune, Masafumi Koike and Joe Sato, Phys. Rev **D56**, 3093 (1997).

[21] William J. Marciano, arXiv: hep-phy/0108181, 22 Aug 2001.

[22] Irina Mociouiu and Robert Schrock, arXiv: hep-ph/0106139v3, 15 Nov. 2001

[23] By L. Wolfenstein (Carnegie Mellon U.). 1978. In *West Lafayette 1978, Proceedings, Neutrinos '78*, West Lafayette 1978, C3-C6 and *Washington 1978, Proceedings, Long-distance Neutrino Detection*, 108-112.

[24] S. Ozaki et al., eds., *Feasibility Study-II of a Muon-Based Neutrino Source* (June 14, 2001), http://www.cap.bnl.gov/mumu/studyii/FS2-report.html M. Zisman, Status of Neutrino Factory and Muon Collider R&D, PAC2001, WOAB008

[25] J. Wei et al. *Low-loss design for the high-intensity accumulator ring of the Spallation Neutron Source*, Phys. Rev. ST Accel. Beams 3, 080101 (2000).

[26] A. Ruggiero, *Design Considerations on a Proton Superconducting Linac*, BNL Internal Report 62312, 1995.

[27] R. Garoby, *Bunch Merging and Splitting Techniques in the Injectors for High Energy Hadron Colliders*, CERN/PS 98-048.

[28] M. Bai et al., *Adiabatic excitation of longitudinal bunch shape oscillations*, Phys. Rev. ST Accel. Beams 3, 064001, 2000.

[29] "Proposal to Study Production for the Neutrino Factory and for the Atmospheric Neutrino Flux", CERN-SPSC/99-35

[30] H. Kirk et al., "Target Studies with BNL E951 at AGS," PAC2001, TPAH137

[31] "A Facility to Study Proton-Nucleus and Heavy Ion Collisions Using a Large Acceptance Detector with Particle Identification Capabilities", BNL.

[32] K. Brown, et al., "First Beam Tests of the Muon Collider Target Test Beam Line at the AGS," PAC2001, TPAH129

[33] N. Simos, et al., "Thermal Shock Analysis of Windows Interacting with Energetic, Focused Beam of the BNL Muon Target Experiment," PAC2001, TPAH085

[34] R.B. Oswald, et al., " One-Dimensional Thermoelastic Response of Solids to Pulsed Energy Deposition," Journal of Applied Physics, Vol. 42, No. 9, pp. 3463-3473, 1971

[35] D. Burgreen, "Thermoelastic Dynamics of Rods, Thin Shells and Solid Spheres", Nucl. Sc. And Eng., 12, 203-217, 1962 P. Sievers, "Elastic Stress Waves in Matter due to Rapid Heating by Intense High-Energy Particle Beam," LAB.II/BT/74-2, CERN, 1974

[36] H. Conrad, "On Elastic Stress Waves in Targets", Institut fur Festkorperforschung, 1994

[37] N.V. Mokhov, "The MARS Code System User Guide, Version 13 (95)", 1995

[38] ANSYS Engineering Analysis of Systems, Swanson Analysis Systems Inc.

[39] 3M Collaboration: Proposal titled: Megaton Modular Multi-Purpose Neutrino Detector, Nov. 26, 2001.

[40] Physics Potential and Feasibility of UNO, UNO collaboration, June 2001.

[41] D.B. Cline, F. Sergiampietri, J.G. Learned, K.T. McDonald, *LANNDD, A Massive Liquid Argon Detector for Proton Decay, Supernova and Solar Neutrino Studies, and a Neutrino Factory Detector* (May 24, 2001), astro-ph/0105442
Also see F. Sergiampietri, *On the Possibility to Extrapolate Liquid Argon Technology to a Supermassive Detector for a Future Neutrino Factory*, presented at NuFACT'01 (May 26, 2001),

[42] F. Arneodo, et al., Nucl. Instrum. Meth. **A461** 324 (2001)

[43] F. Arneodo et al., Nucl. Instrum. Meth. **A471** 272-275 (2000)

[44] M. Diwan, S. Kahn, R.B. Palmer (Brookhaven). Mar 1999. Published in *New York 1999, Particle Accelerator, vol. 5* 3023-3025

[45] M.V. Diwan et al., *Proposal to Measure the Efficiency of Electron Charge Sign Determination up to 10 GeV in a Magnetized Liquid Argon Detector (μLANNDD)*, submitted to BNL (April 12, 2002),
http://www.hep.princeton.edu/m̃cdonald/nufact/bnl_loi/argonprop.pdf

[46] We have consulted Bill Foster at Fermilab to design and calculate the cost of the accumulator ring proposed here.

[47] Muon Electric Dipole Moment experiment.
http://www.bnl.gov/edm/

[48] Rare Symmetry Violating Processes,
http://meco.ps.uci.edu/RSVP.html